Novel Disease Genes Underlying Rare Recessively Inherited Forms Of Osteogenesis Imperfecta

Rachel Beth Keller

A dissertation

submitted in partial fulfillment of the

requirement for the degree of

Doctor of Philosophy

University of Washington

2018

Reading Committee:

Peter H. Byers, Chair

Raj P. Kapur, Member

Carol B. Ware, Member

Program Authorized to Offer Degree:

Pathology

University of Washington

Abstract

Novel Disease Genes Underlying Rare Recessively Inherited Forms Of Osteogenesis Imperfecta

Rachel Beth Keller

Chair of the Supervisory Committee:

Peter H. Byers

Department of Pathology

Osteogenesis imperfecta (OI) is a rare inherited connective tissue disorder affecting bone. Defining features are fragile bones that are highly susceptible to fracture ("brittle bone") and bone deformation. There is a high degree of variability in the clinical skeletal features of OI, even sometimes within families. Presentations range on a spectrum from mild with few fractures, normal stature, and normal life expectancy to severe with intrauterine fractures and disrupted skeletal development leading to early lethality. Variability in a number of extraskeletal features is also observed. The underlying cause of OI has long been understood to be defects in type I collagen, the most abundant protein component of bone, tendon, and ligaments. Variants in the primary collagen genes *COL1A1* and *COL1A2* are the cause of OI in the majority of affected individuals in an autosomal dominant fashion and affect the quantity or quality of type I collagen molecules. In the last decade, very rare cases of OI have been identified that are caused by

variants in a growing list of genes (*IFITM5*, *SERPINF1, CRTAP*, *P3H1*, *PPIB*, *SERPINH1, FKBP10*, *SP7, BMP1*, *TMEM38B*, *WNT1*, *CREB3L1*, *SPARC, MBTPS2*, *MESDC2*) with a diversity of roles in collagen and bone biology, almost all of which are recessively-inherited conditions. The work presented in this dissertation reflects contributions to this relatively new awareness in the OI community including: 1) the second case of *CREB3L1*-associated OI reported in the literature; 2) exploration of the pathogenic mechanism of *CREB3L1*-associated OI using human induced pluripotent stem cell (hiPSC) *in vitro* OI disease models; and 3) report of the first identified OI-causing variants in *MESDC2*. This work emphasizes the importance of cellular secretion and WNT signaling pathways in bone development and may be the basis of advances in further disease gene discovery, in drug development, and in the creation of novel therapeutics for OI and related conditions.

For my incredible parents, Stephen and Rebecca, whose unfailing love and encouragement I felt every day of these past five years from clear across the country and who taught me how to think in the first place. For my sweet brother, Samuel, who has always been supportive of his brainy little sister.

And for the One whose great and good work is revealed through our discoveries.

TABLE OF CONTENTS

ACKNOWLEDGEMENTS

The work herein was supported by the National Institute Of Arthritis & Musculoskeletal & Skin Diseases (F31AR069971), the Freudmann Research Fund, the Cell & Molecular Biology Training Grant (NIGMS 5T32GM007270, UW MCB), the Molecular Medicine Training Grant (NIGMS 5T32GM095421, UW Pathology), the HHMI Molecular Medicine Scholar Award (UW Pathology), the UW Department Of Pathology, and the Collagen Diagnostic Laboratory (UW). hiPSC and hESC work were greatly facilitated by the generous help of Christopher Cavanaugh, and Jennifer Hesson at the Tom & Sue Ellison Stem Cell Core (Institute For Stem Cell & Regenerative Medicine, UW). Additional thanks to Christopher Cavanaugh for surgical excision of teratomas. Other contributors to the work presented herein include: the UW Center For Mendelian Genomics for providing exome sequencing services; Diana Chen (UW Pathology) for performing the collagen analysis; Raj Kapur (Seattle Children's Hospital, UW Pathology) for the histological analysis of teratomas; and Michelle Krutein (UW Pathology) for running flow cytometry on hiPSCs. This work was overseen by a graduate committee with members David R. Eyre, Raj P. Kapur, Raymond J. Monnat, and Carol B. Ware and chaired by Peter H. Byers, who deserves particular mention for his significant contributions to designing and directing all projects. Especial thanks to the OI families who agreed to participate in research studies and to the OI clinical and research communities.

LIST OF FIGURES

LIST OF TABLES

Chapter 1: Many A Mickle Makes A Muckle – The Mounting Genetic Causes Of Recessively Inherited Forms Of Osteogenesis Imperfecta

INTRODUCTION & BACKGROUND

Descriptions of the clinically heterogeneous skeletal dysplasia "brittle bone disease" were recorded as early as 1788, but a comprehensive clinical classification for osteogenesis imperfecta (OI) did not exist until the efforts of David Sillence and colleagues in 1979 who categorized patients into numbered groups based on clinical presentation: I and IV represented milder forms of the disease, while II and III were, correspondingly, lethal and severe (Table 1-1).[1] Contemporaneously, a mechanistic understanding of the disorder, or rather group of disorders, began to be gleaned from the study of patient dermal fibroblasts, and procollagen type I, the major protein component of bone extracellular matrix (ECM), was found to be the culprit.[2]

Procollagen type I is a heterotrimeric protein consisting of two α1(I) chains and one α2(I) chain (Figure 1-1) encoded by the genes *COL1A1* and *COL1A2*. Compromise of either *COL1A1* or *COL1A2* by certain genetic defects is the root cause of OI in more than 90% of affected individuals and leads to a reduction in the quantity or quality (or both) of collagen type I molecules that are produced[3; 4] with quantitative defects generally aligning with a more mild phenotype (e.g., OI Type I) and qualitative defects correlating with moderate disease (e.g., OI Type IV). Genotype-phenotype correlations – the location and nature of variants in *COL1A1* and *COL1A2,* consequent effects on collagen biochemistry, and corresponding clinical outcomes – are complex and have been extensively reviewed by others[5] and an excellent overview of some of these discoveries within the historical context, including a discussion on the initially perplexing case of parental mosaicism in OI Type II, is offered by Byers & Pyott.[6]

Recognition of the existence of recessively inherited forms of OI can be attributed to Sillence *et al*.[1] who cited consanguinity in affected families and recurrence risks in sibships as evidence that OI Types II and III were autosomal recessive. However, it is now accepted that genetic defects in the primary collagen genes (*COL1A1*, *COL1A2*) are autosomal dominant and the cause of all "classical" forms of OI (Types I-IV). Because Sillence and his colleagues were reliant on clinical information, imaging, and pedigree data in want of a current knowledge of medical genetics, it is suspected some families in their studies harbored recessive variants in non-collagenous OI disease genes, which had not yet been identified, a hypothesis substantiated by follow-up studies in our lab (unpublished data).

In the 1990s, with the sequencing and characterization of more and more *COL1A1* and *COL1A2* variants, it became evident that a subset of families with clear clinical OI phenotypes had normal *COL1A1* and *COL1A2* sequences. Electrophoretic analysis of collagen protein (Box 1-1) in some of these families revealed abnormalities (delays in procollagen chain mobility due to overmodification). While some of these cases could be explained by primary collagen variants in the COOH-terminal propeptide and COOH-terminal telopeptide regions, others remained enigmatical. The infrequency of families large enough for linkage studies slowed the search for mechanisms of recessive inheritance, but eventually, studies identified first Procollagen-Lysine, 2-Oxoglutarate 5-Dioxygenase 2 (*PLOD2*) encoding Lysyl Hydroxylase 2 (LH2) in individuals with an OI-related condition called Bruck Syndrome (features include fractures and contractures)[7] and then Cartilage-Associated Protein (*CRTAP*) in a First Nations Canadian population.[8] With continued targeted gene studies (comprehensively reviewed by Byers & Pyott)[9], it became clear that variants not only in collagen genes, but also in genes encoding

proteins that interact with collagens (e.g., collagen processing, posttranslational modification, and chaperoning; crosslinking of collagen fibrils; matrix mineralization, etc.) underlie forms of OI. In the last decade, Next Generation Sequencing (NGS) has empowered the OI community to solve the mystery of recessive inheritance in more families.

While the adoption of the OI "type" descriptions was initially helpful in diagnosis and counseling, it has faltered somewhat in this new era of genetic discovery. A new nomenclature[10] (Table 1-2), defined by functional genetics rather than by clinical observations, has risen to replace it, though it has become unwieldy as discoveries have multiplied, excludes gene discovery in clinically-overlapping syndromes (i.e., *PLOD2*, *PLS3*, *P4HB*, and *SEC24D* do not have type designations), and has admittedly limited clinical utility. Nevertheless, it is the nomenclature used herein. Since Byers & Pyott published their review[9], seven further genes have been identified in the pathogenesis of novel forms of recessively inherited OI (OI Types XII, XIV-XIX). It is the aim of this review to update the field and present new discoveries, including recently published (Chapter 2)[42] and unpublished (Chapters 3 & 4) research presented in this dissertation.

A STANDALONE CASE – A VARIANT IN *SP7* ENCODING THE TRANSCRIPTION FACTOR OSTERIX (OI TYPE XII)

One additional disease gene would be discovered through more traditional methods before whole exome sequencing (WES) began to dominate the field of OI disease gene discovery. Homozygosity mapping in a consanguineous OI Egyptian family led to the identification of Specificity Protein 7 (*SP7*), which encodes the osteoblast-specific transcription factor Osterix (OSX) (OI Type XIII).[11] The phenotype of the 8-year-old proband aligned with an OI Type IV

clinical picture with recurrent fractures after minimal trauma starting at 3 months of age, bowed limbs, wormian bones, delayed tooth eruption, normal hearing, and white sclerae. The candidacy of *SP7* over other genes in regions of homozygosity (ROH) was decided based on published studies of the *Sp7*$^{-/-}$ mouse. In these animals, preosteoblasts could not undergo complete differentiation to functional osteoblasts and no bone formation occurred.[12] In the proband, a single base-pair deletion in *SP7* was sequenced (c.1052delA). The variant was predicted to cause a frameshift leading to premature termination of the transcript (p.E351GfsX19) and loss of the third finger of a zinc-finger domain in OSX, likely impairing the DNA-binding ability of the transcription factor.

Because *Sp7*$^{-/-}$ mice express another key osteoblast transcription factor, Runt-Related Transcription Factor 2 (*Runx2*), whereas *Runx2*$^{-/-}$ mice are absent both transcripts, it is thought that RUNX2 must operate upstream of OSX. Progenitor mesenchymal stem cell cells (MSCs) first express *RUNX2* to become bi-potential preosteoblasts (progenitors of both osteoblasts and cartilage-forming chondrocytes) and further expression of *SP7* drives the expression of additional bone markers (e.g., *SPP1, BGLAP*, and high levels of *COL1A1*) and a commitment to an osteoblast fate.[12] Interestingly, common variants in the regions surrounding *SP7* had been reported in genome-wide association studies as correlating with bone mineral density (BMD) and these regions are considered potential osteoporosis susceptibility loci.[13-15] No additional cases of *SP7* variants in OI have since been reported.

A NEAR MISS – VARIANTS IN *TMEM38B* ENCODING TRIC-B (OI TYPE XIV)

The next novel gene would be identified through the study of multiplex Saudi Arabian families through autozygome analysis (ascertainment of genomic regions in an individual that are identical by descent) followed by exome sequencing. Affected individuals from three autosomal recessive OI families with fractures, osteopenia, and no notable secondary features were found to share a ROH on chromosome 9, yet exome sequencing of the region did not reveal any novel coding or splicing variants. Shaheen *et al*. were keen when they reviewed the SNP calls from the exomes and found that failure to call a single SNP (rs10978220) was common to all affected individuals owing to nullizygosity for exon 4 (c.455_542del) of Transmembrane Protein 38B (*TMEM38B*) (OI Type XIV).[16] The same deletion was independently identified in several Israeli Bedouin families whose ancestors migrated from the Arabian Peninsula, hinting that the exon 4 deletion may represent an ancient founder mutation.[17] Additional reported mutations include: deletion of exons 1 and 2 in an Albanian girl with a milder bone phenotype than both the Saudi Arabian and Israeli Bedouin populations, with the added symptom of mild conductive hearing loss[18]; point mutations in two Han Chinese families located in exon 3 (c.455-7T>G [p.R151_G152insVL]) and exon 4 (c.507G>A [p.W169X])[19]; the same exon 4 variant in a Pakistani individual with consanguineous parentage; and an interesting case in which two affected siblings of English, Scottish, and German descent each bore two separate variants – a maternally-inherited duplication introducing a termination codon (c.63dupT [p.D22X]) and a paternally-inherited deletion identical to that described in the previously reported Albanian proband – such that both alleles were independently compromised.[20]

TMEM38B encodes Trimeric Intracellular Cation Channel Type B (TRIC-B) which is

ubiquitously expressed on the endoplasmic reticulum (ER) of mammalian tissues and functions as a counter-ion channel (primarily for K^+) to balance the release of Ca^{2+} from intracellular stores.[21] *Tmem38b*$^{-/-}$ mice die early from respiratory failure caused by compromised Ca^{2+} release in alveolar type II cells. No skeletal phenotype was described.[22] Thoughts as to the mechanism of *TMEM38B*-associated OI are that disruption of calcium homeostasis in the ER affects rough ER (rER)-resident collagen-modifying enzymes and collagen chaperones (e.g., levels of the calcium-stabilized protein FKBP65 were halved in *TMEB38B*-variant fibroblasts and osteoblasts) leading to abnormal posttranslational modification and folding of collagen type I, the creation of low-stability collagen species, a drop in the rate of collagen secretion, and, overall ECM insufficiency.[20] Calcium is also of known importance for both the differentiation and growth of osteoblasts[23], with the release of Ca^{2+} that accompanies bone resorption triggering signaling pathways by multiple mechanisms, and the regulation of osteoclasts, which have plasma membrane-bound Ca^{2+} sensors by which they can monitor ambient Ca^{2+} and thereby fine-tune their resorptive activity.[24]

BONE & BRAIN (?) – VARIANTS IN *WNT1* & *MESDC2* (OI TYPES XV & XIX)

WES in three separate laboratories led to the near simultaneous discovery of variants in Wingless Type MMTV Integration Site Family, Member 1 (*WNT1*), implicating a vital signaling pathway for embryological development in the pathogenesis of OI (OI Type XV).[25-27] In one study, homozygous *WNT1* variants in all four unrelated families studied (including one family from Newfoundland and another of Hmong Chinese origin) resulted in moderately severe, progressive OI analogous to classical OI Type III.[25] Another study noted a similar range of severity from moderate to progressively-deforming (with one case of early infant death) due to homozygous

variants. An apparently dominant *WNT1* mutation (c.703C>T [p.Arg235Trp]) was also identified by this group in a multi-generational family with early-onset osteoporosis.[26] A third study reported *WNT1* variants in four children with a clinical diagnosis of OI Type IV.[27]

In addition to skeletal findings, some individuals presented with brain malformations and developmental delays (in 3 of 4 families in one study[25] and in 1 of 5 families in another[26]). There were no noticeable neurological features in affected individuals from the third study.[27] In mice, *Wnt1* is highly expressed during neural development and contributes to the proper formation of a substantial portion of the early central nervous system (CNS); *Wnt1*$^{-/-}$ mice lack large portions of the cerebellum and midbrain and die within 24 hours of birth[28] and the spontaneous mutant *swaying* (*sw*) mouse was found to possess a variant in *Wnt1* and presented with malformations in the anterior cerebellum causing ataxia.[29] Why *WNT1* variants in humans are not associated with ataxia or the same neural malformations in all cases could be due to differences in the location and nature of mutations in human *WNT1* versus mouse *Wnt1* or to differences in the requirement for specific WNTs during CNS development in either species. Whether the neurologic findings in this subset of OI patients are even associated with *WNT1* variants is a lingering question, though evidence that there is a causal connection continues to mount.[30]

In bone, WNT signaling pathways are involved in the differentiation of MSC progenitors into osteoblasts, credibly upstream of RUNX2 and OSX. Though not all aspects of WNT signaling in bone are fully understood, recent work in a conditional mouse model in which *Wnt1* was specifically targeted in late osteoblasts/osteocytes has advanced our understanding, suggesting that the primary source of WNT1 in bone is the osteocytes and that WNT signaling from

osteocytes to osteoblasts is disturbed by OI-causing *WNT1* variants.[31] Canonical WNT signaling begins with the binding of WNTs to the cell surface receptor Frizzled (FZD) and its co-receptors Low-Density Lipoprotein Receptor-Related Protein 5 (LRP5) and LRP6 to initiate signal transduction and ends in β-catenin-mediated gene transcription.[32] Pathogenic variants in *LRP5* were the first indication that WNT signaling mattered for bone, being the cause of Osteoporosis-Pseudoglioma Syndrome (OPPG)[33] on the one hand and high bone mass (HBM) phenotypes on the other.[34-36] Both LRP5 and LRP6 are folded in the rER and properly localized to the cell surface with the aid of the ER-resident chaperone Mesoderm Development Protein (MESD) encoded in humans by Mesoderm Development Candidate 2 (*MESDC2*), the newest addition to the OI disease gene family. Using WES followed by targeted sequencing of *MESDC2* in additional families, biallelic variants were identified in three unrelated families with severe OI phenotypes (OI Type XIX). All three variants resulted in loss of the KDEL-like ER retention signal (REDL) and were expected to disrupt WNT signaling (Chapter 4).

"TRAFFIC JAMS" IN BONE-FORMING CELLS – VARIANTS IN *CREB3L1* & *MBTPS2* (OI TYPES XVI & XVIII)

In their discussion of the rER-resident proteins CRTAP, Prolyl-3 Hydroxylase 1 (P3H1), and Cyclophilin B (CyPB) and their involvement in recessive forms of OI, Byers & Pyott proved prescient when they noted that the "voyage" of collagen type I to forming bone ECM involves additional steps and cellular locations and suggested that study of Golgi-resident proteins and constituent proteins of secretory vesicles might prove productive in the search for additional OI-causal genes.[9] In 2013, homozygosity for a large genomic deletion resulting in complete loss of Cyclic-AMP Responsive Element Binding Protein 3-Like 1 (*CREB3L1*), along with the first exon of an adjacent gene, was identified by ArrayCGH analysis of a Turkish family with two

severely-affected pregnancies (OI Type XVI).[37] Following uninformative genetic testing for all known OI genes, targeted genetic testing of *CREB3L1*, encoding the ER-stress transducer Old Astrocyte Specifically-Induced Substance (OASIS), was pursued based on descriptions of *Creb3l1*$^{-\backslash-}$ mice, which were reported to suffer from severe osteopenia and spontaneous fractures.[38] The mechanistic understanding of the role of OASIS in bone formation at the time was informed by the observations that, 1) activated OASIS induced expression of *Col1a1*, 2) the collagen type I content of bone matrix in calvaria and tibiae of *Creb3l1*$^{-\backslash-}$ mice was reduced, and 3) *Creb3l1*$^{-\backslash-}$ osteoblasts had distended rERs full of bone matrix proteins (procollagen type I and osteocalcin).[38] Emphasis was placed on *COL1A1* as a transcriptional target of OASIS and this was submitted as a satisfactory explanation for the OI phenotype in humans, but the true mechanism would prove more intricate.

The next novel OI gene described would serve as confirmation of the importance of OASIS and associated pathways for bone biology. In two independent OI pedigrees, linkage analysis followed by NGS identified variants in Membrane-Bound Transcription Factor Peptidase, Site 2 (*MBTPS2*) (OI Type XVIII).[39] This gene codes for the protein Site-2 Protease (S2P) which, along with its sibling Site-1 Protease (S1P), are Golgi-localized serine proteases that sequentially cleave membrane-bound regulatory proteins resulting in their activation through a process called Regulated Intramembrane Proteolysis (RIP).[40] RIP figures prominently in the control of lipid metabolism where targets are the Sterol Regulatory Element Binding Proteins (SREBPs) and in the Unfolded Protein Response (UPR) where targets include Activating Transcription Factor 6 (ATF6) and, notably, OASIS.[41] Protein analysis of patient fibroblasts and osteoblasts bearing *MBTPS2* variants in which mild ER stress had been induced (to drive OASIS activation) showed

a high level of S1P-cleaved OASIS paired with a low level of activated (both S1P *and* S2P cleaved) OASIS fragment, whereas protein from control fibroblasts was almost all double-cleaved.[39] Lindert *et al.* (2015) had demonstrated a functional effect on a regulatory protein that controls the activity of a known OI-related protein, but no further explanation of downstream mechanisms leading to a bone phenotype (beyond debatable claims of reduced collagen secretion from patient fibroblasts) was proffered.

Some much-needed clarity about the pathogenic mechanism would come with the second report of *CREB3L1* variants in OI. In 2017, we reported WES of multiple members of a consanguineous Lebanese OI family who bore a trinucleotide deletion (c.934_936delAAG [p.Lys312del]) that disrupted the OASIS conserved DNA-binding motif (Chapter 2).[42] The homozygous proband had been terminated at 16 weeks gestation due to suspected OI on the basis of ultrasound imaging. Clinical features were comparable to that of classical OI Type II, though collagen analysis was normal, unlike in the classic case. Based on structural and functional similarity to another RIP-regulated transcription factor expressed highly in chondrocytes, BBF2 Human Homolog On Chromosome 7 (BBF2H7), we explored the possibility of an OASIS-mediated transcriptional effect on the gene *SEC23A*, encoding a coat protein II (COPII) component.[42] While no such effect was seen in HEK293 overexpressing *CREB3L1*, an effect on a gene encoding another COPII structural component, *SEC24D*, was observed.

SEC23A and SEC24D together form the inner "coat" of COPII complexes, intracellular carriers that ferry secreted proteins from the rER to the Golgi for processing, packaging, and secretion. The transport of bulky proteins, including collagens, necessitates the formation of mega-sized

COPII carriers, which is accomplished with the action of helper proteins including TANGO1 and cTAGE5 (covered in detail elsewhere).[43; 44] In bone-forming osteoblasts, the stress of high levels of protein production and accompanying secretory demand multiplied by the need for extra-large COPII, given that 90% of bone ECM is comprised of collagen type I, presents a formidable task for these cells. It was proposed that OASIS activation and actions represent an evolutionary coping mechanism, not unlike the UPR, in highly-secreting ("professional secretory") cell types. Studies in thyroid cells, which also express *CREB3L1*, revealed an expanded role for OASIS, adding transcriptional regulation of genes encoding proteins in other compartments (e.g., GM130 and RAB1B in the Golgi) and enlargement of the Golgi itself to the list of functions.[45] In our follow-up studies, osteoblast-like cells differentiated from patient human induced pluripotent stem cells (hiPSCs) homozygous for the *CREB3L1* variant exhibited a cellular phenotype in keeping with the proposed role of OASIS as a mediator of secretory pathway capacity. These cells produced undermineralized, collagen-type I-deficient ECM, the outcome of a secretion defect evinced by collagen type I accumulation in enlarged rER lumens (Chapter 3). With the report of variants in *SEC24D* proper being the cause of a syndromic form of OI known as Cole-Carpenter Syndrome (bone deformities and fractures with ocular proptosis, craniosynostosis, hydrocephalus, and facial dysmorphism)[46], in which procollagen type I secretion was also found to be deficient,[47] our understanding of the clinical impact of OI-causing variants affecting this pathway was rounded out (i.e., S2P → OASIS → SEC24D).

Of special clinical note for OI Type XVI, is the finding that both homozygotes and heterozygotes can be affected, with zygosity dictating clinical severity: monoallelic variants cause mild OI (akin to OI Type I), while biallelic variants cause lethal OI (akin to OI Type II). While not

emphasized in the original report, Symoens *et al*. (2013) noted that the heterozygous individuals in that family had blue sclerae and some had non-skeletal OI findings (soft skin, conductive hearing loss), though fractures were absent in all.[37] In the Lebanese family we reported, 3 of 4 heterozygous individuals had blue sclerae and mild to moderate osteopenia and 2 of 4 had recurrent fractures. The heterozygous father was seemingly unaffected.[42]

COLLAGEN-ASSOCIATED – VARIANTS IN *SPARC* ENCODING THE MATRICELLULAR PROTEIN OSTEONECTIN (OI TYPE XVII)

Using WES, two unrelated girls with delayed onset of severe bone fragility and features evocative of OI Type IV, but absent variants in *COL1A1*, *COL1A2*, or any of the known recessive OI disease genes, were found to harbor variants in Secreted Protein, Acidic, Cysteine-Rich (*SPARC*) encoding a collagen type I-binding glycoprotein (OI Type XVII).[48] Individual 1 was of North African origin. Her parents were non-consanguineous but did share common ancestry. No skeletal abnormalities were apparent at birth, but she suffered her first fracture (right proximal femur) at 15 months of age. Later evaluation identified vertebral compression fractures and both severe scoliosis and severe kyphosis. Her clinical picture was not dissimilar to that of OI Type VI (caused by variants in *SERPINF1*), but normal serum levels of Pigment Epithelium-Derived Factor (PEDF) excluded that diagnosis.[49] Individual 2 was of Indian descent with consanguineous parentage. At 10 weeks, left hip dislocation was observed, but even with serial casting, she demonstrated gross motor developmental delay. She sustained her first fracture (midshaft transverse femur) at age 5 years. Mild scoliosis and mild kyphosis, in addition to vertebral compression fractures, were noted later. Exome sequencing revealed homozygous variants in *SPARC* in both girls (Individual 1 – c.497G>A [p.Arg166His]; Individual 2 – c.787C>A [p.Glu263Lys]).

SPARC, also called BM-40 or osteonectin (ON), is one of several non-collagenous proteins (NCPs) found in bone ECM.[50] It is counted among the matricellular proteins, a group of secreted glycoproteins that do not structurally contribute to ECM, but that modulate cell-matrix interactions through binding to ECM structural elements, e.g. collagen type I.[51] The attachment of cells to surrounding ECM must be dynamic since activities such as cell differentiation and cell division (as occur during tissue development, tissue remodeling, and wound healing) require morphological changes, e.g., cellular rounding, and cellular movement. The matricellular proteins exhibit "anti-adhesive" properties, helping to break cell-matrix interactions when neccessary.[51] The importance of this action for bone homeostasis is evident from study of the *Sparc*$^{-/-}$ mouse which suffers low-turnover osteopenia with decreased bone mass and low osteoblast and osteoclast numbers.[52] In addition to its established role in bone ECM, it has been postulated that SPARC might double as a chaperone protein for collagens in the rER, possibly in partnership with HSP47 in humans.[53] Indeed, pulse-chase experiments showed a slight delay in procollagen type I secretion from both Individual 1 and 2 fibroblasts.[48] The Arg166 and Glu263 residues affected by variants in Individuals 1 and 2, respectively, form a salt bridge that maintains the structure of a binding pocket by which SPARC interacts with fibrillar collagens.[54] Whether this association occurs in just the ECM or in both the ECM and the rER, it is a crucial interaction. It is reasonable to conclude that constraint of the matricellular protein activity of SPARC is the primary driver of OI, causing a deficiency in bone remodeling that becomes apparent with growth and time.

CLINICAL IMPLICATIONS OF DISEASE GENE DISCOVERY FOR OI & OTHER BONE PATHOLOGIES

There exists no cure for osteogenesis imperfecta. As it is a genetic disorder affecting development, "prevention" is an elusive concept, exceptions being genetic testing for known variants in families with a history of OI and prenatal screening, which can detect the severest clinical forms and inform decisions about the continuation of affected pregnancies. Current treatments for OI are merely palliative and management is symptom-specific. To attend the musculoskeletal symptoms of OI, interventions can include: orthopaedic surgery, such as attempts to realign deformed bones with rodding; rehabilitation, both after fracture events and after surgery, to preserve muscle strength and, when possible, mobility; and the pharmacological use of bisphosphonates (anti-resorptive) and growth hormones with the aim of producing and maintaining more bone, even more poor-quality bone, if it might confer some benefit. Other extraskeletal manifestations (pulmonary insufficiency, cardiovascular abnormalities, conductive deafness, and dentinogenesis imperfecta, among others) must be monitored and addressed by specialists as becomes necessary.[55]

Innovative therapeutic modalities have emerged from biomedical research. After excessive Transforming Growth Factor β (TGF-β) signaling was found to be common to both dominant and recessive OI mice (*Col1a2*$^{tm.1Mcbr}$ and *Crtap*$^{-/-}$), the use of anti-TGF-β antibodies as a potential therapeutic was proposed.[56] Neutralizing antibodies against another target, sclerostin, are also promising. Sclerostin is expressed in osteocytes and was found to antagonize WNT signaling, a key stimulus of osteoblast differentiation and function, by competitively binding LRP5 and LRP6.[57] Clinical trials of the monoclonal anti-sclerostin antibody Romosozumab

(Amgen & UCB Pharma) have shown increased BMD[58] and a lessened incidence of vertebral fractures in osteoporotic post-menopausal women[59]. Whether the impact of blocking sclerostin will be as effective in OI bone awaits to be seen.

Another promising avenue in OI therapeutics is gene therapy. In the case of classical OI types with quantitative defects, the goal would be to introduce normal *COL1A1* or *COL1A2* genes to balance the haploinsufficiency. With qualitative defects, this must be coupled with silencing of the mutant allele to counter the dominant negative effect of abnormal collagen molecules. In fact, success in just the latter effort could be enough to downgrade severe disease to a milder form. Transcript-specific suppression has proven successful with a number of approaches, e.g., antisense oligonucleotides[60] and short interfering RNA (siRNA).[61] Such an approach may not, however, prove efficacious in the other fifteen highly heterogeneous forms of OI.

The clinical contribution of novel gene discovery lies in filling the gaps in our knowledge of both OI disease pathology *and* the basic biology of bone. With every pathway that is elucidated, more druggable targets and potential therapeutic targets become known. Insight into not only the differences between distinct OI pathologies, but also especially the commonalities, will lead to advances. Some discoveries may have implications for only a single form of the disease while others may be generalizable – to OI or to any number of other bone pathologies, both common (e.g., osteoporosis) and uncommon. In the following chapters, new understandings about collagen secretion (Chapters 2 & 3) and WNT signaling (Chapter 4), both of which are implicated in the pathogenesis of newly-characterized forms of recessive OI (Types XVI & XIX,

respectively), along with discussions about the significance of this new knowledge to the OI community, will be presented. While the description of OI as a collagen disorder remains apposite, it is far more multifaceted than was appreciated when only *COL1A1* and *COL1A2* variants were known. In Chapter 5, combined insight from several fields of study will inform a discussion of the "brittle" feature of OI bone, the common thread in a tangle of diverse OI pathologies.

FIGURES & TABLES

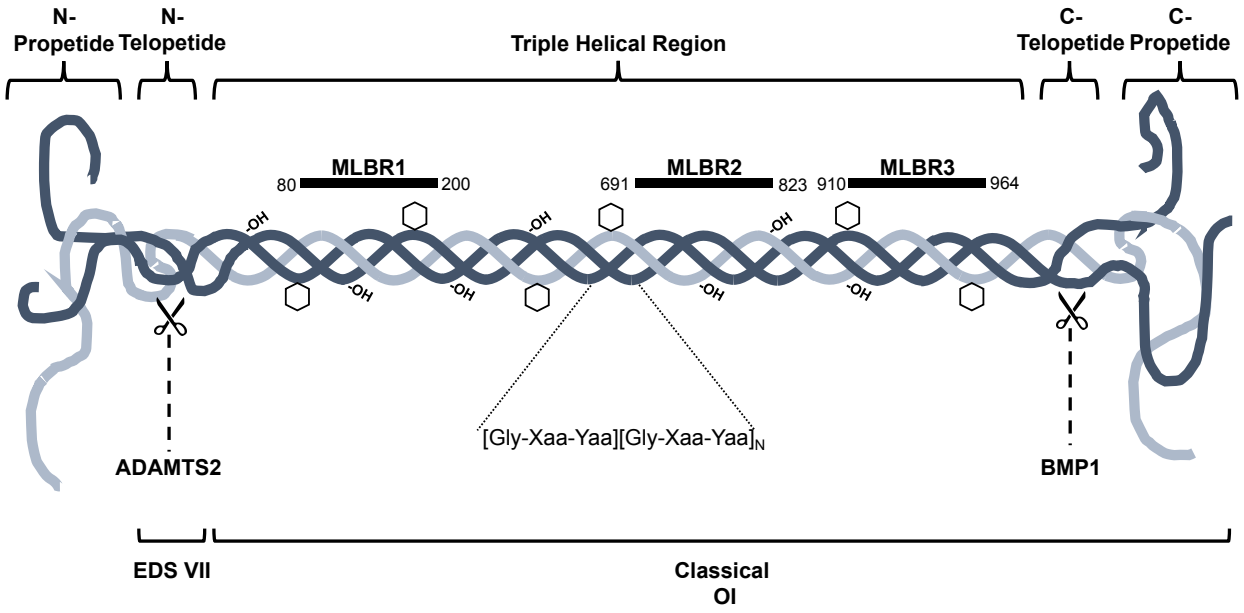

Figure 1-1. Structure Of Procollagen Type I. Procollagen type I consists of two α1(I) chains (**dark blue**) and one α2(I) chain (**light blue**). The bulk of the procollagen type I protein is the 1014-residue triple helical region consisting of Gly-Xaa-Yaa repeats in which Xaa and Yaa can be any amino acid except cysteine and tryptophan and are often (~20%) proline, with the glycine residues situated internally within the triple helix. Important posttranslational modifications include hydroxylation (-OH) of proline and lysine residues, glycosylation (hexagons) of hydroxylated lysines, and the hydroxylation of carbon-3 on the isolated proline residues α1(I)Pro986 and α2(I)Pro707. There are three major ligand binding regions (MLBRs) by which mature collagen type I associates with other proteins. The triple helical region is capped on both ends by globular propeptides, which are important for chain association. Winding of the triple helix progresses from the COOH-terminus to the NH_2-terminus. When procollagen reaches the extracellular matrix, the NH_2- and COOH-propeptides are cleaved off at specific sites in the telopeptide regions by the enzymes ADAMTS2 and BMP1, respectively, to form mature collagen type I. Where variants fall within the various regions of the procollagen structure can be a broad predictor of biochemical effect and, to some extent, phenotype (e.g., because of the COOH-to-NH_2 terminal direction of helix formation, helical glycine substitutions near the COOH-terminal end greatly disrupt procollagen assembly and are associated with moderate and lethal outcomes, whereas substitutions closer to the NH_2-terminal end are minimally disruptive and associated with non-lethal disease). A detailed discussion of the many types of primary collagen defects is outside the scope of this review. Variants in the triple helical region and in the COOH-telopeptide and COOH-propeptide regions cause classical osteogenesis imperfecta (OI), whereas variants in the NH_2-telopeptide instead cause a form of Ehlers-Danlos Syndrome (EDS).

Table 1-1. Sillence Classification Of Osteogenesis Imperfecta

Numerical Type	Clinical Severity	Clinical Features	Historical Synonyms & Eponyms
I	Mild	blue sclerae, normal stature, late-onset hearing loss	Dominantly Inherited OI w/Distinctly Blue Sclerae, Van der Hoeve's Sydrome, Trias Fragilitas Ossium, OI Tarda Levis, OI Tarda Type II, OI (Mild Long Bone Deformity), Eddowe's Syndrome
II	Lethal	perinatal lethality	Lethal Perinatal OI, OI Letalis Vrolik, Lethal OI Congenita
III	Severe	progressive deforming	Progressively Deforming OI w/Normal Sclerae, OI Congenita, OI Tarda Gravis, OI (Severe Long Bone Deformity), OI Congenita Type Vrolik, Periosteal Dysplasia of Porak and Durante, Osteopsathyrosis Idiopathica of Lobstein
IV	Moderate	white sclerae, short stature, dentinogenesis imperfecta	Dominantly Inherited OI w/Normal Sclerae, Osteopsathyrosis Idiopathica of Lobstein, Ekman-Lobstein Disease

(Adapted from Sillence *et al.* J Med Genet 1979)

Box 1-1. Electrophoretic Analysis Of Collagens. In the 1970s and 1980s, before Sanger sequencing greatly simplified the task of identifying pathogenic variants in *COL1A1* and *COL1A2* (and eventually other OI-causing genes), the standard OI diagnostic was analysis of collagen protein secreted by cultured dermal fibroblasts. Fibroblasts were grown with ^{3}H-radiolabeled proline, which incorporates into forming procollagen and collagen molecules and allows detection of collagens with SDS-PAGE and fluorography. Using this technique, quantitative alterations in OI Types I and III and qualitative alterations (observable as changes in the electrophoretic mobility of procollagen and collagen alpha chains) in OI Types II and IV could be determined. In the example analysis below of fibroblasts from a patient with lethal OI Type II caused by a glycine substitution variant (gel images reproduced from Bonadio *et al.* 1985)[62], it is apparent that two discrete forms of both proα1(I) and proα2(I) were secreted from patient fibroblasts into the medium: one chain with normal mobility and another with delayed mobility (arrows). Similar analysis of the collagen content of the cells themselves shows slight retention of the procollagen forms with delayed mobility. To obtain mature α1(I) and α2(I) chains, collagens were digested with pepsin to cleave off the NH_2- and COOH-propeptides. Doublets and delayed chain mobility of alpha chains is evident, suggesting there is a biochemical effect on the triple helical region rather than the procollagen telopeptide or propeptide regions. The delay in chain mobility in these cells is due to excessive posttranslational modification, a consequence of delayed helix folding that causes the procollagen molecule to be resident in the rER for longer. Overmodification of chains is also seen in OI cells with COOH-propeptide and COOH-telopeptide variants, which disrupt chain association and thus folding, and in OI cells bearing certain recessive variants, e.g., variants in *CRTAP,* which encodes a component of a complex directly involved in the hydroxylation of proline residues.

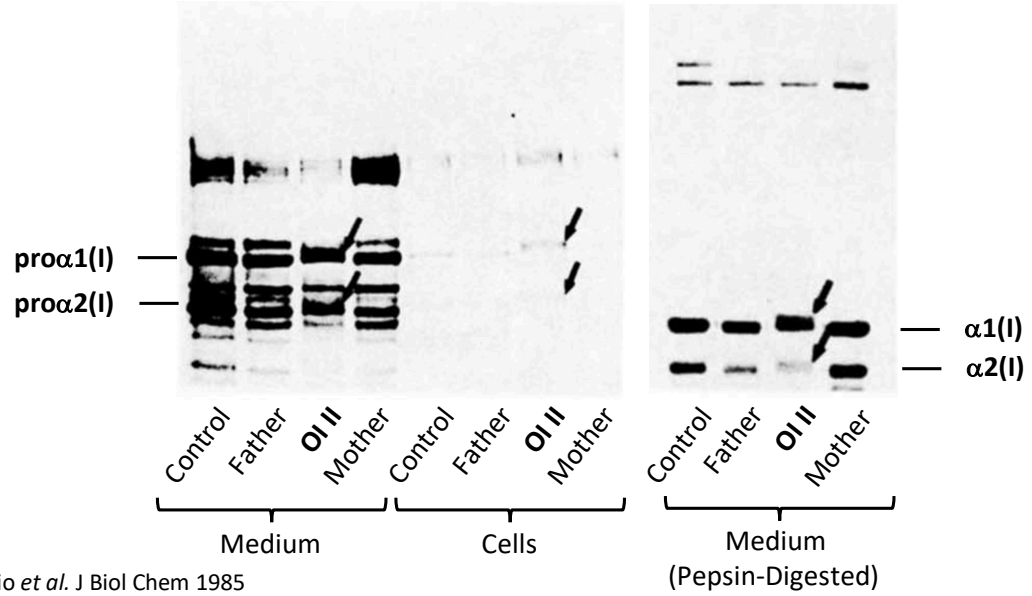

Bonadio *et al.* J Biol Chem 1985

Table 1-2. Functional-Genetic Classification Of Osteogenesis Imperfecta

Numerical Type	Inheritance	Associated Gene	Encoded Protein	Unique Features
I **II** **III** **IV**	AD AD	*COL1A1* *COL1A2*	Collagen Type 1, Alpha-1 [α1(I)] Collagen Type 1, Alpha-2 [α2(I)]	"classical" OI (refer to Table 1)
V	AD	*IFITM5*	Bone-Restricted Interferon-Induced Transmembrane Protein-Like Protein 5 (BRIL)	intraosseous membrane ossifications; radial head dislocation; subepiphyseal metaphyseal radiodense band
VI	AR	*SERPINF1*	Pigment Epithelium-Derived Factor (PEDF)	osteoid (unmineralized matrix) present; "fish-scale" appearance of lamellar bone under polarized light; elevated ALP; reduced serum PEDF
VII	AR	*CRTAP*	Cartilage-Associated Protein (CRTAP)	rhizomelia
VIII	AR	*P3H1 (LEPRE1)*	Prolyl-3 Hydroxylase 1 (P3H1)	rhizomelia
IX	AR	*PPIB*	Cyclophilin B (CyPB)	grey sclerae
X	AR	*SERPINH1*	Heat-Shock Protein 47 (HSP47)	skin abnormalities (blisters and bullae); inguinal hernia
XI	AR	*FKBP10*	65kDa FK506-Binding Protein (FKBP65)	congenital contractures (clinical overlap w/Bruck and Kuskokwim Syndromes)
XII	AR	*SP7*	Specificity Protein 7; Osterix (SP7/OSX)	delayed tooth eruption; midface hypoplasia
XIII	AR	*BMP1*	Bone Morphogenetic Protein 1 (BMP1)	HBM; umbilical hernia
XIV	AR	*TMEM38B*	Trimeric Intracellular Cation Channel Type B (TRIC-B)	absent secondary OI features, typically
XV	AR, AD	*WNT1*	Oncogene INT1 (WNT1)	neurological defects (?); dominant mutations associated with early-onset osteoporosis
XVI	AR, AD	*CREB3L1*	Old Astrocyte Specifically-Induced Substance (OASIS)	clinical severity depends on zygosity: monoallelic variants cause mild OI (blue sclerae, fractures), while biallelic variants cause severe OI (*in utero* fractures, bone deformity)
XVII	AR	*SPARC*	Osteonectin (ON)	delayed onset of bone fragility and deformity
XVIII	XLR	*MBTPS2*	Site-2 Protease (S2P)	scoliosis; pectoral deformity
XIX (*suggested*)	AR	*MESDC2*	Mesoderm Development Gene (MESD)	severe, sometimes lethal, phenotype

AD, Autosomal Dominant; AR, Autosomal Recessive; XLR, X-Linked Recessive; HBM, High Bone Mass; ALP, Alkaline Phosphatase

*Genes associated with OI-related conditions – *LRP5* (Osteoporosis-Pseudoglioma Syndrome; OPPG), *PLOD2* (Bruck Syndrome), *P4HB* (Cole-Carpenter Syndrome/Unknown OI Type) and *SEC24D* (Cole-Carpenter Syndrome/Unknown OI Type) – are omitted here as they have not, up to this point, warranted numerical OI type designations.

(Adapted from Forlino *et al*. Lancet 2016)

REFERENCES

1. Sillence, D., Senn, A., and Danks, D. (1979). Genetic heterogeneity in osteogenesis imperfecta. J Med Genet, 101-116.
2. Martin, G., Lichtenstein, J., McKusick, V., Penttinen, R., Rowe, D., Pope, F., and Sussman, M. (1975). The molecular basis of certain inherited diseases of connective tissues involving collagen. Birth Defects Orig Artic Ser 11, 11-13.
3. Barsh, G., and Byers, P. (1981). Reduced secretion of structurally abnormal type I procollagen in a form of osteogenesis imperfecta. Proc Natl Acad Sci 78, 5142-5146.
4. Bonadio, J., and Byers, P. (1985). Subtle structural alterations in the chains of type I procollagen produce osteogenesis imperfecta type II. Nature 316, 363-366.
5. Marini, J.C., Forlino, A., Cabral, W.A., Barnes, A.M., San Antonio, J.D., Milgrom, S., Hyland, J.C., Korkko, J., Prockop, D.J., De Paepe, A., et al. (2007). Consortium for osteogenesis imperfecta mutations in the helical domain of type I collagen: regions rich in lethal mutations align with collagen binding sites for integrins and proteoglycans. Hum Mutat 28, 209-221.
6. Byers, P., and Pyott, S. (2012). Recessively inherited forms of osteogenesis imperfecta. Annu Rev Genet 46, 475-497.
7. Van der Slot, A., Zuurmond, A., Bardoel, A., Wijmenga, C., Pruijs, H., Sillence, D., Brinckmann, J., Abraham, D., Black, C., Verzijl, N., et al. (2003). Identification of PLOD2 as telopeptide lysyl hydroxylase, an important enzyme in fibrosis. J Biol Chem 278, 40967.
8. Van Dijk, F., Nesbitt, I., Nikkels, P., Dalton, A., Bongers, E., Van de Kamp, J., Hilhorst-Hofstee, Y., Den Hollander, N., Lachmeijer, A., Marcelis, C., et al. (2009). CRTAP mutations in lethal and severe osteogenesis imperfecta: the importance of combining biochemical and molecular genetic analysis. Eur J Hum Genet 17, 1560-1569.
9. Byers, P.H., and Pyott, S.M. (2012). Recessively inherited forms of osteogenesis imperfecta. Annu Rev Genet 46, 475-497.
10. Forlino, A., and Marini, J.C. (2016). Osteogenesis imperfecta. Lancet 387, 1657-1671.
11. Lapunzina, P., Aglan, M., Temtamy, S., Caparros-Martin, J.A., Valencia, M., Leton, R., Martinez-Glez, V., Elhossini, R., Amr, K., Vilaboa, N., et al. (2010). Identification of a frameshift mutation in osterix in a patient with recessive osteogenesis imperfecta. Am J Hum Genet 87, 110-114.
12. Nakashima, K., Zhou, X., Kunkel, G., Zhang, Z., Deng, J.M., Behringer, R.R., and de Crombrugghe, B. (2002). The novel zinc finger-containing transcription factor osterix is required for osteoblast differentiation and bone formation. Cell 108, 17-29.
13. Rivadeneira, F., Styrkarsdottir, U., Estrada, K., Halldorsson, B.V., Hsu, Y.H., Richards, J.B., Zillikens, M.C., Kavvoura, F.K., Amin, N., Aulchenko, Y.S., et al. (2009). Twenty bone-mineral-density loci identified by large-scale meta-analysis of genome-wide association studies. Nat Genet 41, 1199-1206.
14. Styrkarsdottir, U., Halldorsson, B.V., Gretarsdottir, S., Gudbjartsson, D.F., Walters, G.B., Ingvarsson, T., Jonsdottir, T., Saemundsdottir, J., Snorradottir, S., Center, J.R., et al. (2009). New sequence variants associated with bone mineral density. Nat Genet 41, 15-17.
15. Timpson, N.J., Tobias, J.H., Richards, J.B., Soranzo, N., Duncan, E.L., Sims, A.M., Whittaker, P., Kumanduri, V., Zhai, G., Glaser, B., et al. (2009). Common variants in the

region around Osterix are associated with bone mineral density and growth in childhood. Hum Mol Genet 18, 1510-1517.
16. Shaheen, R., Alazami, A.M., Alshammari, M.J., Faqeih, E., Alhashmi, N., Mousa, N., Alsinani, A., Ansari, S., Alzahrani, F., Al-Owain, M., et al. (2012). Study of autosomal recessive osteogenesis imperfecta in Arabia reveals a novel locus defined by TMEM38B mutation. J Med Genet 49, 630-635.
17. Volodarsky, M., Markus, B., Cohen, I., Staretz-Chacham, O., Flusser, H., Landau, D., Shelef, I., Langer, Y., and Birk, O.S. (2013). A deletion mutation in TMEM38B associated with autosomal recessive osteogenesis imperfecta. Hum Mutat 34, 582-586.
18. Rubinato, E., Morgan, A., D'Eustacchio, A., Pecile, V., Gortani, G., Gasparini, P., and Faletra, F. (2014). A novel deletion mutation involving TMEM38B in a patient with autosomal recessive osteogenesis imperfecta. Gene 545, 290-292.
19. Lv, F., Xu, X.J., Wang, J.Y., Liu, Y., Asan, Wang, J.W., Song, L.J., Song, Y.W., Jiang, Y., Wang, O., et al. (2016). Two novel mutations in TMEM38B result in rare autosomal recessive osteogenesis imperfecta. J Hum Genet 61, 539-545.
20. Cabral, W.A., Ishikawa, M., Garten, M., Makareeva, E.N., Sargent, B.M., Weis, M., Barnes, A.M., Webb, E.A., Shaw, N.J., Ala-Kokko, L., et al. (2016). Absence of the ER Cation Channel TMEM38B/TRIC-B Disrupts Intracellular Calcium Homeostasis and Dysregulates Collagen Synthesis in Recessive Osteogenesis Imperfecta. PLoS Genet 12, e1006156.
21. Yazawa, M., Ferrante, C., Feng, J., Mio, K., Ogura, T., Zhang, M., Lin, P.H., Pan, Z., Komazaki, S., Kato, K., et al. (2007). TRIC channels are essential for Ca2+ handling in intracellular stores. Nature 448, 78-82.
22. Yamazaki, D., Komazaki, S., Nakanishi, H., Mishima, A., Nishi, M., Yazawa, M., Yamazaki, T., Taguchi, R., and Takeshima, H. (2009). Essential role of the TRIC-B channel in Ca2+ handling of alveolar epithelial cells and in perinatal lung maturation. Development 136, 2355-2361.
23. Zayzafoon, M. (2006). Calcium/calmodulin signaling controls osteoblast growth and differentiation. J Cell Biochem 97, 56-70.
24. Zaidi, M., Adebanjo, O., Moonga, B., Sun, L., and Huang, L. (1999). Emerging insights into the role of calcium ions in osteoclast regulation. JBMR 14, 669-674.
25. Pyott, S., Tran, T., Leistritz, D., Pepin, M., Mendelsohn, N., Temme, R., Fernandez, B., Elsayed, S., Elsobky, E., Verma, I., et al. (2013). WNT1 mutations in families affected by moderately severe and progressive recessive osteogenesis imperfecta. Am J Hum Genet 92, 590-597.
26. Keupp, K., Beleggia, F., Kayserili, H., Barnes, A.M., Steiner, M., Semler, O., Fischer, B., Yigit, G., Janda, C.Y., Becker, J., et al. (2013). Mutations in WNT1 cause different forms of bone fragility. Am J Hum Genet 92, 565-574.
27. Fahiminiya, S., Majewski, J., Mort, J., Moffatt, P., Glorieux, F.H., and Rauch, F. (2013). Mutations in WNT1 are a cause of osteogenesis imperfecta. J Med Genet 50, 345-348.
28. McMahon, A., and Bradley, A. (1990). The Wnt1 (int-1) proto-oncogene is required for development of a large region of the mouse brain. Cell 62, 1073-1085.
29. Thomas, K., Musci, T., Neumann, P., and Capecchi, M. (1991). Swaying is a mutant allele of the proto-oncogene wnt-1. Cell 67, 969-976.

30. Laine, C.M., Joeng, K.S., Campeau, P.M., Kiviranta, R., Tarkkonen, K., Grover, M., and Makitie, O. (2013). WNT1 mutations in early-onset osteoporosis and osteogenesis imperfecta. NEJM 368, 1809-1816.
31. Joeng, K.S., Lee, Y.C., Lim, J., Chen, Y., Jiang, M.M., Munivez, E., Ambrose, C., and Lee, B.H. (2017). Osteocyte-specific WNT1 regulates osteoblast function during bone homeostasis. J Clin Invest 127, 2678-2688.
32. Kubota, T., Michigami, T., and Ozono, K. (2009). Wnt signaling in bone metabolism. J Bone Miner Metab 27, 265-271.
33. Gong, Y., Slee, R.B., Fukai, N., Rawadi, G., Roman-Roman, S., Reginato, A.M., Wang, H., Cundy, T., Glorieux, F.H., Lev, D., et al. (2001). LDL receptor-related protein 5 (LRP5) affects bone accrual and eye development. Cell 107, 513-523.
34. Boyden, L.M., Mao, J., Belsky, J., Mitzner, L., Farhi, A., Mitnick, M.A., Wu, D., Insogna, K., and Lifton, R.P. (2002). High bone density due to a mutation in LDL-receptor-related protein 5. NEJM 346, 1513-1521.
35. Little, R.D., Carulli, J.P., Del Mastro, R.G., Dupuis, J., Osborne, M., Folz, C., Manning, S.P., Swain, P.M., Zhao, S.C., Eustace, B., et al. (2002). A mutation in the LDL receptor-related protein 5 gene results in the autosomal dominant high-bone-mass trait. Am J Hum Genet 70, 11-19.
36. Van Wesenbeeck, L., Cleiren, E., Gram, J., Beals, R.K., Benichou, O., Scopelliti, D., Key, L., Renton, T., Bartels, C., Gong, Y., et al. (2003). Six novel missense mutations in the LDL receptor-related protein 5 (LRP5) gene in different conditions with an increased bone density. Am J Hum Genet 72, 763-771.
37. Symoens, S., Malfait, F., D'hondt, S., Callewaert, B., Dheedene, A., Steyaert, W., Bachinger, H., De Paepe, A., Kayserili, H., and Coucke, P. (2013). Deficiency for the ER-stress transducer OASIS causes severe recessive osteogenesis imperfecta in humans. Orphanet J Rare Dis 8, e154.
38. Murakami, T., Saito, A., Hino, S., Kondo, S., Kanemoto, S., Chihara, K., Sekiya, H., Tsumagari, K., Ochiai, K., Yoshinaga, K., et al. (2009). Signalling mediated by the endoplasmic reticulum stress transducer OASIS is involved in bone formation. Nat Cell Biol 11, 1205-1211.
39. Lindert, U., Cabral, W.A., Ausavarat, S., Tongkobpetch, S., Ludin, K., Barnes, A.M., Yeetong, P., Weis, M., Krabichler, B., Srichomthong, C., et al. (2016). MBTPS2 mutations cause defective regulated intramembrane proteolysis in X-linked osteogenesis imperfecta. Nat Commun 7, 11920.
40. Brown, M.S., Ye, J., Rawson, R.B., and Goldstein, J.L. (2000). Regulated Intramembrane Proteolysis. Cell 100, 391-398.
41. Rawson, R.B. (2013). The site-2 protease. Biochim Biophys Acta 1828, 2801-2807.
42. Keller, R.B., Tran, T.T., Pyott, S.M., Pepin, M.G., Savarirayan, R., McGillivray, G., Nickerson, D.A., Bamshad, M.J., and Byers, P.H. (2017). Monoallelic and biallelic CREB3L1 variant causes mild and severe osteogenesis imperfecta, respectively. Genet Med. Advance Online Publication: doi:10.1038/gim.2017.115.
43. Malhotra, V., and Erlmann, P. (2011). Protein export at the ER: loading big collagens into COPII carriers. EMBO J 30, 3475-3480.
44. Unlu, G., Levic, D., Melville, D., and Knapik, E. (2014). Trafficking mechanisms of extracellular matrix macromolecules: insights from vertebrate development and human diseases. Int J Biochem Cell Biol 47, 57-67.

45. Garcia, I.A., Torres Demichelis, V., Viale, D.L., Di Giusto, P., Ezhova, Y., Polishchuk, R.S., Sampieri, L., Martinez, H., Sztul, E., and Alvarez, C. (2017). CREB3L1-mediated functional and structural adaptation of the secretory pathway in hormone-stimulated thyroid cells. J Cell Sci 130, 4155-4167.
46. Cole, D., and Carpenter, T. (1987). Bone fragility, craniosynostosis, ocular proptosis, hydrocephalus, and distinctive facial features: a newly recognized type of osteogenesis imperfecta. J Pediatr 110, 76-80.
47. Garbes, L., Kim, K., Riess, A., Hoyer-Kuhn, H., Beleggia, F., Bevot, A., Kim, M.J., Huh, Y.H., Kweon, H.S., Savarirayan, R., et al. (2015). Mutations in SEC24D, encoding a component of the COPII machinery, cause a syndromic form of osteogenesis imperfecta. Am J Hum Genet 96, 432-439.
48. Mendoza-Londono, R., Fahiminiya, S., Majewski, J., Care4Rare Canada, C., Tetreault, M., Nadaf, J., Kannu, P., Sochett, E., Howard, A., Stimec, J., et al. (2015). Recessive osteogenesis imperfecta caused by missense mutations in SPARC. Am J Hum Genet 96, 979-985.
49. Rauch, F., Husseini, A., Roughley, P., Glorieux, F.H., and Moffatt, P. (2012). Lack of circulating pigment epithelium-derived factor is a marker of osteogenesis imperfecta type VI. J Clin Endocrinol Metab 97, e1550-1556.
50. Termine, J., Kleinman, H., Whitson, S., Conn, K., McGarvey, M., and Martin, G. (1981). Osteonectin, a bone-specific protein linking mineral to collagen. Cell 26, 99-105.
51. Sage, E., and Bornstein, P. (1991). Extracellular matrix proteins that modulate cell-matrix interactions. J Biol Chem 266, 14831-14834.
52. Delany, A., Amling, M., Priemel, M., Howe, C., Baron, R., and Canalis, E. (2000). Osteopenia and decreased bone formation in osteonectin-deficient mice. J Clin Invest 105, 915-923.
53. Martinek, N., Shahab, J., Sodek, J., and Ringuette, M. (2007). Is SPARC an evolutionarily conserved collagen chaperone? J Dent Res 86, 296-305.
54. Sasaki, T., Hohenester, E., Gohring, W., and Timpl, R. (1998). Crystal structure and mapping by site-directed mutagenesis of the collagen-binding epitope of an activated form of BM-40/SPARC/osteonectin. EMBO J 17, 1625-1634.
55. Marini, J.C., Forlino, A., Bachinger, H.P., Bishop, N.J., Byers, P.H., Paepe, A., Fassier, F., Fratzl-Zelman, N., Kozloff, K.M., Krakow, D., et al. (2017). Osteogenesis imperfecta. Nat Rev Dis Primers 3, 17052.
56. Grafe, I., Yang, T., Alexander, S., Homan, E.P., Lietman, C., Jiang, M.M., Bertin, T., Munivez, E., Chen, Y., Dawson, B., et al. (2014). Excessive transforming growth factor-beta signaling is a common mechanism in osteogenesis imperfecta. Nat Med 20, 670-675.
57. Li, Y., Lu, W., He, X., and Bu, G. (2006). Modulation of LRP6-mediated Wnt signaling by molecular chaperone Mesd. FEBS Lett 580, 5423-5428.
58. McClung, M.R., Grauer, A., Boonen, S., Bolognese, M.A., Brown, J.P., Diez-Perez, A., Langdahl, B.L., Reginster, J.Y., Zanchetta, J.R., Wasserman, S.M., et al. (2014). Romosozumab in postmenopausal women with low bone mineral density. N Engl J Med 370, 412-420.
59. Cosman, F., Crittenden, D.B., Adachi, J.D., Binkley, N., Czerwinski, E., Ferrari, S., Hofbauer, L.C., Lau, E., Lewiecki, E.M., Miyauchi, A., et al. (2016). Romosozumab Treatment in Postmenopausal Women with Osteoporosis. N Engl J Med 375, 1532-1543.

60. Wang, Q., and Marini, J.C. (1996). Antisense oligodeoxynucleotides selectively suppress expression of the mutant alpha 2(I) collagen allele in type IV osteogenesis imperfecta fibroblasts. A molecular approach to therapeutics of dominant negative disorders. J Clin Invest 97, 448-454.
61. Millington-Ward, S., McMahon, H.P., Allen, D., Tuohy, G., Kiang, A.S., Palfi, A., Kenna, P.F., Humphries, P., and Farrar, G.J. (2004). RNAi of COL1A1 in mesenchymal progenitor cells. Eur J Hum Genet 12, 864-866.
62. Bonadio, J., Holbrook, K.A., Gelinas, R.E., Jacob, J., and Byers, P.H. (1985). Altered triple helical structure of type I procollagen in lethal perinatal osteogenesis imperfecta. J Biol Chem 260, 1734-1742.

Chapter 2: Monoallelic & Biallelic *CREB3L1* Variant Causes Mild And Severe Osteogenesis Imperfecta, Respectively†

INTRODUCTION

Osteogenesis imperfecta (OI [MIM: 166200, 166210, 259420, 166220]), is a genetically and phenotypically heterogeneous disorder characterized by brittle bones and variable bone deformity.[1] Severity ranges from intrauterine fractures and significantly shortened long bones with perinatal lethality to few fractures with normal stature and life expectancy.[1] Extraskeletal features may include blue sclerae, dentinogenesis imperfecta, adult-onset hearing loss, joint hypermobility, and hyperlaxity of skin.[1] In the majority (>90%) of affected individuals, mutations in *COL1A1* [MIM: 120150] and *COL1A2* [MIM: 120160], which encode the proα1(I) and proα2(I) chains of mature type I procollagen, respectively, account for the phenotype.[2] Genes involved in collagen processing (*CRTAP* [MIM: 605497], *P3H1* [MIM: 610339], *PPIB* [MIM: 123841], *FKBP10* [MIM: 607063], *SERPINH1* [MIM: 600943], *BMP1* [MIM: 112264], *PLOD2* [MIM: 601865]), bone cell differentiation and signaling (*SP7* [MIM: 606633], *WNT1* [MIM: 164820]), bone cell association with extracellular matrix (*SPARC* [MIM: 182120]), and matrix mineralization (*SERPINF1* [MIM: 172860], *TMEM38B* [MIM: 611236]) have been implicated in rarer forms of recessively-inherited disease.[2,3] Additionally, mutations in *IFITM5* [MIM: 614757], through mechanisms that are not fully understood, cause autosomal dominant forms of OI with unique features, e.g. hyperplastic callus formation [MIM: 610967].[4,5] Recently, an X-linked form of OI caused by mutations in *MBTPS2* [MIM: 300294] was reported.[6]

† Keller, R.B., Tran, T.T., Pyott, S.M., Pepin, M.G., Savarirayan, R., McGillivray, G., Nickerson, D.A., Bamshad, M.J., and Byers, P.H. (2017). Monoallelic and biallelic CREB3L1 variant causes mild and severe osteogenesis imperfecta, respectively. Genet Med. Advance Online Publication: doi:10.1038/gim.2017.115

Even with this expanded catalog of OI disease genes, the underlying cause of OI in a subset of families has still not been identified. From exome sequence analysis of members of a consanguineous family of Lebanese descent (Figure 2-1A), we identified a trinucleotide deletion in Cyclic AMP Responsive Element Binding Protein 3-Like 1 (*CREB3L1*) [MIM: 616215] that corresponds to an in-frame single amino acid deletion in Old Astrocyte Specifically-Induced Substance (OASIS), and results in a mild OI phenotype in heterozygotes and a lethal phenotype in homozygotes. Previously, homozygosity for whole gene deletion of *CREB3L1* was shown to result in lethal OI [MIM: 616229] in a Turkish family.[7] Our study confirms that mutations in *CREB3L1* result in an OI phenotype wherein disease severity is determined by whether mutations are monoallelic or biallelic, and identifies a potential mechanism of action.

MATERIALS & METHODS

Exome & Confirmatory Sequencing: Written informed consent was obtained for all individuals in the study. Exome sequencing was performed by the University Of Washington Center For Mendelian Genomics as previously described.[8] Variants were sorted as described in the text. The variant in *CREB3L1* was confirmed with Sanger sequencing. Primers for amplification of exon 7 are listed in Supplementary Table 2-1 (Integrated DNA Technologies, Coralville, IA, USA). Exon 7 was amplified using AmpliTaq Gold Polymerase (Applied Biosystems, Foster City, CA, USA). The program used for cycling was: 95°C for 12 minutes, 95°C for 10 seconds, 61°C for 40 seconds, 72°C for 50 seconds for 35 cycles, then, 72°C for 7 minutes. Amplicons were treated with ExoSAP according to a standard protocol. Sequencing reactions were set up using Big Dye v3.1 (Applied Biosystems, Foster City, CA, USA) with the following program: 96°C for 10 seconds, 50°C for 5 seconds, 60°C for 4 minutes for 40 cycles.

Sequencing was run on an ABI 3730. Sequences were analyzed using Mutation Surveyor v4.0.9 software (Softgenetics, State College, PA, USA).

Collagen Analysis: Culture of skin fibroblasts and analysis of procollagens was performed as previously described.[9]

In Vitro Transcription/Translation (IVT) & Western Blot: IVT was performed using the 1-Step Human Coupled IVT Kit – DNA (ThermoFisher Scientific, Waltham, MA, USA). Templates for IVT were generated using a PCR-based method (ThermoScientific Tech Tip #72 PCR Protocol For Generating Optimized Templates For Pierce Human *In Vitro* Expression Kits).[10] WT and VT312 full-length *CREB3L1* cDNA sequences were amplified from plasmids "WT312" and "VT312", generated for overexpression experiments in mammalian cell lines (see "Over-Expression Plasmids" below). Primers for creation of IVT templates are listed in Supplementary Table 2-1 (Integrated DNA Technologies, Coralville, IA, USA). IVT reactions were assembled according to kit instructions and incubated for 6 hours at 30°C. 1µl of each IVT reaction was run on 10% sodium dodecyl sulfate-polyacrylamide gel. IVT with no DNA input or with a construct bearing GFP DNA (pCFE-GFP; ThermoFisher Scientific, Waltham, MA, USA) were included as (–) and (+) controls, respectively, for IVT. Detection by Western blot was performed with the following primary antibodies: OASIS (sc-514635; Santa Cruz Biotechnology, Santa Cruz, CA, USA) at 1:1000 and TurboGFP (PA5-22688; ThermoFisher Scientific, Waltham, MA, USA) at 1:10,000. Secondary antibodies used were: Goat Anti-Mouse Secondary IgG (TA130004; OriGene, Rockville, MD, USA) and Goat Anti-Rabbit IgG H&L (ab6721; Abcam, Cambridge, MA, USA), both at 1:20,000. Detection was achieved using Amersham ECL Western Blotting Detection Reagent (GE Healthcare, Pittsburgh, PA, USA).

Electrophoretic Mobility Shift Assay (EMSA): EMSA was performed using the Gel Shift Assay Core System (Promega, Madison, WI, USA). WT and VT312 IVT OASIS proteins were incubated with a 40bp fragment of the human *COL1A1* promoter that was synthesized as a duplex oligonucleotide (Integrated DNA Technologies, Coralville, IA, USA). Oligonucleotide sequences are listed in Supplementary Table 2-1. The oligonucleotides were labeled with γ^{32}P ATP (Perkin Elmer, Waltham, MA, USA) using T4 polynucleotide kinase. Unincorporated label was removed using Micro Bio Spin P-30 Gel Columns (BIORAD, Redmond, WA, USA). Protein and labeled oligonucleotide (and in the case of competition samples, unlabeled oligonucleotide) were incubated together at 4°C for 1 hour. Samples were run on a 6% non-denaturing polyacrylamide gel. Gel was dried for 4 hours at 72°C and exposed to film overnight.

Over-Expression (OE): A human cDNA ORF clone with *CREB3L1* placed under a CMV promoter (RC204968) was purchased from OriGene (Rockville, MD, USA) along with an empty pCMV6-Entry vector (PS100001) as a transfection control. The *CREB3L1* expression construct is referred to herein as "WT312". The family deletion (VT312) was introduced using the QuickChange II Site-Directed Mutagenesis Kit to create "VT312". Primers for site-directed mutagenesis were purchased as PAGE-purified primers and are listed in Supplementary Table 2-1 (Integrated DNA Technologies, Coralville, IA, USA). Constructs were transiently transfected into HEK293 using XtremeGene 9 Transfection Reagent (Roche, USA) at a 3:1 (μl reagent: μg plasmid) ratio and incubated for 48 hours before harvest. For the dimerization experiment, WT312 and VT312 were transfected at the indicated ratios equaling 1μg total of plasmid (3:1 =

0.75µg WT312 + 0.25µg VT312; 1:1 = 0.5µg WT312 + 0.5µg VT312, 1:3 = 0.25µg WT312 + 0.75µg VT312).

RT-qPCR: Total RNA was isolated from cells using the RNeasy Mini Kit (Qiagen, Valencia, CA, USA). First-strand cDNA snythesis of 1µg of DNAseI-treated RNA was performed using iScript Reverse Transcription Supermix (BIORAD, Hercules, CA, USA) in 20µl reactions. One µl of cDNA was used for RT-qPCR in 20µl reactions using iTaq Universal SYBRGreen Supermix (BIORAD, Hercules, CA, USA). Samples were run on a CFX96 Touch (BIORAD, Hercules, CA, USA) using the following program: 95°C for 30 seconds, 95°C for 5 seconds, 60°C for 30 seconds for 40 cycles. Each sample was run in triplicate and the mean Ct values were analyzed using the 2^-[delta][delta]Ct method.[11] Expression was normalized to the reference gene GAPDH. Primers for RT-qPCR are listed in Supplementary Table 2-1 (Integrated DNA Technologies, Coralville, IA, USA).

Immunoblotting: Protein lysates were prepared from transfected cells using a buffer containing 0.05 M Tris-HCl at pH 8.0, 0.15 M NaCl, 5.0 mM EDTA, 1% NP-40 and a protease inhibitor cocktail at 4°C. 50µg of lysate was loaded in each lane on a 10% sodium dodecyl sulfate-polyacrylamide gel in loading buffer containing 7.7mg/ml dithiothreitol (DTT). Detection for Western blot was performed with primary antibodies to SEC24D (ab191566; Abcam, Cambridge, MA, USA) at 1:2000, SEC23A (ab179811; Abcam, Cambridge, MA, USA) at 1:100, OASIS (ab33051; Abcam, Cambridge, MA, USA) at 1:1000, and GAPDH (ab37168; Abcam, Cambridge, MA, USA) at 1:2000. The secondary antibodies Goat Anti-Rabbit IgG H&L (ab6721; Abcam, Cambridge, MA, USA) and Goat Anti-Mouse Secondary IgG (TA130004; OriGene, Rockville, MD, USA) were used at a 1:2,000 dilution. Detection was achieved using

Amersham ECL Western Blotting Detection Reagent (GE Healthcare, Pittsburgh, PA, USA). Quantitation of blot signals was achieved using ImageJ.[12] Adjusted signal intensities were obtained by normalizing to GAPDH signal to control for loading differences between lanes.

Statistical Analysis: Statistical analysis was performed using GraphPad Prism 7.0a software (GraphPad, San Diego, CA, USA). The RT-qPCR data are expressed as the mean +/- S.D. from three independent experiments. Statistical significance was determined by running analysis of variance (ANOVA) and the indicated tests for Multiple Comparisons (see figure legends).

RESULTS

Case Report

The proband (VI-7, Figure 2-1) was identified on ultrasound at 12 weeks gestation due to shortened and angulated humeri, multiple fractures of the long bones of both legs, and apparently reduced skull mineralization. Spine and ribs appeared normal. Imaging at 14 weeks confirmed micromelia and angulated long bones. The ribs were normal length, but appeared angulated, consistent with fractures. Hypomineralization of the skull was not convincing at this time. At 16 weeks, the pregnancy was terminated due to suspected OI. Molecular genetic analysis of DNA extracted from skin fibroblasts excluded mutations in all genes known at the time to cause OI. Biochemical analysis of cultured fibroblasts from VI-7 demonstrated normal amounts and mobility of type I collagen and procollagen chains in contrast to altered electrophoresis due to overmodification of type I collagen chains from a typical OI type II patient with a heterozygous *COL1A1* mutation that resulted in substitution of a triple helical glycine (p.Gly818Cys) (Figure

2-1B).

Two prior pregnancies had been terminated because of *in utero* findings consistent with severe skeletal dysplasia. The first of these pregnancies (VI-3) (Figure 2-1C) was terminated at 18 weeks. Radiographs showed severe long bone deformity with crumpling, angulation, and marked rhizomelic and mesomelic shortening. The ribs were fractured, but not beaded in appearance. The calvarial bones were paper thin and soft. There was almost no ossification of the cranial vault and severe demineralization was noted. There were no wormian bones identified. Detailed clinical information on the second of the previous affected pregnancies (VI-6) was not available. An earlier pregnancy (VI-2) was lost to fetal demise at 27 weeks. The cause was unclear, but fetal lungs showed pulmonary hypoplasia.

Three individuals in the family appeared to be mildly affected and exhibited some OI-like features. The proband's brother (VI-4) (Figure 2-1D) had a fractured right femur at birth with acute angulation in the midshaft. Otherwise, long bones, ribs, and thorax were normal in length and shape. He did not have wormian bones. He was treated for Vitamin D deficiency postnatally (levels were 22nmol/L; lower limit of the normal range is 50nmol/L), as was his mother. X-ray of the pelvis at six weeks of age showed osteopenia. At 15 years of age, he had blue sclerae and osteopenia, but no additional fractures. The affected sister (VI-5) had blue sclerae and mild osteopenia, which was diagnosed at 2 years of age on x-ray of the knee when the long bones were also noted to be gracile, but she has no history of fractures. The mother (V-4) had blue sclerae and had recurrent fractures in childhood, including a fractured pelvis with minimal trauma at age 1 and a spiral fracture of one femur at age 16. Her father, too, (IV-1) had recurrent

fractures. A great grandfather of the proband (III-4) and a maternal granduncle (IV-5) reportedly had fractures and may also be mildly affected (Supplementary Figure 2-1). The family members in generation IV were not available for clinical assessment.

Variant Identification

Exome sequence analysis was performed on samples from seven family members: V-3, V-4, VI-1, VI-4, VI-5, VI-7, and VI-8. We identified 56,634 variants that differed from the consensus genomic sequence (GRCh37/hg19) among the seven individuals. We removed variants in intergenic and intronic regions, variants found in dbSNP, and variants found more than 10 times in the Exome Sequencing Project Exome Variant Server (EVS). This reduced the list to 4254 variants. Variants shared by affected members of the family and the unaffected siblings were discarded, leaving 659 variants. We then looked for changes that were homozygous in the proband (72 variants), but that were heterozygous in the mildly affected siblings. This left six genes as candidates: *CREB3L1*, *FADS2*, *UQCC3*, *CTSF, MMP17* and *C11orf49* (Table 2-1). We found a 3bp in-frame deletion (c.934_936delAAG [p.Lys312del]) in exon 7 of the *CREB3L1* gene that segregated with the phenotypes in the family (Figure 2-1A). While the proband (VI-7) is homozygous for the deletion, all mildly affected individuals (V-4, VI-4, VI-5) are heterozygous for the change. The two healthy siblings (VI-1, VI-8) are homozygous for the normal allele. The father (V-3), who is reportedly unaffected, is also heterozygous. Either his phenotype is so mild it has not come to clinical attention or the mutation is not penetrant in him. He declined multiple offers of clinical assessment. The lysine residue that is lost is highly conserved (GERP[13]=4.69; PhastCons[14]=1) (Figure 2-2).

Expression of *CREB3L1* has been described in a select few cell types thus far, including in osteoblasts.[15-18] The protein product of *CREB3L1*, OASIS, is synthesized as an endoplasmic reticulum (ER) transmembrane protein with the NH_2-terminal end (residues 1-374) in the cytoplasmic compartment. The NH_2-terminal end contains a basic leucine zipper (bZIP) domain and an overlapping nuclear localization signal. The COOH-terminal end (residues 394-519) is resident in the ER (Figure 2-2).[15] Upon detection of ER stress, proteolytic cleavage releases the NH_2-terminal fragment. This fragment is transported to the nucleus where it functions as a transcription factor.[15] Target genes of OASIS vary among cell types.[15-18] Knockout of *Creb3l1* in mice results in growth retardation and fractures. Micro-computed tomography (μCT) of these mice revealed low bone mineral density in femoral trabecular bone. By this and additional bone metrics, Murakami *et al*. concluded that *Creb3l1*$^{-\backslash-}$ mice suffer from severe osteopenia.[16] Based on the mouse study, on the previous report of lethal OI caused by *CREB3L1* deletion[7], and on the genetics of the family described here, the variant identified in *CREB3L1* was thought to be the cause of both mild and severe forms of OI.

Based on the literature, the remaining five genes – *FADS2* [MIM: 606149], *UQCC3* [MIM: 616097], *CTSF* [MIM: 603539], *MMP17* [MIM: 602285], and C11orf49 – were no longer reasonable candidates. *FADS2* encodes Delta-6 Desaturase (D6D). D6D is involved in the synthesis of long-chain polyunsaturated fatty acids. Single nucleotide polymorphisms in D6D and other fatty acid desaturases have been associated with a heightened risk of cardiovascular disease, including coronary artery disease and ischemic stroke.[19] UQCC3 (Ubiquinol-Cytochrome C Reductase Complex Assembly Factor 3) is required for Complex III assembly. Mutations in *UQCC3* cause Mitochondrial Complex III Deficiency, Nuclear Type 9.[20] *CTSF*

encodes Cathepsin F, a lysosomal degradation enzyme implicated in Type B Kufs disease, a neuronal ceroid-lipofuscinosis.[21] *MMP17* encodes Matrix Metalloproteinase 17, an enzyme that is able to cleave extracellular matrix components. Variants in *MMP17* are thought to predispose to aortic aneurysm[22] and *MMP17* is expressed in some cancers.[23,24] *C11orf49* encodes a protein of unknown function.

Effect Of The Variant On OASIS Function

Fibroblasts from the proband (VI-7) were available, but *CREB3L1* is expressed at such low levels in skin[15,16] that we could not examine the altered function of the protein in those cells. To study the effect of the variant, we performed *in vitro* transcription/translation of wild type (WT) and variant (VT312) *CREB3L1* sequences. With IVT, VT312 *CREB3L1* was expressed and produced a stable, full-length (~80kDa) OASIS protein (Figure 2-3A). The deletion is located within both a predicted bipartite nuclear localization signal (NLS) (RVRRKIKNKISAQESRRKK**K**EY)[25] and a DNA-binding motif (RRKK**K**EY) shared among CREB/ATF family members[26] (Figure 2-2). Disruption of either of these domains could prevent OASIS from transducing its targets due to, respectively, failure of the active NH_2-terminal fragment to reach the nucleus or by interfering with DNA-binding to gene regulatory elements.

To determine if DNA-binding was affected by the deletion, we performed an electrophoretic mobility shift assay (EMSA) to assess binding of OASIS to an Unfolded Protein Response Element (UPRE)-like sequence (CGACGTGG) in the *COL1A1* promoter to which OASIS was previously shown to bind.[16] While the WT OASIS protein bound the UPRE-like sequence, demonstrated by a band shift, no shift was detected after incubation with the VT312 protein,

indicating that the variant protein did not bind to DNA (Figure 2-3B). On this basis, we concluded that the mutation is pathogenic.

We attempted ICC in transfected cells treated with ER-stress inducing drugs (e.g., tunicamycin) to look at the effect of the variant on the subcellular localization of OASIS, however, we were unable to obtain reliable staining (data not shown). As the EMSA shows that the DNA-binding ability of VT312 OASIS is eliminated, we decided determination of the effect of the mutation on localization was unnecessary. Whether VT312 OASIS can reach its nuclear targets or not, it cannot bind them.

OASIS Is A Regulator Of Cellular Secretion

Another CREB/ATF family member with high sequence similarity to OASIS, BBF2H7 (BBF2 Human Homolog On Chromosome 7, encoded by *CREB3L2* [MIM: 608834]), was found to regulate expression of *SEC23A* (SEC23 Homolog A) [MIM: 610511], a component of the inner wall of the coat protein II (COPII) complex.[27] COPII carriers are involved in the trafficking of secreted proteins from the rER to the Golgi.[28] To assess whether OASIS also regulates *SEC23A*, we overexpressed WT and VT312 OASIS separately in HEK293 cells (Supplementary Figure 2-2) and looked for an effect on *SEC23A* expression. Though the data showed a slight increase in expression of *SEC23A* in the presence of VT312 OASIS ($P = 0.03$), there was no significant difference in *SEC23A* mRNA levels between WT overexpression and the empty vector control, nor between WT and VT312 overexpression. We concluded that expression of *SEC23A* was not affected (Figure 2-4A), consistent with the previously published finding that OASIS could not rescue *Sec23a* expression in Bbf2h7$^{-/-}$ chondrocytes.[27]

However, mRNA levels of another COPII component, *SEC24D* [MIM: 607186], were significantly upregulated in the presence of functional OASIS protein (P = 0.007 versus empty vector; P = 0.009 versus VT312), but not when the Lys312del protein variant was present (Figure 2-4B). Immunoblotting of whole cell lysates from transfected cells was consistent with the expression studies (Figure 2-4C). More SEC24D protein was seen in cells overexpressing WT OASIS than in those expressing the nonfunctional VT312 OASIS or in the empty vector control (Figure 2-4C & D), while SEC23A protein levels were unchanged with OASIS overexpression (Figure 2-4C & E). Without sufficient *SEC24D* expression, we suspect COPII formation is disrupted and osteoblasts cannot efficiently secrete type I collagen and other bone matrix proteins. While we did not see abnormal retention of type I procollagen or type I collagen alpha chains in proband (VI-7) fibroblasts (Figure 2-1D), we would not expect to see evidence of defective secretion in the collagen analysis we performed, as *CREB3L1* is not expressed in skin.

OASIS Transcriptional Target Specificity

The binding ability of many bZIP transcription factors is determined by the formation of homo- and/or heterodimers. It has been proposed that switching out the binding partners in these dimers could alter specificity.[29] This could help explain the variability of OASIS target genes in different cell types in which expression has been reported. To examine whether OASIS forms homodimers to promote expression of *SEC24D*, we overexpressed WT and VT312 OASIS simultaneously at varying ratios (WT:VT312 ratios of 3:1, 1:1, 1:3) with the expectation that, if OASIS formed homodimers, the increasing presence of variant, nonfunctional OASIS protein would result in the abrogation of target gene expression. The presence of any WT OASIS altered *SEC24D* expression significantly over both empty vector control and VT312 overexpression

alone, but there were no significant differences in *SEC24D* expression levels among cells transfected with the vectors at different ratios (Supplementary Figure 2-3). This suggested that if OASIS forms dimers, it partners with other proteins and not itself.

DISCUSSION

This is the second report of a family with OI-like phenotypes caused by variants in *CREB3L1* and confirms *CREB3L1* as an OI disease gene.[7] Clues to the mechanisms by which alteration of OASIS function might result in OI come from looking at a closely related gene, *CREB3L2*. Knockout of *Creb3l2* in mice resulted in severe chondrodysplasia due to failure to secrete type II procollagen with the resultant disruption of hypertrophic zone formation in cartilage tissue. Type II collagen and other cartilage matrix proteins accumulated in the rER lumen of *Creb3l2*$^{-/-}$ chondrocytes.[27] The protein product of *Creb3l2*, Bbf2h7, promotes transcription of *Sec23a,* which encodes a component of the COPII complex.[27] In human dermal fibroblasts, *CREB3L2* knockdown suppressed *SEC23A* expression and caused Golgi dysmorphology (irregularly-curved cisternae and aggregation), indicative of problems with subcellular trafficking.[30] Molecular and cellular analysis of *Creb3l1*$^{-\backslash-}$ mice revealed similar cellular and tissue phenotypes, but in bone tissue, rather than in cartilage. *Creb3l1*$^{-\backslash-}$ primary osteoblasts had distended rERs full of bone matrix proteins (type I procollagen and osteocalcin) and there was significantly reduced collagen content in the bone matrix, leading to severe osteopenia and fractures.[16] Because BBF2H7 is important for COPII formation and for secretion of type II collagen and other cartilage matrix proteins from chondrocytes during chondrogenesis, we proposed that OASIS has an analogous role in the secretion of type I collagen and other bone matrix proteins from osteoblasts during osteogenesis.

COPII complexes are involved in the trafficking of secreted proteins from the rER to the Golgi and are specifically involved in rER export.[28] Carrier structure consists of an inner coat formed by SEC23 and SEC24 proteins and an outer coat consisting of SEC13 and SEC31 proteins[31], which are thought to confer stability.[32] Vesicle formation is aided by SAR1, SEC12, and SEC16.[31] Shuttling of large proteins, such as procollagen, requires the creation of extra-large COPII carriers.[31] Auxiliary proteins TANGO1 (Transport And Golgi Organization 1) and cTAGE5 (Cutaneous T-cell-Lymphoma-Associated 5) are found at rER exit sites and help with loading of large COPII.[31] They bind SEC23 and SEC24 proteins in the inner coat on the cytoplasmic side of the rER membrane and procollagens on the luminal side, both guiding procollagens into the forming vesicle and inhibiting association of the outer coat with the inner coat (Supplementary Figure 2-4). This latter action delays vesicle fission, giving sufficient time for a larger vesicle to form.[31] Sedlin, another helper protein, is recruited by TANGO1 and is thought to stabilize the inner coat and prevent premature membrane constrictions.[31] The absence of COPII structural or helper proteins could result in the creation of hypoplastic carriers and the cell may be unable to secrete large proteins efficiently. We have shown that OASIS regulates the expression of the COPII component *SEC24D*.

The importance of secretory pathways in osteogenesis is already appreciated. Recessive mutations in *SEC24D* itself cause a syndromic form of OI with features that resemble Cole Carpenter Syndrome [MIM: 616294] (skull ossification defects, fractures).[33] It is possible OASIS lies upstream of additional components of the COPII complex and plays a larger role in construction of these carriers. We hypothesize that OASIS-mediated secretory pathways, specifically the OASIS-SEC24D interaction, are necessary for normal bone development.

Furthermore, a recent report identified an X-linked form of OI associated with mutations in Membrane-Bound Transcription Factor Peptidase, Site 2 (*MBTPS2)* [MIM: 300294], which encodes Site-2 Metalloprotease (S2P).[6] S2P is a serine protease that cleaves OASIS in response to the sensing of ER stress, and thereby regulates OASIS activity.[34,35] Taken together, the discovery of these novel disease genes demonstrates the critical contributions of secretory pathways to bone development and bone homeostasis (Supplementary Figure 2-4) and should give direction to continued efforts to identify the genetic causes of OI and other bone dysplasias.

Notably, expression of OASIS has also been reported in astrocytes[26], pancreatic β-cells[17] and goblet cells.[18] Along with physiological ER stress pathways that involve OASIS (as others have hypothesized)[16,29], secretory pathways involving OASIS may be unique to "professional" secretory cell types in which the demand for protein production is especially high[36] and may be cytoprotective. Given the suspected importance of OASIS for these tissues, it is notable that none of the individuals in the family appear to have neural, pancreatic, or intestinal abnormalities. Heterozygosity for the deletion may be insufficient to cause significant abnormalities in these tissues, unlike in bone. It is possible evidence of such abnormalities would be found in homozygous individuals if they survived longer. Future studies will further elucidate the importance of OASIS for the development of bone and other tissue types.

FIGURES & TABLES

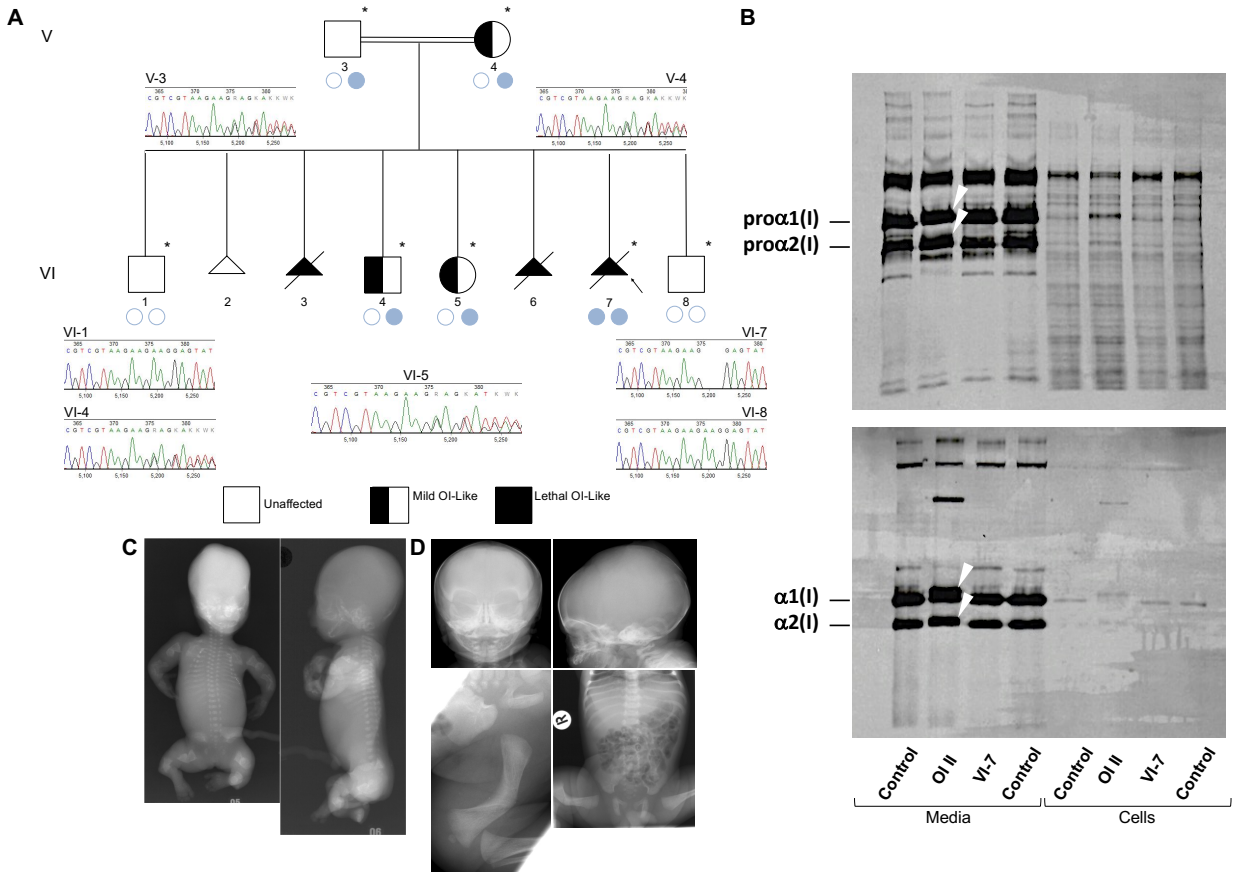

Figure 2-1. Homozygosity And Heterozygosity For A 3bp Deletion In *CREB3L1*. A) Pedigree of the family with *CREB3L1*-associated OI. Arrow indicates the proband. Asterisks denote the family members whose exomes were sequenced. Circles below denote alleles (empty – normal; **filled** – variant) and chromatograms from Sanger sequencing confirming the variants (c.934_936delAAG [p.Lys312del]) are shown. B) Effect of the *CREB3L1* variant on type I collagen biochemistry. Collagen alpha chains synthesized by skin fibroblasts from the proband (VI-7) are structurally equivalent to those from control fibroblasts, in contrast to those from a typical OI type II patient (OI II) with a *COL1A1* glycine substitution (p.Gly818Cys), in which overmodification results in both delayed procollagen chain mobility (upper panel) (arrows) and delayed α1(I) and α2(I) chain mobility when procollagens are digested with pepsin (lower panel) (arrows). We do not see abnormal retention of procollagen nor of collagen alpha chains in the proband fibroblasts; as skin fibroblasts do not express *CREB3L1*, we would not expect OASIS to have a role in regulating secretion in these particular cells. C) Anterior-posterior (left) and lateral (right) radiographs from VI-3 (suspected to have been homozygous for the 3bp deletion in *CREB3L1*) following 18 weeks gestation termination. There is virtually no calvarial mineralization. Bones in all visible extremities are telescoped and very irregular. The ribs are thin and wavy and there is mild platyspondyly. D) Radiographs of VI-4 (heterozygous for the 3bp deletion in *CREB3L1*) at birth. The calvarium is thin and the anterior and posterior fontanelles are large, but there are no wormian bones. The ribs are thin and there is mild platyspondyly. There is marked bowing of the right femur.

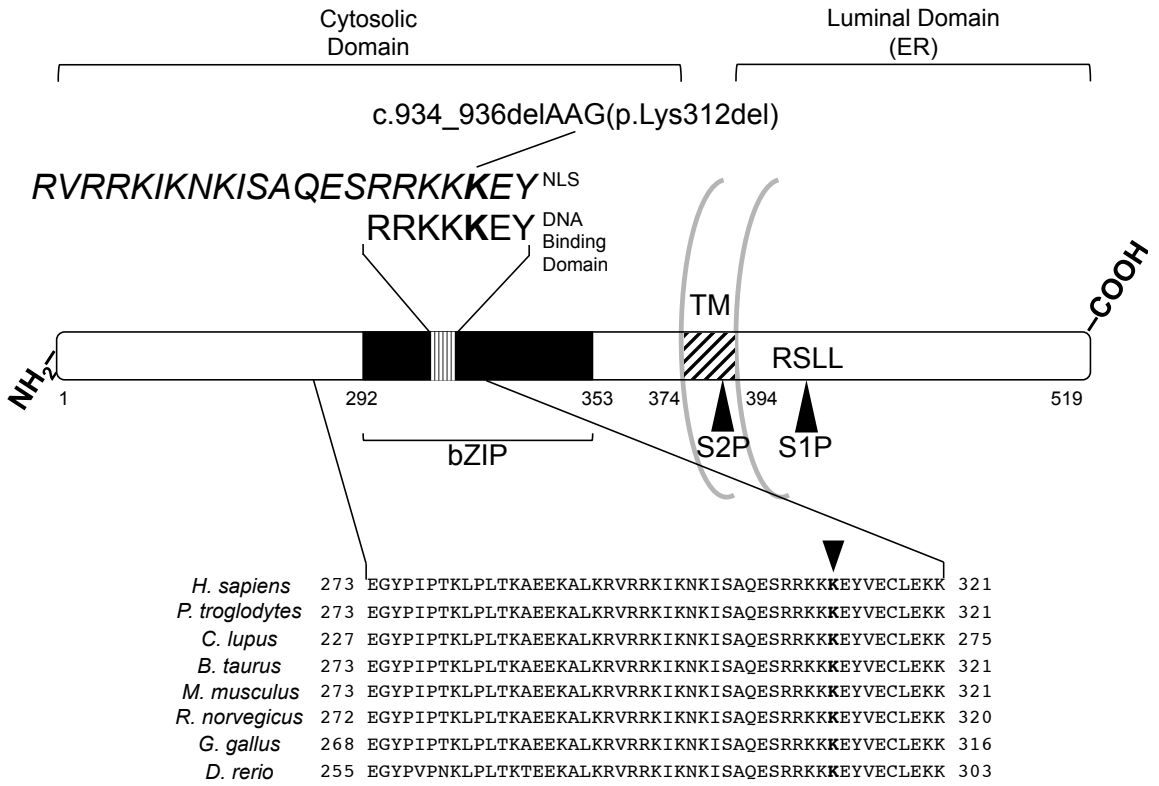

Figure 2-2. Old Astrocyte Specifically-Induced Substance (OASIS). OASIS is a 519aa protein with a basic leucine zipper (bZIP) domain common to other CREB/ATF family members and a transmembrane domain (TM) that anchors it in the ER membrane. When ER stress challenges the cell, the full-length OASIS protein is freed from the ER membrane and is activated upon sequential cleavage by S1P and S2P at the indicated sites. The conserved DNA binding domain is shown, with the deleted lysine residue in **bold**. *Italics* above show an overlapping predicted bipartite nuclear localization sequence (NLS). The deleted lysine residue is conserved in vertebrates (GERP=4.69; PhastCons=1).

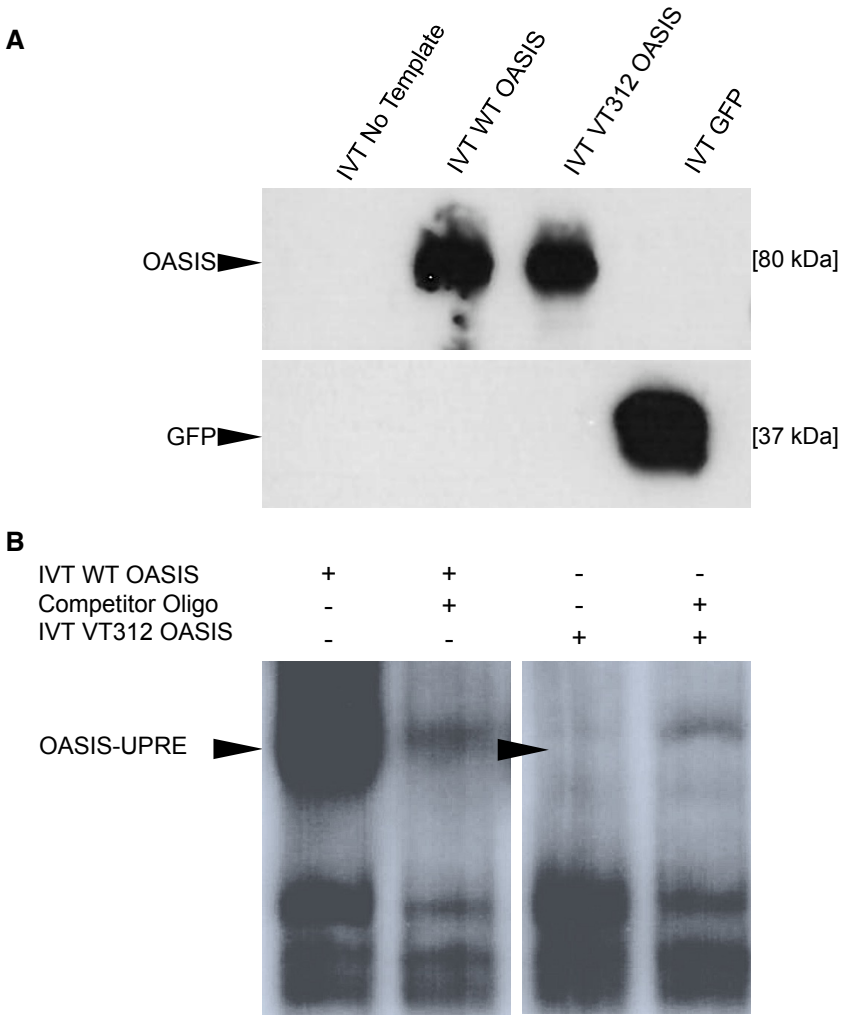

Figure 2-3. Effect Of The Variant On OASIS Function. A) The variant OASIS protein (VT312) is stably expressed and does not appear truncated compared to wild type (WT) protein. IVT with no DNA input or with a construct bearing GFP DNA were included as (–) and (+) controls, respectively. IVT. B) The family variant causes a defect in DNA binding. A shift is seen when IVT WT OASIS is incubated with the radiolabeled oligo containing a UPRE-like sequence (lane 1). This shift is competed away when unlabeled oligo is added (lane 2). The shift is absent when radiolabeled oligo is incubated with IVT VT312 OASIS (lane 3). Background bands are likely binding interactions between labeled oligo and proteins from the HeLa lysate used to perform IVT. EMSA.

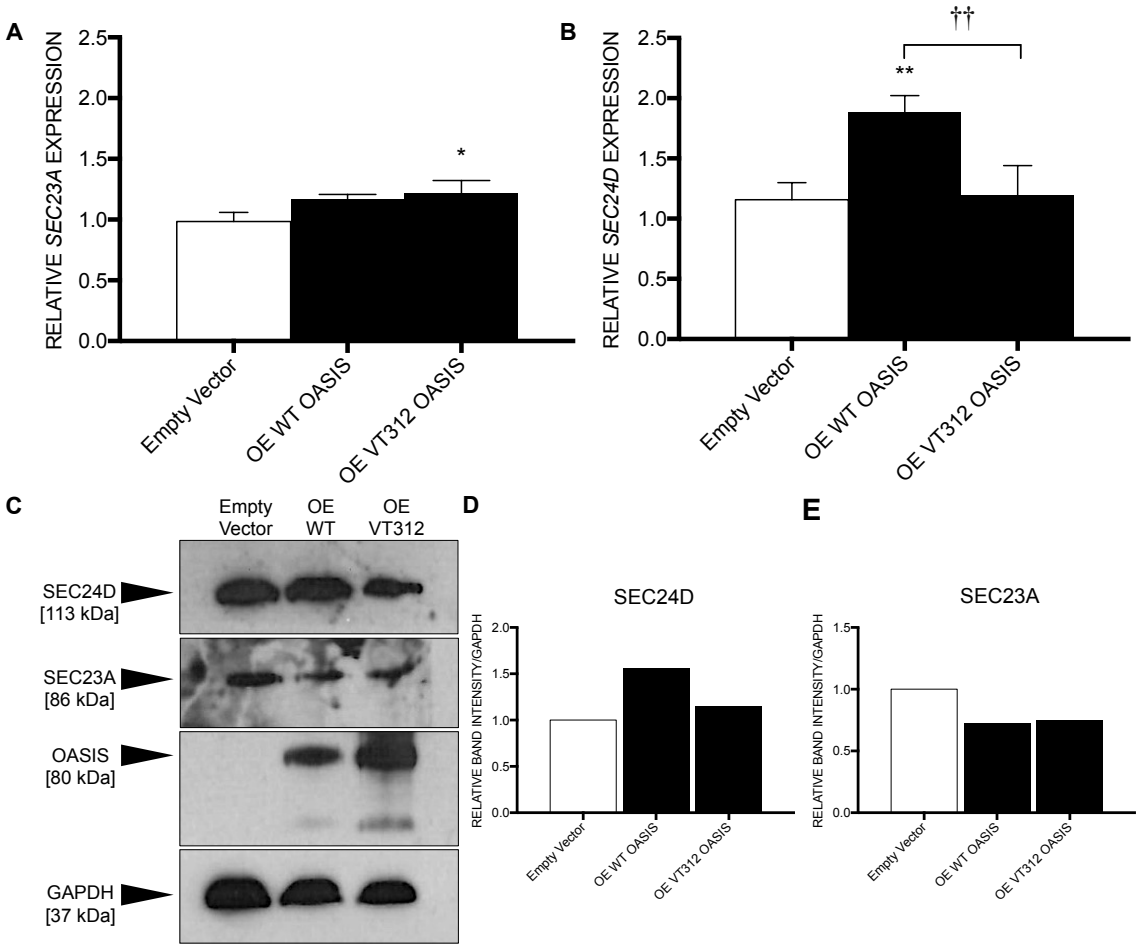

Figure 2-4. OASIS Regulates Expression Of *SEC24D*, But Not *SEC23A*. A) *SEC23A*, which encodes a component of the COPII complex, is not significantly upregulated in the presence of WT OASIS under normal conditions. Apparently increased expression in the presence of VT312 OASIS is significant (P = 0.03), but given there is no significant difference in *SEC23A* expression between WT- and VT312-overexpressing cells, we conclude that *SEC23A* is not regulated by OASIS. *P < 0.05 versus empty vector-transfected control (Tukey Test). RT-qPCR. B) A gene that encodes another component of the COPII complex, *SEC24D*, is significantly upregulated in the presence of WT OASIS (P = 0.007 versus empty vector; P = 0.009 versus VT312-transfected), but not in the presence of non-functional VT312 OASIS. **P < 0.01 versus empty vector-transfected control. ††P < 0.01 versus the indicated group (Tukey Test). Y-axes represent relative mRNA expression normalized by the level of GAPDH. Values shown are the means of three independent experiments (n = 3). Error bars, S.D. RT-qPCR. C) Immunoblotting of whole cell lysates from HEK293 overexpressing either WT or VT312 OASIS is consistent with the expression studies, showing that D) the amount of SEC24D protein was augmented upon WT OASIS overexpression, while E) SEC23A protein levels were static.

Chromosomal Location	Gene	Protein	Coding Change	Protein Change	Alteration	Clinical Associations
Chromosome 11: 46,277,661-46,321,422	*CREB3L1* MIM 616215	Old Astrocyte Specifically-Induced Substance (OASIS)	c.934_936delAAG	p.Lys312del	in-frame deletion	severe recessive osteogenesis imperfecta (OI)[7]; osteopenia (*m. musculus*)[16]
Chromosome 11: 46,936,689-47,164,385	*C11ORF49*	N/A	c.822_823insT	p.(*275Leuext*52)	frameshift	associated with D-dimer levels, but function unknown
Chromosome 11: 61,792,980-61,867,354	*FADS2* MIM 606149	Delta-6 Desaturase (D6D)	c.310G>A	p.Gly104Ser	missense	coronary artery disease; ischemic stroke[19]
Chromosome 11: 62,670,273-62,673,687	*UQCC3* MIM 616097	Ubiquinol-Cytochrome C Reductase Complex Assembly Factor 3 (UQCC3)	c.254_263delAGGCGGCGC	p.86_88delGlyGlyAla	in-frame deletion	Mitochondrial Complex III Deficiency, Nuclear Type 9[20]
Chromosome 11: 66,563,463-66,568,841	*CTSF* MIM 603539	Cathepsin F (CTSF)	c.320C>T	p.Ser107Asn	missense	Type B Kufs Disease (neuronal ceroid-lipofuscinosis)[21]
Chromosome 12: 131,828,393-131,851,783	*MMP17* MIM 602285	Matrix Metalloproteinase 17 (MMP17)	c.89C>T	p.Ala30Val	missense	aortic aneurysm[22]; cancer[23,24]

REFERENCES

1. Rauch, F., and Glorieux, F. (2004). Osteogenesis Imperfecta. Lancet 363, 1377-1385.
2. Byers, P., and Pyott, S. (2012). Recessively inherited forms of osteogenesis imperfecta. Annu Rev Genet 46, 475-497.
3. Harrington, J., Sochett, E., and Howard, A. (2014). Update on the evaluation and treatment of osteogenesis imperfecta. Pediatr Clin North Am 61, 1243-1257.
4. Semler, O., Garbes, L., Keupp, K., Swan, D., Zimmermann, K., Becker, J., Iden, S., Wirth, B., Eysel, P., Koerber, F., et al. (2012). A mutation in the 5'-UTR of IFITM5 creates an in-frame start codon and causes autosomal-dominant osteogenesis imperfecta type V with hyperplastic callus. Am J Hum Genet 91, 349-357.
5. Guillen-Navarro, E., Ballesta-Martinez, M.J., Valencia, M., Bueno, A.M., Martinez-Glez, V., Lopez-Gonzalez, V., Burnyte, B., Utkus, A., Lapunzina, P., and Ruiz-Perez, V.L. (2014). Two mutations in IFITM5 causing distinct forms of osteogenesis imperfecta. Am J Med Genet 164A, 1136-1142.
6. Lindert, U., Cabral, W.A., Ausavarat, S., Tongkobpetch, S., Ludin, K., Barnes, A.M., Yeetong, P., Weis, M., Krabichler, B., Srichomthong, C., et al. (2016). MBTPS2 mutations cause defective regulated intramembrane proteolysis in X-linked osteogenesis imperfecta. Nat Commun 7, 11920.
7. Symoens, S., Malfait, F., D'hondt, S., Callewaert, B., Dheedene, A., Steyaert, W., Bachinger, H., De Paepe, A., Kayserili, H., and Coucke, P. (2013). Deficiency for the ER-stress transducer OASIS causes severe recessive osteogenesis imperfecta in humans. Orphanet J Rare Dis 8, e154.
8. Pyott, S., Tran, T., Leistritz, D., Pepin, M., Mendelsohn, N., Temme, R., Fernandez, B., Elsayed, S., Elsobky, E., Verma, I., et al. (2013). WNT1 mutations in families affected by moderately severe and progressive recessive osteogenesis imperfecta. Am J Hum Genet 92, 590-597.
9. Bonadio, J., Holbrook, K.A., Gelinas, R.E., Jacob, J., and Byers, P.H. (1985). Altered triple helical structure of type I procollagen in lethal perinatal osteogenesis imperfecta. J Biol Chem 260, 1734-1742.
10. ThermoScientific. Tech Tip #72: PCR protocol for generating optimized templates for pierce human in vitro expression kits. 2017. https://tools. thermofisher.com/content/sfs/brochures/TR0072-IVT-PCR-protocol.pdf. Accessed 28 February 2017.
11. Livak, K.J., and Schmittgen, T.D. (2001). Analysis of relative gene expression data using real-time quantitative PCR and the 2(-Delta Delta C(T)) Method. Methods 25, 402-408.
12. Rasband, W. (1997). ImageJ. In. (Bethesda, MD, US National Institutes Of Health.
13. Davydov, E., Goode, D., Sirota, M., Cooper, G., Sidow, A., and Batzoglou, S. (2010). Identifying a high fraction of the human genome to be under selective constraint using GERP++. PLoS Comput Biol 6, e1001025.
14. Siepel, A., Bejerano, G., Pederson, J., Hinrichs, A., Hou, M., Rosenbloom, K., Clawson, H., Spieth, J., Hillier, L., Richards, S., et al. (2005). Evolutionarily conserved elements in vertebrate, insect, worm, and yeast genomes. Genome Res 15, 1034-1050.
15. Kondo, S., Murakami, T., Tatsumi, K., Ogata, M., Kanemoto, S., Otori, K., Iseki, K., Wanaka, A., and Imaizumi, K. (2005). OASIS, a CREB/ATF-family member, modulates UPR signalling in astrocytes. Nat Cell Biol 7, 186-194.

16. Murakami, T., Saito, A., Hino, S., Kondo, S., Kanemoto, S., Chihara, K., Sekiya, H., Tsumagari, K., Ochiai, K., Yoshinaga, K., et al. (2009). Signalling mediated by the endoplasmic reticulum stress transducer OASIS is involved in bone formation. Nat Cell Biol 11, 1205-1211.
17. Vellanki, R., Zhang, L., Guney, M., Rocheleau, J., Gannon, M., and Volchuk, A. (2010). OASIS/CREB3L1 induces expression of genes involved in extracellular matrix production but not classical endoplasmic reticulum stress response genes in pancreatic beta-cells. Endocrinology 151, 4146-4157.
18. Asada, R., Saito, A., Kawasaki, N., Kanemoto, S., Iwamoto, H., Oki, M., Miyagi, H., Izumi, S., and Imaizumi, K. (2012). The endoplasmic reticulum stress transducer OASIS is involved in the terminal differentiation of goblet cells in the large intestine. J Biol Chem 287, 8144-8153.
19. Yang, Q., Yin, R., Cao, X., Wu, D., Chen, W., and Zhou, Y. (2015). Association of two polymorphisms in the FADS1/FADS2 gene cluster and the risk of coronary artery disease and ischemic stroke. Int J Clin Exp Pathol 8, 7318-7331.
20. Wanschers, B.F., Szklarczyk, R., Van den Brand, M.A., Jonckheere, A., Suijskens, J., Smeets, R., Rodenburg, R.J., Stephan, K., Helland, I.B., Elkamil, A., et al. (2014). A mutation in the human CBP4 ortholog UQCC3 impairs complex III assembly, activity and cytochrome b stability. Hum Mol Genet 23, 6356-6365.
21. Smith, K.R., Dahl, H.H., Canafoglia, L., Andermann, E., Damiano, J., Morbin, M., Bruni, A.C., Giaccone, G., Cossette, P., Saftig, P., et al. (2013). Cathepsin F mutations cause Type B Kufs disease, an adult-onset neuronal ceroid lipofuscinosis. Hum Mol Genet 22, 1417-1423.
22. Martin-Alonso, M., Garcia-Redondo, A.B., Guo, D., Camafeita, E., Martinez, F., Alfranca, A., Mendez-Barbero, N., Pollan, A., Sanchez-Camacho, C., Denhardt, D.T., et al. (2015). Deficiency of MMP17/MT4-MMP proteolytic activity predisposes to aortic aneurysm in mice. Circ Res 117, e13-26.
23. Sohail, A., Sun, Q., Zhao, H., Bernardo, M.M., Cho, J.A., and Fridman, R. (2008). MT4-(MMP17) and MT6-MMP (MMP25), A unique set of membrane-anchored matrix metalloproteinases: properties and expression in cancer. Cancer Metastasis Rev 27, 289-302.
24. Wang, Y., Yu, S.J., Li, Y.X., and Luo, H.S. (2015). Expression and clinical significance of matrix metalloproteinase-17 and -25 in gastric cancer. Oncol Lett 9, 671-676.
25. Kosugi, S., Hasebe, M., Tomita, M., and Yanagawa, H. (2009). Systematic identification of cell cycle-dependent yeast nucleocytoplasmic shuttling proteins by prediction of composite motifs. Proc Natl Acad Sci 106, 10171-10176.
26. Honma, Y., Kanazawa, K., Mori, T., Tanno, Y., Tojo, M., Kiyosawa, H., Takeda, J., Nikaido, T., Tsukamoto, T., Yokoya, S., et al. (1999). Identification of a novel gene, OASIS, which encodes for a putative CREB/ATF family transcription factor in the long-term cultured astrocytes and gliotic tissue. Mol Brain Res 69, 93-103.
27. Saito, A., Hino, S., Murakami, T., Kanemoto, S., Kondo, S., Saitoh, M., Nishimura, R., Yoneda, T., Furuichi, T., Ikegawa, S., et al. (2009). Regulation of endoplasmic reticulum stress response by a BBF2H7-mediated Sec23a pathway is essential for chondrogenesis. Nat Cell Biol 11, 1197-1204.
28. Canty, E., and Kadler, K. (2005). Procollagen trafficking, processing and fibrillogenesis. J Cell Sci 118, 1341-1353.

29. Asada, R., Kanemoto, S., Kondo, S., Saito, A., and Imaizumi, K. (2011). The signalling from endoplasmic reticulum-resident bZIP transcription factors involved in diverse cellular physiology. J Biochem 149, 507-518.
30. Ishikura-Kinoshita, S., Saeki, H., and Tsuji-Naito, K. (2012). BBF2H7-mediated Sec23A pathway is required for endoplasmic reticulum-to-Golgi trafficking in dermal fibroblasts to promote collagen synthesis. J Invest Dermatol 132, 2010-2018.
31. Unlu, G., Levic, D., Melville, D., and Knapik, E. (2014). Trafficking mechanisms of extracellular matrix macromolecules: insights from vertebrate development and human diseases. Int J Biochem Cell Biol 47, 57-67.
32. Copic, A., Lathan, C., Horlbeck, M., D'Arcangelo, J., and Miller, E. (2012). ER cargo properties specifiy a requirement for COPII coat rigidity mediated by Sec13p. Science 335, 1359-1362.
33. Garbes, L., Kim, K., Riess, A., Hoyer-Kuhn, H., Beleggia, F., Bevot, A., Kim, M., Huh, Y., Kweon, H., Savarirayan, R., et al. (2015). Mutations in SEC24D, encoding a component of the COPII machinery, cause a syndromic form of osteogenesis imperfecta. Am J Hum Genet 96, 432-439.
34. Omori, Y., Imai, J., Suzuki, Y., Watanabe, S., Tanigami, A., and Sugano, S. (2002). OASIS is a transcriptional activator of CREB/ATF family with a transmembrane domain. Biochem Bioph Res Co 293, 470-477.
35. Murakami, T., Kondo, S., Ogata, M., Kanemoto, S., Saito, A., Wanaka, A., and Imaizumi, K. (2006). Cleavage of the membrane-bound transcription factor OASIS in response to endoplasmic reticulum stress. J Neurochem 96, 1090-1100.
36. Wu, J., and Kaufman, R. (2006). From acute ER stress to physiological roles of the Unfolded Protein Response. Cell Death Differ 13, 374-384.

Chapter 3: OASIS-Mediated Expansion Of Secretory Capacity Is Necessary For Proper Formation Of Bone Matrix As Evidenced By Mutations That Cause Osteogenesis Imperfecta

INTRODUCTION

While all cells secrete to some degree, select specialized cell types, including bone-forming osteoblasts, are highly secretory. Osteogenesis begins with the laying down of collagenous bone matrix by osteoblasts. This function levies a significant demand on these cells in terms of protein production and secretion that cellular systems have evolved to accommodate. As an example, the rough endoplasmic reticulum (rER) is the site of folding of secreted proteins. When the synthesis of cargo proteins (e.g. bone matrix proteins such as type I procollagen) overwhelms the available contingent of rER-resident protein-folding chaperones, the accumulation of unfolded proteins in the rER lumen initiates the Unfolded Protein Response (UPR), a signal transduction pathway that triggers the production of additional chaperones and enzymes to handle the excess demand on the protein-folding machinery.[1]

While the UPR is an effective response to crisis in the rER, "traffic jams"[2] can occur in other stages of the secretory pathway. After folding, procollagens are trafficked from the rER to the Golgi for further post-translational processing and packaging for secretion. Vesicular carriers called coat protein II (COPII) complexes bud off from the rER carrying their procollagen cargo and traffic to the Golgi in what is known as anterograde transport.[2; 3] This stage of the secretory pathway is disrupted in a recently-described form of the inherited skeletal dysplasia osteogenesis imperfecta (OI) associated with mutations in Cyclic AMP Responsive Element-Binding Protein 3-Like 1 (*CREB3L1*), which encodes the ER-resident transcription factor Old Astrocyte Specifically-Induced Substance (OASIS).[4; 5]

OASIS, along with other transducers of the UPR, is activated in response to ER stress.[6] Activation is achieved through two cleavage events, which release the active NH_2-terminal fragment, a transcription factor, from the ER membrane and allow it to localize to the nucleus. This mechanism of activation (Regulated Intramembrane Proteolysis or RIP) ensures a rapid response since the transcription factor is pre-made.[6] In HEK293 cells that overexpress *CREB3L1*, we showed a significant increase in the expression of *SEC24D*, which encodes a key structural component of COPII complexes. We hypothesized that OASIS functions in osteoblasts by boosting COPII formation to allow efficient trafficking of large amounts of type I procollagen, and possibly other bone matrix proteins, during the critical period of bone formation.[4] This represents another mechanism cells have adapted to handle high secretory demand. Recently, further evidence of this mechanism was demonstrated by a study in thyroid cells, in which OASIS was found to increase expression of a number of other transport factors (e.g., RAB1B and GM130) in multiple compartments of the secretory pathway, in addition to stimulating an increase in Golgi volume and enhanced organelle complexity. Overall, OASIS seems to augment the capacity of the secretory machinery in these cell types.[7]

It remains to verify the role of OASIS in osteoblasts, in the process of bone tissue formation, and in the pathogenesis of *CREB3L1*-associated OI. Continued study of this form of OI (OI XVI) is complicated by the tissue-dependent and temporal expression of *CREB3L1*. *In situ* hybridization of developing mouse embryos showed that *Creb3l1* mRNA levels in the embryonic tooth bud, salivary gland, and rib peak on embryonic days E14.5-16.5 and wane by E18.5.[8] In human thyroid cells, OASIS protein levels are elevated up to 14 hours after thyrotropin (TSH)-

stimulation and dropped to basal levels after 24 hours.[7] These observations suggest that expression and/or activation of OASIS occurs in a short temporal window. Additionally, the transcriptional targets of OASIS are cell-type specific.[6; 7; 9-11] With the use of human induced pluripotent stem cells (hiPSCs) from OI patients, coupled with directed differentiation, we hoped to generate a model that could overcome these obstacles – to produce osteoblasts and assess them as they differentiate, mature, and begin *in vitro* matrix formation when OASIS would be expected to be activated and relevant pathways are operative.

We generated OI XVI hiPSCs from the homozygous proband in the family we previously reported[4] who exhibited severe disease (*in utero* fractures, lethality) reminiscent of OI Type II in accordance with the original Sillence classification.[12] After differentiation, iOI XVI osteoblast-like cells produced type I collagen-deficient, under-mineralized matrix and displayed unresolved ER stress evidenced by grossly distended rER lumens laden with procollagen type I aggregates. This cellular phenotype is likely the consequence of OASIS dysfunction and the failure to expand secretory pathway capacity in response to the high secretory demands of bone matrix formation.

MATERIALS & METHODS

Cellular Reprogramming, hiPSC Culture and Characterization: To obtain hiPSC, skin fibroblasts that harbored a homozygous *CREB3L1* variant (c.934_936delAAG [p.Lys312del]) and cells heterozygous for a pathogenic *COL1A1* variant (c.2452G>T [p.Gly818Cys]) were virally transduced with non-integrating Sendai viral (SeV) vectors that encoded human *OCT3/4*, *SOX2*, *KLF4*, and c-*MYC* from the CytoTune-iPS 2.0 Sendai Reprogramming Kit (Life

Technologies) at an MOI of 5:5:3 (KOS [hKlf4, hOct3/4, hSox2] MOI=5; hc-Myc MOI=5; hKlf4 MOI=3) per kit instructions. We chose this reprogramming method to mitigate the possibility of integration so that any observed phenotype could reliably be attributed to the disease variants and not to artefactual genetic alterations resulting from the reprogramming process. Transduction of 2 x 10^5 cells was performed. Patient iPSC lines are referred to as "iOI XVI" for the *CREB3L1* variant line and "iOI II" for the *COL1A1* variant line, respectively. Seven days posttransduction, 1-2 x 10^5 cells were passaged onto irradiated mouse embryonic fibroblast (MEF) feeders. After 2-4 weeks, emerging colonies were manually picked and expanded on MEFs. A normal human male iPSC line, "iWT" (a gift from the Tom & Sue Ellison Stem Cell Core, Institute for Stem Cell and Regenerative Medicine, University of Washington) was also reprogrammed using CytoTune-iPS 2.0. Cells on MEFs were maintained with medium containing F12/DMEM (Invitrogen) supplemented with 20% Knockout Serum Replacer (Gibco), 0.1mM Sodium Pyruvate (Gibco), 1nM NEAA (Gibco), 0.1mM β-mercaptoethanol (Sigma), 50 IU/mL penicillin, 50μg/mL streptomycin, and 5ng/mL FGF (Invitrogen). Media was changed every 1-3 days. Cells were passaged following dissociation with 1.925 IU/mL Dispase (Gibco Life Sciences). All cells were transitioned to feeder-free culture on Matrigel (Corning) and maintained in mTESR1 (Stem Cell Technologies). G-banded chromosome analysis of cell lines (n = 20) was performed by Diagnostic Cytogenetics, Inc. (Seattle, WA) on feeder-free clones with a band level resolution of 450-500. For immunocytochemistry of colonies, hiPSCs were passaged onto Matrigel-covered sterile glass slides and cultured. Colonies were fixed with 4% paraformaldehyde/PBS for 15 minutes, permeabilized with 0.1% Triton X-100 for 2 minutes and incubated with 2.5% normal horse serum/PBS (Vector Laboratories) for 20 minutes at room temperature to block nonspecific binding of antibodies. The cells were then incubated with

primary antibody to Oct3/4 (sc-5279; Santa Cruz Biotechnology, Inc.) at 1:100 at 4°C overnight. This was followed by incubation with AlexaFluor488 Goat Anti-Mouse IgG (H&L) (A11029; ThermoFisher Scientific) secondary antibody, 1:500, at room temperature for 1 hour. This stepwise process was repeated for Nanog (AF1997; R&D Systems) at 5μg/mL with Northern Lights Donkey Anti-Goat IgG NL557 (NL001; R&D Systems) at 1:200. The cells were counterstained with DAPI, mounted on slides, and confocal images were acquired with a Leica TCS SPE.

Teratoma Generation: For teratoma generation, 2 x 10^6 cells were harvested, washed, brought up in 150μl of a Pro-Survival Cocktail[13], and subcutaneously injected into 6-8 week-old female SCID mice (Charles River Laboratories International, Inc.). Tumors were removed when they reached ~1cm in size, which took 8-14 weeks post-transplantation. The tumors were fixed in 4% paraformaldehyde/PBS overnight, paraffin-embedded, sectioned, hematoxylin and eosin (H&E) stained, and examined.

Directed Differentiation, Characterization, & Mineralization Assay: hiPSCs were pushed down the osteoblast lineage using a differentiation method that does not employ an embryoid body (EB) step, as inclusion of this step is reportedly associated with a lower efficiency of *in vitro* mineralization[14], one of the primary readouts of our study. Briefly, colonies were disaggregated with Accutase (Corning) and plated as single cells at high density (10^5/cm^2) in αMEM (Cat No. 12571-063; Gibco) supplemented with 10% FBS, 50 IU/mL penicillin, 50μg/mL streptomycin, and 10μM Y27632 (Cat No. 04-0012-02; Stemgent) overnight. Beginning the next day, cells were cultured in osteoblast differentiation media (ODM) consisting

of αMEM supplemented with 10% FBS, 100nM dexamethasone (Cat No. D2915; Sigma-Aldrich), 50μg/mL ascorbic acid, 5mM β-glycerophosphate (Cat No. G9422; Sigma-Aldrich), 50 IU/mL penicillin, and 50μg/mL streptomycin, for 21 days. Media was changed every 3-4 days. On D21, some cells were passaged 1:5 onto sterile glass slides and cultured in ODM. On D25, these cells were fixed for 10 minutes in methanol and blocked for 20 minutes with 2.5% normal horse serum/PBS (Vector Laboratories). The cells were incubated with an AlexaFluor488-conjugated primary antibody to RUNX2 (ab215954; Abcam) at 1:500 at 4°C overnight. Cells were counterstained with DAPI, mounted on slides, and confocal images were acquired with a Leica TCS SPE. To assess mineralization, cells were differentiated for 21 days in 48-well plates. Typically, *in vitro* mineralization is measured using histochemical methods including alizarin red and von Kossa staining. Alizarin red forms a chelate upon reacting with calcium cations[15], while von Kossa staining reacts with phosphates and carbonates in calcium.[16] Both methods, therefore, depend on the detection of subcomponents of hydroxyapatite, the mineral phase of bone, but neither is specific for it. As an alternative, we used the OsteoImage Mineralization Assay offered by Lonza, which claims specific binding to hydroxyapatite. The OsteoImage Mineralization Assay (Lonza) was performed according to kit instructions and imaged on a Zeiss Imager A1. Quantification of mineralization from the images was achieved with Fiji (National Institutes Of Health). A detailed protocol and raw images for this quantification are presented in the Supplementary Material for this chapter.

RT-qPCR: For quantitative reverse transcription PCR (RT-qPCR), total RNA was isolated from cells with either the RNeasy Mini Kit or the AllPrep DNA/RNA/Protein Mini Kit (Qiagen) according to kit instructions. First strand synthesis of 200ng of RNA was achieved using iScript

Reverse Transcription Supermix (BIORAD) in 20µl reactions. 0.5µl of cDNA was used for RT-qPCR in 20µl reactions using iTaq Universal SYBRGreen Supermix (BIORAD). Samples were run on a CFX96 Touch (BIORAD) using the following program: 95°C for 30 seconds, 95°C for 5 seconds, 60°C for 30 seconds for 40 cycles. Each sample was run in triplicate and the mean Ct values were analyzed using the 2^-[delta][delta]Ct method.[17] Expression was normalized to the reference gene GAPDH. Primers for RT-qPCR targets are listed in Supplementary Table 1 (Integrated DNA Technologies).

Immunocytochemistry (ICC) Of Matrix And Of Collagen In Differentiated Single Cells: For ICC of extracellular matrix, hiPSCs were plated on Matrigel-coated glass slides and differentiated for 21 days. On D21, the cell sheets were fixed with 4% paraformaldehyde/PBS for 15 minutes. Blocking and staining was performed as described above. Primary antibodies used were against type I collagen (LF68)[18] at 1:200 and osteopontin (OPN) (ab8448; abcam) at 1:200 with the respective secondary antibodies AlexaFluor594 Goat Anti-Rabbit IgG (H&L) (A11037; ThermoFisher Scientific) and AlexaFluor405 Goat Anti-Rabbit IgG (H&L) (A31556; ThermoFisher Scientific), both at 1:500. For ICC of differentiated single cells, passaged D25 cells were fixed with methanol for 10 minutes. Blocking and staining was performed as described previously. Primary antibodies used were for type I procollagen (LF41)[18] at 1:200 and for KDEL, an ER marker, (ab176333; Abcam) at 1:250. Secondary antibodies used were AlexaFluor488 Goat Anti-Rabbit IgG (H&L) (A11034; ThermoFisher Scientific) and AlexaFluor594 Goat Anti-Rabbit IgG (H&L) (A11037; ThermoFisher Scientific), both at 1:800. Images were acquired with a Zeiss Imager A1.

Transmission Electron Microscopy (TEM): For TEM, approximately 5 million differentiated cells were scraped, collected, and fixed in 2% paraformaldehyde/2.5% glutaraldehyde in 0.2M cacodylate buffer at 4°C overnight, post-fixed in 1% osmium tetroxide in 0.1M cacodylate buffer, dehydrated, and embedded in EPONATE 812 (Ted Pella, Inc.). Ultra-thin (~70nm) sections were stained with uranyl acetate and lead citrate and imaged on a JEOL JEM 1400 at 120kV with a Gatan Ultrascan 1000XP. Preparation of samples was performed by the Electron Microscopy Resource at the Fred Hutchinson Cancer Research Institute. rER tubules were measured using Fiji (National Institutes Of Health).

Statistical Analysis: Statistical analysis was performed using GraphPad Prism 7.0d software. The data are expressed as arithmetic means +\- standard deviation, SD. Statistical significance was determined by running analysis of variance (ANOVA) and tests for multiple comparisons as noted in the figure legends.

RESULTS

Generation Of OI hiPSC Lines From Patient Skin Fibroblasts

Dermal fibroblasts (Supplementary Figure 1A) from the proband in a previously reported family[4] bearing a homozygous *CREB3L1* variant (c.934_936delAAG [p.Lys312del]) and fibroblasts from an individual with a *COL1A1* triple-helical glycine substitution variant (c.2452G>T [p.Gly818Cys]), each variant being the genetic cause of a severe OI phenotype in the respective patient, were successfully reprogrammed using non-integrating Sendai virus (SeV)[19; 20] expressing the Yamanaka factors (OCT3/4, SOX2, KLF4, c-MYC).[21] After subcloning, one *CREB3L1* variant clone (iOI XVI) and one *COL1A1* variant clone (iOI II) were fully expanded

and characterized alongside a normal human male iPSC line (iWT), also generated from primary fibroblasts using SeV, as a control.

iOI XVI, iOI II, and iWT hiPSC all demonstrated human ESC-like colony morphology (Figure 1A). The karyotypes of all established clones were normal (n = 20) (Figure 1B). Colonies stained positively for the pluripotency markers Oct4 and Nanog (Figure 1C) and mRNA expression of *POU5F1* (OCT4), *SOX2*, and *NANOG* were comparable to that in ESC unlike in the starting fibroblast populations (OI XVI and OI II) (Figure 1D). Flow cytometry indicated the presence of pluripotent cell surface markers SSEA-3, SSEA-4, and Tra-1-81, while cells lacked SSEA-1, a surface marker on differentiating cells (Supplementary Figure 1B). After many passages, established clones no longer had detectable SeV vector sequences, confirming that integration had not occurred (Supplementary Figure 1C). Sequencing of iOI XVI and iOI II clones confirmed the presence of the original patient mutations in *CREB3L1* and *COL1A1*, respectively, indicating that, genetically, these are OI hiPSC lines (Supplementary Figure 1D). As a final conclusive test of pluripotency[22], injection of a bolus of hiPSCs from each line into nude mice resulted in the generation of teratomas in which tissue types from each of the three germ layers (ectoderm, endoderm, mesoderm) could be identified histologically (Figure 1E-G). We were curious if we would be able to see any striking differences in the quantity or constitution of bone foci in teratomas generated by healthy versus OI hiPSC, but bone generation was infrequent across all tumors and no obvious phenotypes were observable (Supplementary Figure 2).

Directed Differentiation Of OI hiPSC Into Osteoblasts

hiPSCs were disaggregated, plated at high density, and cultured in osteoblast differentiation media (ODM) containing the factors dexamethasone (DEX), ascorbic acid (AA), and β-glycerophosphate (βGP) for 21 days without passaging (Figure 2A). After three weeks in culture, plates were carpeted with dense sheets of cells (Figure 2B). Passaging of the cells allowed for single cell imaging (Figure 2C) revealing fibroblast-like/osteoblast-like morphology, which are indistinguishable in culture[23]. To estimate the efficiency of differentiation, we performed immunocytochemistry and documented expression of RUNX2 (Runt-Related Transcription Factor 2) (Figure 2D), a key transcription factor involved in osteoblast differentiation and one of a select few transcripts that genetically distinguishes fibroblasts from osteoblasts.[23] The observation that cells treated with ODM secreted mineralized matrix *in vitro* (Figure 2E) served as another specific that osteogenic differentiation, even if incomplete, was taking place.[23]

As another means to determine the success of coaxing hiPSCs down the osteoblast lineage, we measured mRNA expression of a panel of bone markers in cells differentiated for 7, 14, and 21 days. While low-level mRNA expression of the transcription factor *RUNX2* and more robust expression of genes coding for the extracellular matrix (ECM) structural protein *COL1A1*, the non-collagenous matrix protein (NCP) *BGLAP* (Bone Gla Protein encoding osteocalcin; OCN), and the matricellular protein *SPARC* (Secreted Protein, Acidic, Cysteine Rich encoding osteonectin; ON) was observed, additional markers of a mature osteoblast phenotype – *ALPL* (Alkaline Phosphatase, Liver), *SP7* (Specificity Protein 7 encoding osterix; OSX), and *IBSP* (Integrin-Binding Sialoprotein encoding Bone Sialoprotein II) – were not detectable (Figure 2F).

These findings are in keeping with other reports of the osteogenic differentiation of both hiPSCs[24] and hESCs[25] and reflect the limitations of current methodologies.

OI Osteoblast-Like Cells Produce Deficient Extracellular Matrix *In Vitro*

The clinical skeletal features of OI – bone fragility, bone deformity, fractures – are the organ-level consequences of a tissue-level defect, namely the improper formation of bone ECM. We wanted to examine the matrix produced by our OI osteoblast-like cells. The deposition of mineralized nodules is a functional hallmark of osteogenic cell cultures[23], the *in vitro* approximation of *in vivo* bone formation. This activity can be recapitulated with differentiated iPSCs.[26] After differentiation, all hiPSC-derived osteoblast-like cell lines deposited mineralized matrix that could be visualized and quantified (Figure 3A, Supplementary Figure 3), however, osteoblast-like cells with OI-causing variants produced significantly less mineral than wild type ($P < 0.001$ for iOI XVI versus iWT; $P = 0.001$ for iOI II versus iWT).

While measuring mineralization allowed for comparative assessment of the inorganic component of matrix deposited by the osteoblast-like cells, we also assessed some of the organic components. The major organic component of bone matrix is type I collagen. In addition to collagenous protein, bone matrix contains a number of non-collagenous proteins – including OCN, ON, and osteopontin (OPN) – which have roles in the binding interactions between collagen and mineral and in regulating mineralization.[27] To look at the relative contributions of specific proteins to the matrix produced by our cells, we performed ICC for type I collagen (COL1) and OPN on the D21 cell sheets. ECM from normal healthy cells (iWT) consisted of many, many strands of COL1 in a thick fibrous network often forming dense rafts of collagenous

matrix, while the bulk of detectable COL1 in iOI II cultures appeared to be retained in cells and not in the secreted matrix (Figure 3B). There was an observable difference between the quality of matrix produced by the two OI cell lines: some amount of type I collagen fibers had been deposited in iOI XVI matrix, though the networks were far sparser than those produced by iWT osteoblast-like cells (Figure 3B).

OI Osteoblast-Like Cells Secrete Collagen Inefficiently

Next, we disaggregated the cell sheets and plated single osteoblast-like cells for ICC. While normal healthy cells efficiently trafficked type I procollagen, those molecules accumulated in the rER and Golgi of iOI II cells (Figure 4A). This is a known consequence of the specific *COL1A1* defect in these cells, substitution of a glycine in the (Gly-Xaa-Yaa)-repeating triple-helix, which inhibits proper folding of the procollagen molecule and causes it to be retained[28]. The well-understood pathogenesis of OI type II is therefore verifiable in our OI II hiPSC model.

Retention of procollagen was also observed in iOI XVI cells (Figure 4A), even though they produce biochemically normal type I collagen (data previously published; Chapter 2, Figure 2-1).[4] What the iOI XVI cells lack, instead, is functional OASIS. Our previous work in an OASIS over-expression model demonstrated the induction of SEC24D, a component of the inner coat of the COPII complex.[4] We had hypothesized that OASIS may be called upon during times of increased protein synthesis, such as occurs during osteogenesis, to drive the formation of COPII carriers and aid in the secretion of bone matrix proteins, especially type I collagen, the trafficking of which requires extra-large COPII due to its size.[3] We found that the *CREB3L1* variant in this family interrupted binding of OASIS to DNA regulatory elements.[4] In this new

model, it is clear that in the absence of functional OASIS, the iOI XVI osteoblast-like cells were far less efficient in secreting procollagen into forming matrix.

Transmission electron microscopy (TEM) of individual cells (Figure 4B) showed markedly distended rERs ($P < 0.001$) in iOI II and iOI XVI cells (average rER tubule thickness = 192nm and 197nm, respectively) compared to normal (average rER tubule thickness = 108nm) (Figure 4C), a sign of unresolved ER stress. Notably, this dramatic cellular phenotype is also seen in osteoblasts from individuals with variants in the *SEC24D* gene itself, that lead to a syndromic form of OI.[29]

DISCUSSION

In our study, OI XVI and OI II osteoblast-like cells differentiated from patient hiPSC formed under-mineralized matrix *in vitro* that was deficient in type I collagen. In both instances, osteoblast-like cells were unable to efficiently secrete collagen, but to different degrees and due to different mechanisms. These observed cellular phenotypes are consistent with our current understanding of the molecular mechanisms underlying these genetically distinct forms of OI. In iOI II osteoblast-like cells, the improper folding of type I collagen molecules (as previously shown by collagen analysis of the un-reprogrammed patient dermal fibroblasts)[4] would be expected to hinder procollagen exit from osteoblast-like cells, to disrupt fibril formation and, thus, disrupt the hierarchical structure of forming bone matrix. In iOI XVI osteoblast-like cells however, in which type I collagen molecules are structurally normal and functional OASIS is absent[4], we think that the secretory pathway needed to shuttle type I collagen out of the cell is

overburdened resulting in the substantial reduction of collagen fibers in the matrix observed compared to iWT.

There is the question of how to reconcile both 1) that the under-mineralization of iOI XVI matrix *in vitro* appears so much more severe than that of iOI II matrix when iOI XVI cells are able to deposit some type I collagen and OI II cells nearly none and 2) that the clinical phenotypes of both an OI II patient and the OI XVI homozygote are similarly severe even though iOI XVI matrix had a slightly better composition. It is possible that this difference reflects limitations of our model. The need for OASIS is dependent on the processes of differentiation, maturation, and bone formation demanding more of the protein-producing machinery than it can handle. This "breaking point" may have been reached in our cultures only on by a subset of cells; maturation of other cells may have been delayed or incomplete. During bone development *in situ*, these stresses may be amplified and more uniform than in our model and the effects of OASIS impairment may be more dramatic. However, the rER expansion data suggests a disease phenotype does exist in our iOI XVI cells. From the work of Garcia *et al*.[7], we know OASIS impacts more than just SEC24D and COPII. The almost complete lack of mineralization in *in vitro* iOI XVI matrix may be the result of this more generalized secretion defect affecting the deposition of additional bone matrix proteins, e.g., NCPs. OI bone tissue is generally found to be hypermineralized compared to normal[30; 31], but this can vary with the causative disease gene and specific mutation. As an example, two *COL1A1* glycine substitutions were reported as causing OI type II in which collagen fibrils formed normally, but were rarely associated with hydroxyapatite crystals (5% of fibrils contained crystallites versus 70% in normal bone).[32]

Alternatively, our seemingly-conflicting observations could be an artifact of *in vitro* versus *in vivo* settings.

The secretion deficiency observed in iOI XVI osteoblast-like cells is consistent with the molecular mechanism proposed by us[4] and by others[7] for this class of secretion-related proteins. In addition to augmenting levels of the transport factor SEC24D[4] and of type I collagen cargo through the transcription of *COL1A1*[9], OASIS was found to regulate the synthesis of several other ER/Golgi transport factors and to dramatically increase Golgi volume in TSH-stimulated thyroid cells.[7] Additionally, Garcia *et al*.[7] identified a list of potential target genes by searching for the *CREB3L1* consensus motif in promoter regions. Notably, *SEC24D* was among those genes, validating our previous finding that *SEC24D* was transcriptionally upregulated in response to OASIS overexpression.[4] It is clear from the severity of both the cellular phenotype and of the clinical phenotype of homozygous individuals that the regulatory role of OASIS in expanding the capacity of the secretory pathway in times of need is highly significant.

At present, methods for the directed differentiation of pluripotent cells to osteoblasts (and to most other cell types) have limitations. Differentiation of both ESCs and iPSCs toward an osteogenic fate is most commonly achieved with addition of the exogenous factors dexamethasone, ascorbic acid, and β-glycerophosphate to culture media[14; 24; 26; 33]: DEX is important for the differentiation of osteoprogenitors[34], AA is a required cofactor in collagen assembly[35], and βGP has a role in matrix mineralization.[35] Alternative approaches to osteogenic differentiation have been attempted including culturing with additional factors (e.g., Bone Morphogenetic Protein 2; BMP2)[33] or with small molecules[36] and bioengineering-based

approaches such as co-culturing with calcium phosphate (CaP)-coated hydroxyapatite mineral particles[37], but these have shown nominal improvement over the method we employed. Efficiency of differentiation is commonly determined by flow cytometry for cell-type specific markers. This was not possible in our study, as a unique profile of cell surface markers that differentiate osteoblasts from progenitor mesenchymal stem cells (MSCs) has not yet been established[38; 39]. Other studies claimed that flow cytometry for ALPL could be used to sort for osteogenic cells[14; 40], but we could not detect an ALPL-positive population in our differentiations (data not shown). Notably, both studies that sorted based on ALPL involved differentiation of ESC, rather than iPSC, and one involved differentiation and characterization of MSCs as an intermediate. The dynamics of an ESC- versus an iPSC-based differentiation are likely very different. The lack of ALPL mRNA expression in our cells and in osteogenic cells differentiated from iPSC by others using current methods[24] calls into question the applicability of an ALPL sorting method in this study. We used nuclear RUNX2 staining as a proxy for efficiency determination here. In spite of the shortcomings of our model, we generated cells with which we were able to answer relevant questions about the biological role of OASIS.

With the same starting number of cells and the same titer of virus, reprogramming of patient fibroblast line OI II yielded hundreds of colonies leading to seven stable clones. Colonies appeared within 9 days and were subcloned as early as D14. In contrast, reprogramming of patient fibroblast line OI XVI yielded only a few semi-stable clones, which were not ready for subculture until D19, D22, and beyond and which ultimately could not be expanded further. We originally hypothesized that the age of the starting cells had hindered the efficiency of the reprogramming. We therefore repeated the reprogramming with earlier passage OI XVI primary

fibroblasts. However, reprogramming of the younger cells resulted in a similarly low efficiency as the first attempt, with only a few colonies appearing by D18 and subcloning starting at D20. The clones that survived were difficult to culture on MEF feeders with high levels of differentiation. Only after the clones were transitioned to a feeder-free culture system did they begin to stabilize. Even feeder-free, they were slow to expand and quick to spontaneously differentiate.

Apart from a technical explanation for the low reprogramming efficiency and instability (e.g., slight differences in the titer of virus delivered to each line) and aside from the known variability in the behavior of cells from different patients, there could be a relevant biological explanation. Dillin and colleagues hypothesized that given the major stresses associated with forcing cells to reprogram (e.g., global cellular remodeling, metabolic shifts), it would make sense that UPR mechanisms are activated and that variability or deficiency in UPR activation or function could have a profound effect on reprogramming efficiency.[41] OASIS is an ER stress transducer. We know OASIS is activated in response to ER stress in some highly secreting cell types in response to physiological demands. Perhaps OASIS has a role in the reprogramming process, as well. If *CREB3L1* is expressed in stem cells and OASIS is activated at some point during reprogramming, this could explain the poor reprogramming potential of OI XVI fibroblasts, a cell line lacking functional OASIS. Further insight into the interactions between OASIS, the UPR, and reprogramming will require additional studies.

Historically, study of OI has used primary dermal fibroblasts as they are relatively easy to acquire and secrete collagens readily. As additional genes have been implicated in the

pathogenesis of OI in pathways beyond collagen production and processing, the limitations of this approach have become evident. The use of hiPSC could be a useful tool for the OI research community going forward as we fill in the remaining gaps in knowledge about OI causative genes and their respective mechanisms, especially when osteoblast-specific genes are implicated.

Of continued interest is the observation that heterozygosity for the *CREB3L1* c.934_936delAAG variant resulted in a far milder phenotype than homozygosity, more akin to OI type I with osteopenia and fractures. In one individual who possessed the variant, there was no report of skeletal abnormalities or fractures at all.[4] This recognition, taken together with the implication of *CREB3L1*-interacting genes in OI and related skeletal disorders (e.g., *SEC24D*[29], a transcriptional target of OASIS and *MBTPS2*[42], encoding SP2, a protein that cleaves OASIS resulting in its activation) raises the question of whether heterozygous variants affecting other transport factors or transcriptional regulators of secretion pathways could contribute to more common and/or late-onset bone phenotypes, e.g., osteoporosis. It remains to mine the available genomic and clinical data to explore this possibility.

FIGURES & TABLES

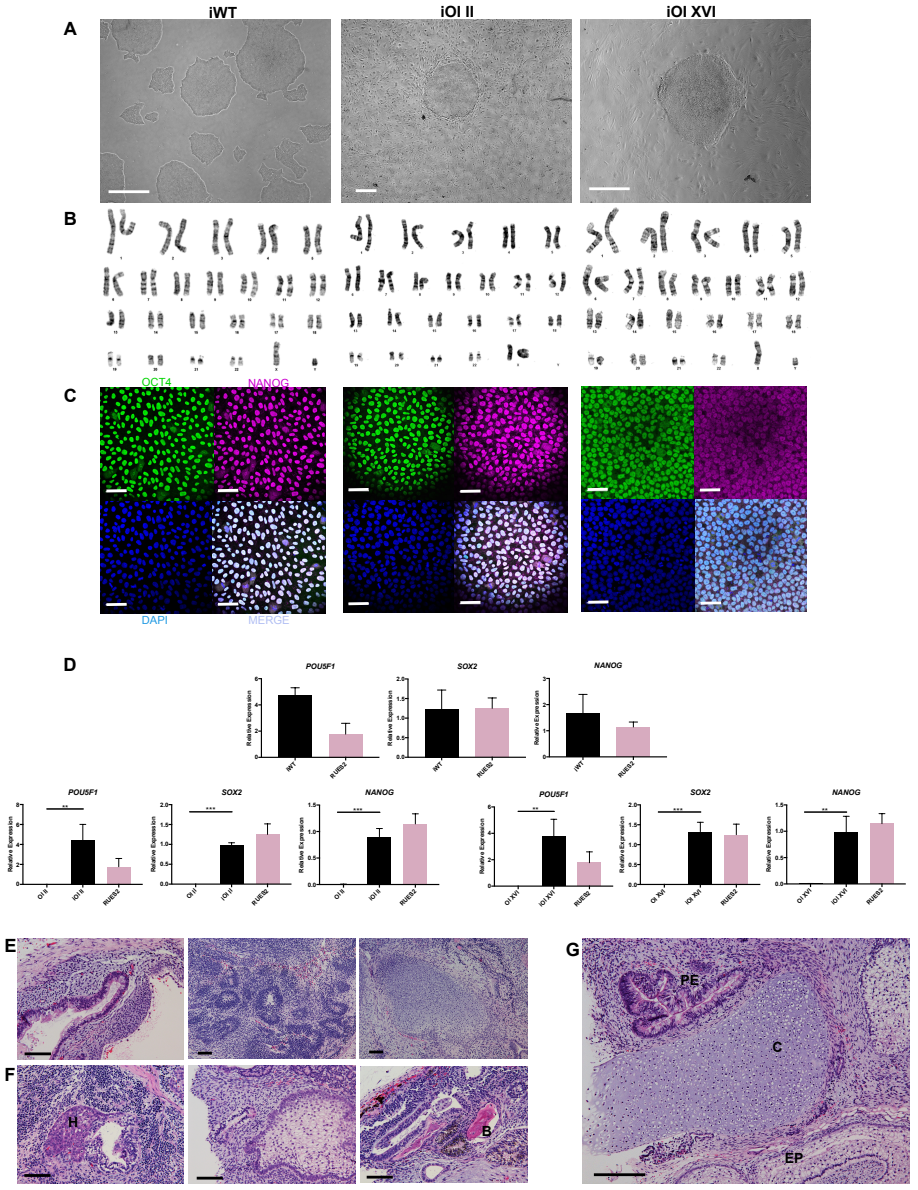

Figure 3-1. Successful Reprogramming Of OI Patient Fibroblasts. A) Reprogrammed cells exhibit typical hiPSC colony morphology. Scale Bars = 500µm. B) hiPSC clones are karyotypically normal (n = 20). C) Colonies stain positively for OCT4 and NANOG. Scale Bars = 50µm. ICC. D) hiPSC express the pluripotency genes *POU5F1* (OCT4), *SOX2*, and *NANOG* at levels comparable to hESC control line RUES2. OI XVI and OI II, the starting patient fibroblast lines, were included as negative controls. **P < 0.01 and ***P < 0.001 versus the respective non-reprogrammed patient fibroblast line (Dunnett Test). Y-axes represent relative mRNA expression normalized by the level of GAPDH. Values shown are the means of three independent experiments (n = 3). Error bars, SD. RT-qPCR. E-G) Histological analysis of teratomas generated from hiPSC lines demonstrate development of tissues from all three germ layers. E) From iWT *left to right*, intestinal epithelium (endoderm), neural tube (ectoderm), and cartilage (mesoderm). F) From iOI II *left to right*, hepatoid tissue **H** (endoderm), epidermis (ectoderm), and bone **B** (mesoderm). G) From iOI XVI, primitive endoderm **PE**, cartilage **C** (mesoderm), and epidermis **E** (ectoderm). Scale Bars = 100µm. H&E.

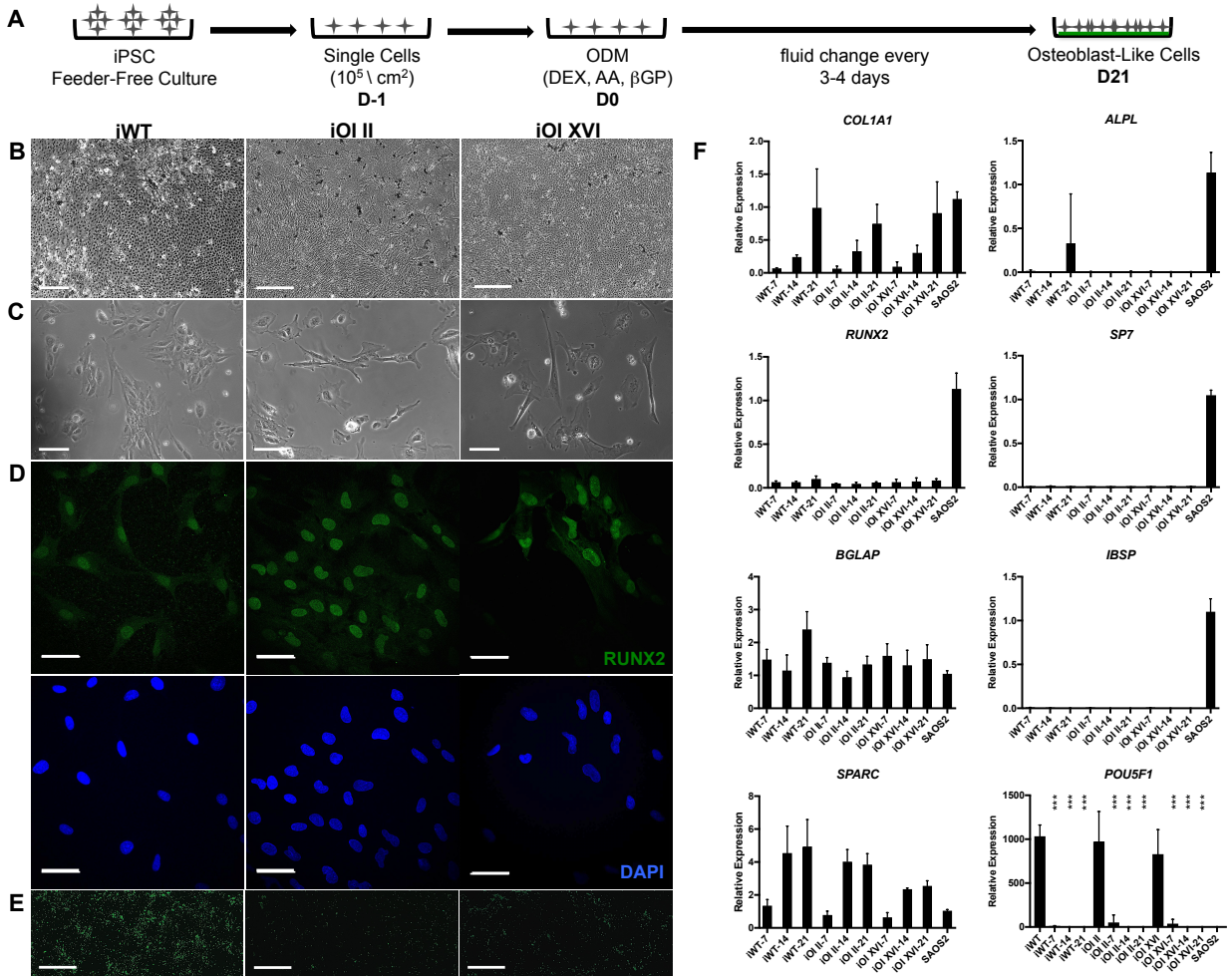

Figure 3-2. Directed Differentiation Of OI hiPSC Into Osteoblast-Like Cells. A) hiPSC colonies were disaggregated and plated as single cells at high density. The next day, plates were switched to osteoblast differentiation media (ODM) supplemented with dexamethasone (DEX), ascorbic acid (AA), and β-glycerophosphate (βGP). Cultures were grown for 21 days with fluid changes every 3-4 days and no further passaging. B) After 21 days in ODM, cells formed dense sheets dotted with mineral. Scale Bars = 200, 500, and 500μm *left to right*. C) The osteoblast-like cells were passaged on D21 and imaged on D22 to better visualize single cell morphology. Scale Bars = 100μm. D) Efficiency of differentiation was determined by staining for nuclear RUNX2, an essential transcription factor in osteoblast differentiation and maturation. Every nuclear DAPI signal aligned with a nuclear RUNX2 signal. Scale Bars = 50μm. ICC. E) After 21 days, deposits of mineralized matrix were detectable *in vitro*. Scale Bars = 1000μm. OsteoImage Mineralization Assay (Lonza). F) Differentiating cells were harvested on D7, D14, and D21. As expected, *POU5F1* expression dropped off once the cells were cultured in ODM, indicating the loss of pluripotency. While expression of some bone markers (*COL1A1*, *RUNX2*, *BGLAP*, and *SPARC*) was evident in the differentiated cell populations, additional markers of an osteoblast fate (*ALPL*, *SP7*, and *IBSP*) were absent. SAOS2, an osteosarcoma line, was included as a positive control for bone marker expression. ***P < 0.001 versus the matched undifferentiated hiPSC line (Bonferroni Test). Y-axes represent relative mRNA expression normalized by the level of GAPDH. Values shown are the means of three independent experiments (n = 3). Error bars, SD. RT-qPCR.

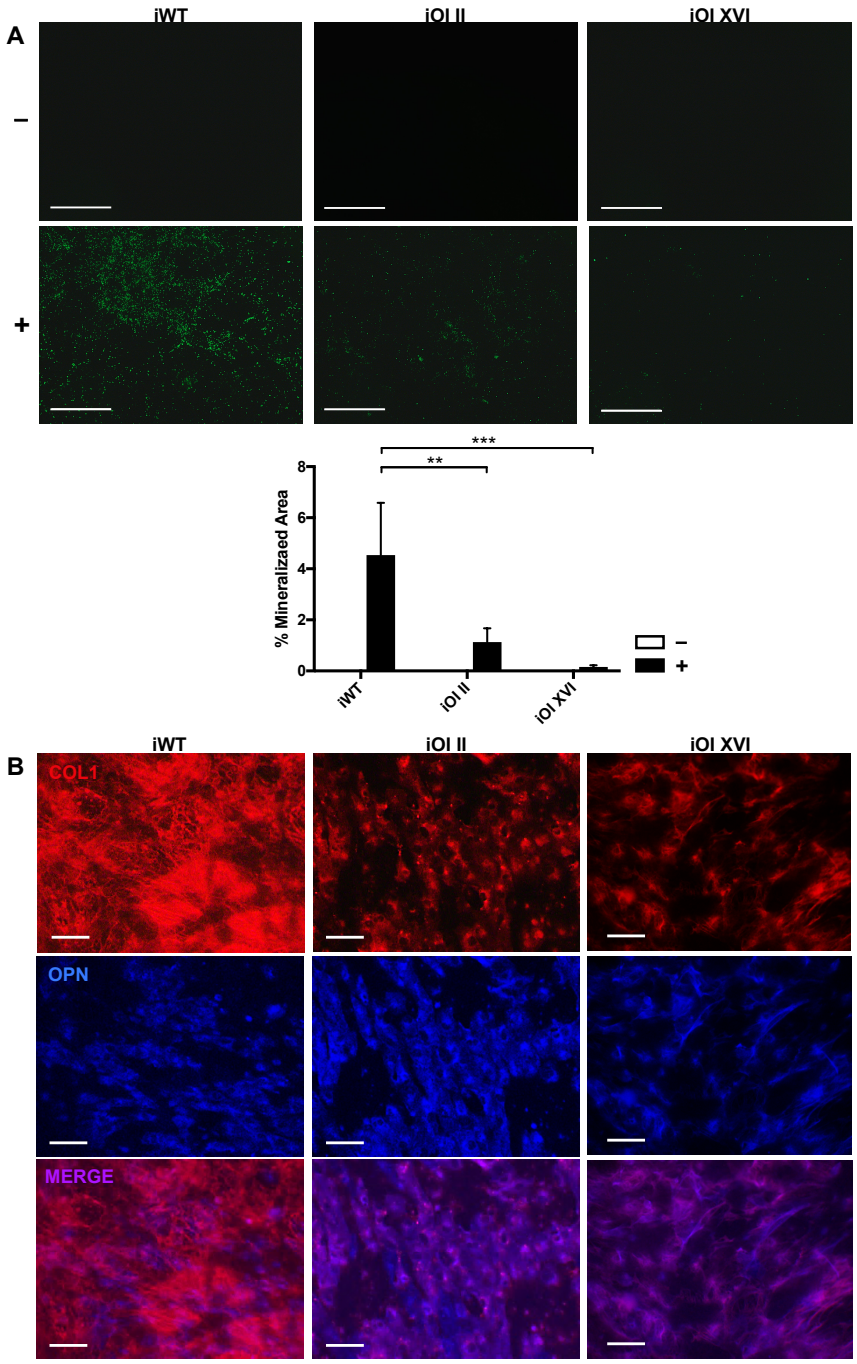

Figure 3-3. OI Osteoblast-Like Cells Produce Deficient Extracellular Matrix. A) Nodules of mineralized matrix were visible after staining with the OsteoImage Mineralization Assay (Lonza). All lines deposited some matrix when cultured in ODM (+) for 21 days, while cells grown in basal media without factors (-) for 21 days did not produce mineralized matrix at all. Both iOI XVI and iOI II osteoblast-like cells produced far less matrix than normal healthy cells (iWT). Scale Bars = 1000μm. **P < 0.01; ***P < 0.001 versus iWT (Tukey Test). Y-axes represent % mineralized area (quantified from imaging). Values shown are the mean of three independent experiments (n = 3). Error bars, SD. B) ECM from normal healthy cells (iWT) consisted of thick networks of type I collagen fibers, while far fewer type I collagen fibers were found in iOI XVI matrix. In stark contrast, type I collagen was largely absent from iOI II matrix and was instead bound up in cells. Scale Bars = 100μm. COL1 = type I collagen; OPN = osteopontin. ICC.

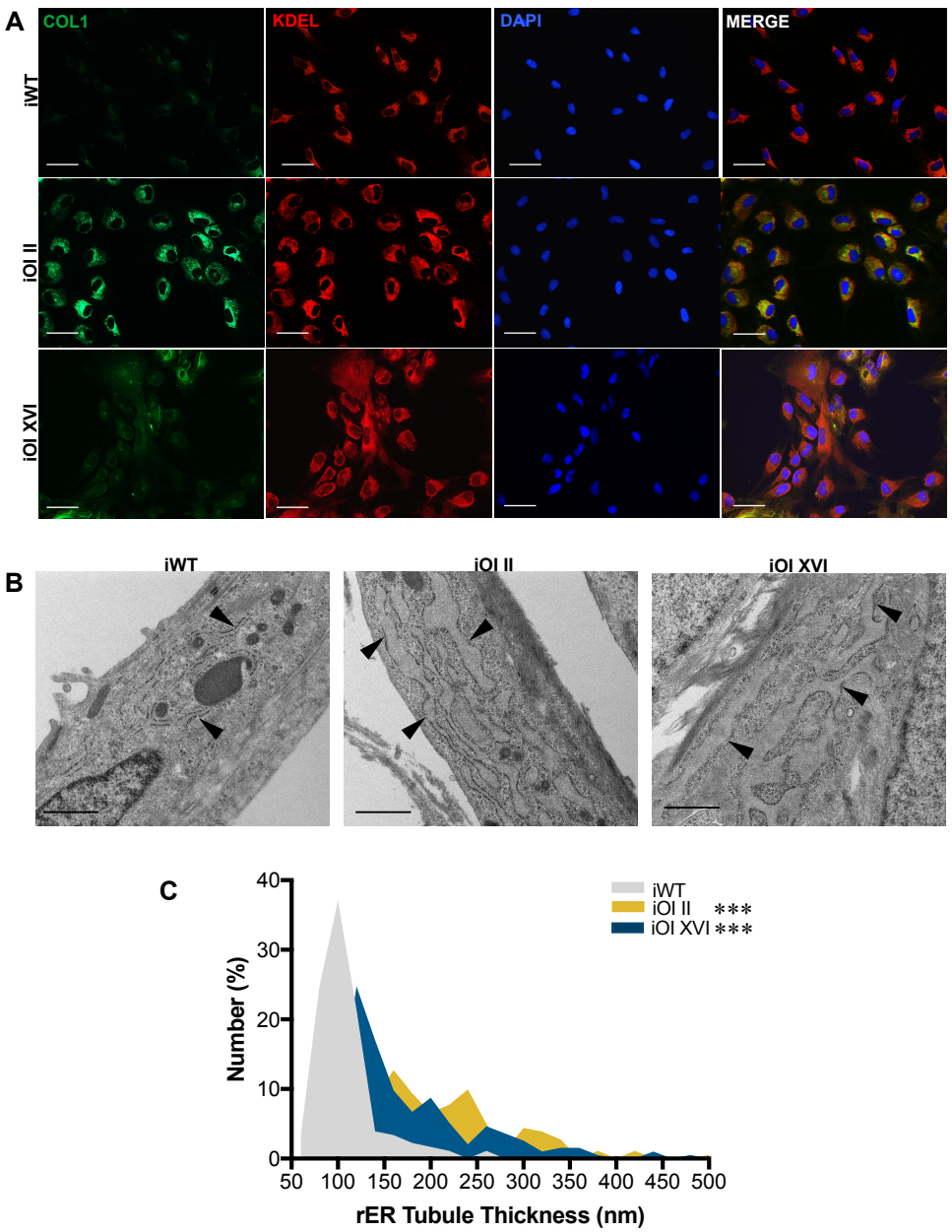

Figure 3-4. OI Osteoblast-Like Cells Secrete Collagen Inefficiently. A) Procollagen type I accumulated in the rER or Golgi of OI osteoblast-like cells but was efficiently trafficked in normal healthy cells (iWT). COL1 = procollagen type I; KDEL = ER. Scale Bars = 100µm. ICC. B) Distention of rER tubules (arrowheads) is evident in OI osteoblast-like cells. Scale Bars = 1µm. TEM. C) rER tubule thickness quantified in osteoblast-like cells. Tubule measurements were binned such that the 100nm tick on the x-axis represents measurements greater than 50nm and equal to or less than 100nm. Y-axis represents the percentage of total measurements from each cell line that fall into the respective bin. The tubules of iOI XVI (average thickness = 197nm) and iOI II (average thickness = 192nm) osteoblast-like cells are significantly distended compared to normal (average thickness = 108nm). ***P < 0.001 versus iWT according to one-way ANOVA (Dunnet Test) where n = 178 (iWT), n = 181 (iOI II), and n = 167 (iOI XVI) tubule measurements, respectively.

REFERENCES

1. Bernales, S., Papa, F.R., and Walter, P. (2006). Intracellular signaling by the unfolded protein response. Annu Rev Cell Dev Biol 22, 487-508.
2. Melville, D., and Knapik, E. (2014). Traffic jams in fish bones. Cell Adhes Migr 5, 114-118.
3. Unlu, G., Levic, D., Melville, D., and Knapik, E. (2014). Trafficking mechanisms of extracellular matrix macromolecules: insights from vertebrate development and human diseases. Int J Biochem Cell Biol 47, 57-67.
4. Keller, R.B., Tran, T.T., Pyott, S.M., Pepin, M.G., Savarirayan, R., McGillivray, G., Nickerson, D.A., Bamshad, M.J., and Byers, P.H. (2017). Monoallelic and biallelic CREB3L1 variant causes mild and severe osteogenesis imperfecta, respectively. Genet Med. Advance Online Publication: doi:10.1038/gim.2017.115.
5. Symoens, S., Malfait, F., D'hondt, S., Callewaert, B., Dheedene, A., Steyaert, W., Bachinger, H., De Paepe, A., Kayserili, H., and Coucke, P. (2013). Deficiency for the ER-stress transducer OASIS causes severe recessive osteogenesis imperfecta in humans. Orphanet J Rare Dis 8, e154.
6. Kondo, S., Murakami, T., Tatsumi, K., Ogata, M., Kanemoto, S., Otori, K., Iseki, K., Wanaka, A., and Imaizumi, K. (2005). OASIS, a CREB/ATF-family member, modulates UPR signalling in astrocytes. Nat Cell Biol 7, 186-194.
7. Garcia, I., Demichelis, V., Viale, D., Giusto, P., Ezhova, Y., Plishchuk, R., Sampieri, L., Martinez, H., Sztul, E., and Alvarex, C. (2017). CREB3L1-mediated functional and structural adaptation of the secretory pathway in hormone- stimulated thyroid cells. J Cell Sci 130, 4155-4167.
8. Nikaido, T., Yokoya, S., Mori, T., Hagino, S., Iseki, K., Zhang, Y., Takeuchi, M., Takaki, H., Kikuchi, S., and Wanaka, A. (2001). Expression of the novel transcription factor OASIS, which belongs to the CREB/ATF family, in mouse embryo with special reference to bone development. Histochem Cell Biol 116, 141-148.
9. Murakami, T., Saito, A., Hino, S., Kondo, S., Kanemoto, S., Chihara, K., Sekiya, H., Tsumagari, K., Ochiai, K., Yoshinaga, K., et al. (2009). Signalling mediated by the endoplasmic reticulum stress transducer OASIS is involved in bone formation. Nat Cell Biol 11, 1205-1211.
10. Vellanki, R., Zhang, L., Guney, M., Rocheleau, J., Gannon, M., and Volchuk, A. (2010). OASIS/CREB3L1 induces expression of genes involved in extracellular matrix production but not classical endoplasmic reticulum stress response genes in pancreatic beta-cells. Endocrinology 151, 4146-4157.
11. Asada, R., Saito, A., Kawasaki, N., Kanemoto, S., Iwamoto, H., Oki, M., Miyagi, H., Izumi, S., and Imaizumi, K. (2012). The endoplasmic reticulum stress transducer OASIS is involved in the terminal differentiation of goblet cells in the large intestine. J Biol Chem 287, 8144-8153.
12. Sillence, D., Senn, A., and Danks, D. (1979). Genetic heterogeneity in osteogenesis imperfecta. J Med Genet, 101-116.
13. Laflamme, M.A., Chen, K.Y., Naumova, A.V., Muskheli, V., Fugate, J.A., Dupras, S.K., Reinecke, H., Xu, C., Hassanipour, M., Police, S., et al. (2007). Cardiomyocytes derived from human embryonic stem cells in pro-survival factors enhance function of infarcted rat hearts. Nat Biotechnol 25, 1015-1024.

14. Karp, J.M., Ferreira, L.S., Khademhosseini, A., Kwon, A.H., Yeh, J., and Langer, R.S. (2006). Cultivation of human embryonic stem cells without the embryoid body step enhances osteogenesis in vitro. Stem Cells 24, 835-843.
15. Wang, Y.H., Liu, Y., Maye, P., and Rowe, D.W. (2006). Examination of mineralized nodule formation in living osteoblastic cultures using fluorescent dyes. Biotechnol Prog 22, 1697-1701.
16. Meloan, S., and Puchtler, H. (1985). Chemical mechanisms of staining methods: von Kossa's technique. What von Kossa really wrote and a modified reaction for selective demonstration of inorganic phosphate. J Histotechol 8, 11-13.
17. Livak, K.J., and Schmittgen, T.D. (2001). Analysis of relative gene expression data using real-time quantitative PCR and the 2(-Delta Delta C(T)) Method. Methods 25, 402-408.
18. Fisher, L., Stubbs, J., and Young, M. (1995). Antiseria and cDNA probes to human and certain animal model bone matrix noncollagenous proteins. Acta Orthop Scand Suppl 266, 61-65.
19. Li, H., Zhu, Y., Asakawa, M., Kuma, H., Hirata, T., Ueda, Y., Lee, Y., Fukumura, M., Iida, A., Kato, A., et al. (2000). A cytoplasmic RNA vector derived from nontransmissible Sendai virus with efficient gene transfer and expression. J Virol 74, 6564-6569.
20. Fusaki, N., Ban, H., Nishiyama, A., Saeki, K., and Hasegawa, M. (2009). Efficient induction of transgene-free human pluripotent stem cells using a vector based on Sendai virus, an RNA virus that does not integrate into the host genome. P Jpn Acad B-Phys 85, 348-362.
21. Takahashi, K., Tanabe, K., Ohnuki, M., Narita, M., Ichisaka, T., Tomoda, K., and Yamanaka, S. (2007). Induction of pluripotent stem cells from adult human fibroblasts by defined factors. Cell 131, 861-872.
22. Przyborski, S.A. (2005). Differentiation of human embryonic stem cells after transplantation in immune-deficient mice. Stem Cells 23, 1242-1250.
23. Ducy, P., Schinke, T., and Karsenty, G. (2000). The osteoblast: a sophisticated fibroblast under central surveillance. Science 289, 1501-1504.
24. Phillips, M.D., Kuznetsov, S.A., Cherman, N., Park, K., Chen, K.G., McClendon, B.N., Hamilton, R.S., McKay, R.D., Chenoweth, J.G., Mallon, B.S., et al. (2014). Directed differentiation of human induced pluripotent stem cells toward bone and cartilage: in vitro versus in vivo assays. Stem Cells Transl Med 3, 867-878.
25. Kuznetsov, S.A., Cherman, N., and Robey, P.G. (2011). In vivo bone formation by progeny of human embryonic stem cells. Stem Cells Dev 20, 269-287.
26. Bilousova, G., Jun, D., King, K., De Langhe, S., Chick, W., Torchia, E., Chow, K., Klemm, D., Roop, D., and Majka, S. (2011). Osteoblasts derived from induced pluripotent stem cells form calcified structures in scaffolds both in vitro and in vivo. Stem Cells 29, 206-216.
27. Stock, S.R. (2015). The mineral-collagen interface in bone. Calcif Tissue Int 97, 262-280.
28. Ishida, Y., Yamamoto, A., Kitamura, A., Lamande, S., Yoshimori, T., Bateman, J., Kubota, H., and Nagata, K. (2009). Autophagic elimination of misfolded procollagen aggregates in the endoplasmic reticulum as a means of cell protection. Mol Biol Cell 20, 2744-2754.
29. Garbes, L., Kim, K., Riess, A., Hoyer-Kuhn, H., Beleggia, F., Bevot, A., Kim, M.J., Huh, Y.H., Kweon, H.S., Savarirayan, R., et al. (2015). Mutations in SEC24D, encoding a component of the COPII machinery, cause a syndromic form of osteogenesis imperfecta. Am J Hum Genet 96, 432-439.

30. Jones, S.J., Glorieux, F.H., Travers, R., and Boyde, A. (1999). The microscopic structure of bone in normal children and patients with osteogenesis imperfecta: a survey using backscattered electron imaging. Calcif Tissue Int 64, 8-17.
31. Lindahl, K., Barnes, A.M., Fratzl-Zelman, N., Whyte, M.P., Hefferan, T.E., Makareeva, E., Brusel, M., Yaszemski, M.J., Rubin, C.J., Kindmark, A., et al. (2011). COL1 C-propeptide cleavage site mutations cause high bone mass osteogenesis imperfecta. Hum Mutat 32, 598-609.
32. Culbert, A.A., Lowe, M.P., Atkinson, M., Byers, P.H., Wallis, G.A., and Kadler, K.E. (1995). Substitutions of aspartic acid for glycine-220 and of arginine for glycine-664 in the triple helix of the proα1(I) chain of type I procollagen produce lethal osteogenesis imperfecta and disrupt the ability of collagen fibrils to incorporate crystalline hydroxyapatite. Biochem J 311, 815-820.
33. Levi, B., Hyun, J., Montoro, D., Lo, D., CHan, C., Hu, S., Sun, N., Lee, M., Grova, M., Connolly, A., et al. (2012). In vivo directed differentiation of pluripotent stem cells for skeletal regeneration. PNAS 109, 20379–20384.
34. Aubin, J. (1999). Osteoprogenitor cell frequency in rat bone marrow stromal populations: role for heterotypic cell-cell interactions in osteoblast differentiation. J Cell Biochem 72, 396-410.
35. Davies, J. (1996). In vitro modeling of the bone/implant interface. Anat Rec 245, 426-445.
36. Kanke, K., Masaki, H., Saito, T., Komiyama, Y., Hojo, H., Nakauchi, H., Lichtler, A.C., Takato, T., Chung, U.I., and Ohba, S. (2014). Stepwise differentiation of pluripotent stem cells into osteoblasts using four small molecules under serum-free and feeder-free conditions. Stem Cell Rep 2, 751-760.
37. Wang, Y., Yu, X., Baker, C., Murphy, W.L., and McDevitt, T.C. (2016). Mineral particles modulate osteo-chondrogenic differentiation of embryonic stem cell aggregates. Acta Biomater 29, 42-51.
38. Graneli, C., Thorfve, A., Ruetschi, U., Brisby, H., Thomsen, P., Lindahl, A., and Karlsson, C. (2014). Novel markers of osteogenic and adipogenic differentiation of human bone marrow stromal cells identified using a quantitative proteomics approach. Stem Cell Res 12, 153-165.
39. Foster, L., Zeeman, P., Li, C., Mann, M., Jensen, O., and Kassem, M. (2005). Differential expression profiling of membrane proteins by quantitative proteomics in a human mesenchymal stem cell line undergoing osteoblast differentiation. Stem Cells 25, 1367–1377.
40. Arpornmaeklong, P., Brown, S.E., Wang, Z., and Krebsbach, P.H. (2009). Phenotypic characterization, osteoblastic differentiation, and bone regeneration capacity of human embryonic stem cell-derived mesenchymal stem cells. Stem Cells Dev 18, 955-968.
41. Dillin A, Simic M, Schinzel RT, Moehle E, Halloran J. The activation of the UPR-ER is an essential step in the acquisition of pluripotency during reprogramming. (Abstract) Presented at the Annual Meeting of the International Society for Stem Cell Research, June 22-25, 2016, San Francisco, CA.
42. Lindert, U., Cabral, W.A., Ausavarat, S., Tongkobpetch, S., Ludin, K., Barnes, A.M., Yeetong, P., Weis, M., Krabichler, B., Srichomthong, C., et al. (2016). MBTPS2 mutations cause defective regulated intramembrane proteolysis in X-linked osteogenesis imperfecta. Nat Commun 7:11920.

Chapter 4: Biallelic Variants In *MESDC2,* Which Encodes A WNT-Signaling Related Protein, In Three Families With Recessively Inherited Osteogenesis Imperfecta

INTRODUCTION

Osteogenesis imperfecta (OI [MIM 166200, 166210, 259420, 166220]) is a heritable bone dysplasia marked by low bone mass and deformed, fragile bones, hence the commonly used description of "brittle bone disease". Genetic studies of individuals with this disorder in the last decade have led to an expanded understanding of the causative mechanisms. Whereas before, OI was thought to be associated only with dominant collagen variants (*COL1A1* [MIM 12050], *COL1A2* [MIM 120160]), it is now appreciated that recessive forms of OI result from variants in almost two dozen genes that encode proteins involved in regulation of collagen production; assembly, transport, chaperoning, and secretion of collagens; extracellular processing; and regulation of signaling pathways.[1] In the course of analysis of individuals with convincing clinical features and family history consistent with a diagnosis of OI, we have ascertained more than 60 patients in whom we have not been able to identify the causative variant. In three such families, we identified apparent homozygosity for mutations in Mesoderm Development Candidate 2 (*MESDC2*) [MIM 607783], which encodes a chaperone protein for Low-Density Lipoprotein Receptor-Related Protein 5 (LRP5) and LRP6, cell surface co-receptors for WNT proteins.[2; 3] This study contributes another addition to the repertoire of genes that underlie forms of OI.

MATERIALS & METHODS

Informed Consent: Written informed consent was obtained for all individuals in this study.

Exome Analysis & Identification Of *MESDC2*: We selected samples from four unrelated infants with severe OI phenotypes for exome sequence analysis and also included the unaffected sibling of one of these patients. (This approach is outlined by Pyott et al.[4] and was successful in identifying one of the first families in whom *WNT1* [MIM 164820] mutations were found to cause OI.) For the analysis, we assumed that the unrelated affected individuals did not have causative variants in the same genes. We also assumed that variants in infants from consanguineous families would be identical in both alleles. In the sibling pair, the affected child was found to be homozygous for a missense variant in *WNT1*[4]. Separately, another infant in the group was found to have a biallelic 20 kilobase deletion that encompassed exon 4 of *TMEM38B* [MIM 611236] and flanking splice sites. Prior to this analysis, this specific *TMEM38B* deletion had been described in other infants. Because of the geographical origin of the infant, we knew to search for that specific alteration.[5] The exome sequence analysis had no coverage in the region of exon 4 of *TMEM38B*, which confirmed the deletion. These three infants (unaffected, *WNT1*, and *TMEM38B*) were used as "unaffected" controls in the analysis of variants from the two remaining unsolved individuals since parental samples were not available.

The analysis identified 55,915 variants from the reference exome seen in one or more of the individuals who were sequenced. Removal of variants found in one unsolved proband that were also found in the other five individuals left 9198 variants. Subtraction of intergenic variants and those variants that appeared more than 10 times in the Exome Sequencing Project Exome Variant Server (EVS) left 936 variants. All heterozygous variants were discarded, as the pedigrees suggested recessive inheritance, which left 123 variants. After intronic variants and synonymous coding variants were discarded, there were 62 candidates left. Those variants with a conservation

score (consScoreGERP) >2 were discarded, leaving 24 variants. Of the 24, 11 genes were identified as potential candidates based on allele frequencies in the ExAC database (Table 4-1). In DNA from one affected infant, we identified apparent homozygosity for a variant in *MESDC2* (Figure 4-1A). We then screened an additional 60 probands with clinical OI in whom sequencing for *COL1A1*, *COL1A2*, and all other genes previously linked to OI was normal. Among these additional patients, we found two probands with biallelic variants in *MESDC2* (Figures 4-1B & 4-1C).

Genomic & cDNA Sequencing: DNA was extracted from patient fibroblasts or blood using the DNeasy Blood & Tissue Kit (Qiagen). RNA was extracted from 1:III-6 fibroblasts using the RNeasy Mini Kit (Qiagen) and cDNA was generated with the Superscript First Strand Synthesis System (Thermofisher Scientific). For confirmatory sequencing of *MESDC2*, exon 3 was amplified from either genomic DNA or cDNA using AmpliTaq Gold Polymerase (Applied Biosystems). The cycling program was: 95°C for 12 minutes, 95 °C for 10 seconds, 61 °C for 40 seconds, 72 °C for 50 seconds for 35 cycles, then, 72 °C for 7 minutes. Amplicons were treated with ExoSAP according to a standard protocol. Sequencing reactions were assembled using Big Dye v3.1 (Applied Biosystems) with the following program: 96°C for 10 seconds, 50 °C for 5 seconds, 60 °C for 4 minutes for 40 cycles. Sequencing was run on an ABI 3730. Sequences were analyzed using Mutation Surveyor v5.0 (Softgenetics). Primers used for genomic and cDNA sequencing of *MESDC2* were as follows: MESDC2 Genomic Sense 5'-TGCTCTGACCCCTTAGCACC-3', MESDC2 Genomic Antisense 5'-GGGCAAAGAGCTCTCCACG-3', MESDC2 cDNA Sense 5'-

GTCGGGTAAGCGCGTCTAGG-3', and MESDC2 cDNA Antisense 5'-AAGAGCTCTCCACGTCCACC-3'.

Immunoblotting: Protein lysates were prepared from primary fibroblasts using a buffer containing 0.05M Tris-HCl at pH 8.0, 0.15M NaCl, 5mM EDTA, 1% NP-40, and a protease inhibitor cocktail at 4 °C. 50μg of lysate was loaded per lane and resolved on a 10% SDS-PAGE gel in loading buffer containing 7.7 mg/ml dithiothreitol (DTT). Proteins were transferred to an Amersham Protran Premium 0.45μm Nitrocellulose Membrane (GE Healthcare). Detection for Western Blot was performed with primary antibodies for MESDC2 (sc-139397; Santa Cruz Biotechnology, Inc.) at 1:00, LRP5 (sc-390267; Santa Cruz Biotechnology, Inc.) at 1:200, LRP6 (sc-25317; Santa Cruz Biotechnology, Inc.) at 1:300, and GAPDH (ab179811: Abcam) at 1:100. Detection was achieved using Amersham ECL Western Blotting Detection Reagent (GE Healthcare).

In Vitro Transcription/Translation (IVTT): In vitro transcription/translation (IVTT) was achieved using the 1-Step Human Coupled IVT Kit–DNA (ThermoFisher Scientific). Templates for IVTT were generated from an *MESDC2* cDNA expression plasmid (SC304244) from OriGene Technologies. Family-specific mutations were introduced into the *MESDC2* sequence using the QuikChange II Site-Directed Mutagenesis Kit (Agilent Technologies). Primers used for mutagenesis were: QuikMESDC2_603-606delTAAA_F 5'-caaaggaggaggaagcaaagagaaaaaacaaagcaagacaa-3'; QuikMESDC2_603-606delTAAA_R 5'-ttgtcttgctttgtttttctctttgcttcctcctcctttg-3'; QuikMESDC2_632dupA_F 5'-caaagcaagacaagggcaaaaaaaaagaaggaaggagatct-3'; QuikMESDC2_632dupA_R 5'-

agatctccttccttctttttttttgcccttgtcttgctttg-3'; QuikMESDC2_c676t_F 5'-ttattcccagctcaattttcttccttggaagaccgaga-3'; and QuikMESDC2-c676t_R 5'-tctcggtcttccaaggaagaaaattgagctgggaataa-3'. Fragments containing the cDNA sequence with upstream T7 promoters were liberated using Sac-I (New England BioLabs) and gel purified using the QIAquick Gel Extraction Kit (Qiagen). Approximately 125ng of linearized template was used in IVTT reactions that were incubated for 6 hours at 30°C. 2µl of each IVT reaction was run on a 10% SDS-PAGE gel in loading buffer containing 7.7 mg/ml dithiothreitol (DTT). Western Blot was performed using primary antibody against MESDC2 (sc-139397; Santa Cruz Biotechnology, Inc.) at 1:100 followed by HRP-Conjugated Goat Anti-Rabbit IgG H&L (ab6721; Abcam) secondary antibody at 1:20,000. Detection was achieved using Amersham ECL Western Blotting Detection Reagent (GE Healthcare).

Immunocytochemistry (ICC): Primary dermal fibroblasts from I:III-6 and from a control patient (A8) cultured in DMEM 10% FBS were fixed in cold methanol for 10 minutes and incubated with 2.5% normal horse serum/PBS (Vector Laboratories) for 20 minutes at room temperature to block nonspecific binding of antibodies. The cells were incubated with primary antibody to MESDC2 (sc-139397; Santa Cruz Biotechnology, Inc.) at 1:50 at 4°C overnight. This was followed by incubation with AlexaFluor488 Goat Anti-Rabbit IgG (H&L) (A11034; ThermoFisher Scientific), 1:500, at room temperature for 1 hour. This stepwise staining process was repeated for KDEL (ab176333; Abcam) at 1:100 with AlexaFluor594 Goat Anti-Rabbit IgG (H&L) (A11037; ThermoFisher Scientific) at 1:800. The cells were counterstained with DAPI and mounted on slides. Images were acquired with a Zeiss Imager A1.

RESULTS

Clinical Presentations

Family 1 – 1:III-6 (Figure 4-1A) died in the neonatal period. She had a small chest and multiple fractures. Analysis of collagen synthesized and secreted by her cultured dermal fibroblasts revealed no alterations in the electrophoretic mobility of the chains of type I procollagen or collagen or the efficiency of secretion (data not shown). Her parents (1:II-1, 1:II-2) were double first cousins. They had two prior pregnancies that were also affected (1:III-4, 1:III-5) and had three unaffected children (1:III-1, 1:III-2, 1:III-3). Radiographs of 1:III-6 showed a thin calvarial mantle (there was not enough clarity to determine if wormian bones were present), thin ribs with fractures, and marked deformity, fracture, and shortening of the long bones (Figure 4-1D). The radiographic features were consistent with severe OI Type III in the original Sillence classification[6]. No other clinical information was available. 1:III-6 was homozygous for a 4bp deletion in the last exon of *MESDC2* (c.603-606delTAAA [p.Asn201Lysfs*15]) (Figure 4-2A) that led to a frameshift and premature termination 15 codons downstream from the deletion and prior to the constitutive termination codon. Sequence analysis of cDNA from cultured skin fibroblasts derived from 1:III-6 showed that all stable transcripts had the deletion (Figure 4-2B). Parental samples were not available to confirm that each carried the variant or to determine if the deletion-bearing transcript was as stable as that encoded by the normal allele.

Family 2 – The proband in Family 2 (2:III-4) was a 5-year-old boy who had been diagnosed with OI at birth as a result of multiple *in utero* fractures. When assessed at the age of 5 years, he had leg and shoulder deformities, triangular facies, and poor muscle tone. He was non-ambulatory.

Most of his teeth had fallen out, but it was unclear whether this was due to dentinogenesis imperfecta (DI) or to other factors (e.g., poor nutrition, gum disease). His parents (2:II-1, 2:II-2) were first cousins. We determined the child was homozygous for a single base pair duplication in the last exon of *MESDC2* (c.632dupA [p.Lys212Glufs*19]) (Figure 4-2A) that led to a frameshift and a premature termination codon 19 codons downstream from the frameshift and upstream of the constitutive termination site. His parents were each heterozygous for the duplication (Figure 4-2B). Cultured fibroblasts were not available from the proband in the family or from the parents.

Family 3 – The proband in Family 3 (3:III-2) was a 5-year-old boy with blue sclerae. He had fractures in his upper and lower limbs, sternum, and ribs. He had left femoral and a right upper limb deformity and underwent surgery (femoral shaft osteotomy and fixation). His parents (3:II-1, 3:II-2) were first cousins once-removed. The boy was homozygous for a variant in *MESDC2* (c.676C>T [p.Arg226*]) (Figure 4-2A) that generates a premature termination codon and deletes the last 9 amino acids of the protein. His father and mother were each carriers of the variant (Figure 4-2B).

Analysis Of mRNA Stability And Protein In Cells From One Proband

All three variants are found in the last exon of *MESDC2* and, thus, are unlikely to lead to nonsense-mediated mRNA decay. We confirmed this assumption by cDNA sequence analysis in cells from the proband in Family 1 (Figure 4-2A). In spite of the presence of stable mRNA, the MESD protein was not detected in the cell lysate from 1:III-6 fibroblasts, while it could be detected in control cells (Figure 4-3A). The loss of the ER retention signal (REDL) due to the

stop-gain could explain this finding. In COS-1 fibroblasts that were overexpressing a mutant MESD protein missing the REDL sequence, MESD was not retrieved from the Golgi and was allowed to travel through the secretory pathway into the media.[7] Levels of LRP5 and LRP6, meanwhile, were similar to control (Figure 4-3A). Cells from affected individuals in Families 2 and 3 were not available, therefore cDNA and protein studies could not be performed. However, the proximity of the variants and the similarity of predicted sequence outcomes suggest that the Family 2 and 3 MESD variant proteins share the same fate (Figure 4-3B).

Loss Of The REDL Sequence Is Likely Pathogenic

To assess the relative stability of the variant proteins (i.e., whether additional residues present in the Family 2 and 3 sequences might affect MESD), we performed coupled *in vitro* transcription/translation (IVTT) using each of the variant sequences and found that all produced stable MESD equivalent to protein produced from the wild type sequence (Figure 4-3C). Observations in COS-1 fibroblasts[7] overexpressing a form of MESD lacking the REDL signal led us to suspect all variants might result in improper MESD localization and be pathogenic for that reason. In further support of this hypothesis, immunocytochemistry for MESD in primary fibroblasts from 1:III-6 showed weak and diffuse staining compared to the strong ER-localized staining observed in control fibroblasts (Figure 4-3D) possibly due, as discussed, to variant MESD not being retained. The Family 1 phenotype is more severe (perinatal lethal) than that of Families 2 and 3. The variant in Family 3 creates two sequences (KEGDL and KEEN) that might substitute for REDL and allow for some degree of retention that might explain a less severe phenotype in that family.

DISCUSSION

Of the candidate genes, none had known clinical implications relating to skeletal disorders, but one gene was involved in a pathway known to be important to bone development, specifically, in OI. *MESDC2* encodes a chaperone protein that is involved in the folding of two WNT co-receptors, LRP5 and LRP6, and in their localization to the cell surface.[7] LRP5 regulates peak bone mass in vertebrates. Homozygosity for inactivating variants in *LRP5* is the cause of reduced bone accrual and eye defects in patients with osteoporosis-pseudoglioma syndrome (OPPG) [MIM 259770].[8] In contrast, *LRP5* gain-of-function variants have been implicated in high bone mass (HBM) phenotypes, including endosteal hyperostosis [MIM 144750], van Buchem disease [MIM 607636], and osteopetrosis [MIM 607634].[9-11] Mice homozygous for a knockout allele of *Mesdc2* failed to establish a primitive streak and lacked a developed mesoderm[12] due to a patterning defect in the proximal epiblast;[7] this patterning defect is similar to the outcome of *Wnt3* knockout in embryos.[13] Additionally, variants in *WNT1* have been linked to severe OI [MIM 615220] and to osteoporosis.[4; 14-16] Because WNT signaling has well-established importance in skeletal development, *MESDC2* was thought to be the best candidate gene in Family 1. We then screened an additional 60 probands with clinical OI in whom sequencing for *COL1A1*, *COL1A2*, and all other genes previously linked to OI was normal. Among these additional patients, we found two more probands with biallelic variants in *MESDC2*.

Canonical WNT signaling involves binding of WNT proteins to the frizzled receptor (FZD) and to the co-receptors LRP5 and LRP6. Formation of this complex leads to the inhibition of glycogen synthase kinase 3β (GSK-3β), which would otherwise phosphorylate β-catenin. Unphosphorylated β-catenin is safeguarded from proteosomal degradation, accumulates, and

moves into the nucleus where it triggers lymphoid enhancer factor (LEF)/T-cell factor (TCF)-mediated gene transcription.[17] While WNT signaling pathways involved in bone biology have not been fully elucidated, targets of WNTs that are important for bone are thought to include Alkaline Phosphatase (*ALPL* [MIM 171760]), which plays a role in bone mineralization, and Specificity Protein 7 (*SP7*) [MIM 606633]), which encodes a transcription factor that controls the preosteoblast-to-osteoblast transition.[18; 19] Variants in *ALPL* cause hypophosphatasia [MIM 146300, 241510][20] and one reported variant in *SP7* was the genetic cause of a form of OI [MIM 613849].[21]

MESD is a 234 amino acid ER-localized protein.[7] MESD has an NH_2-terminal signal sequence (residues 1-33), a chaperone domain (residues 34-164) that facilitates folding of the β-propeller domains of LRP5 and LRP6, an escort domain (residues 165-204), and a COOH-terminal KDEL-like sequence (REDL) that distinguishes it from the secreted proteins it chaperones and allows for retrieval from the Golgi.[22] In all three families, the frameshift or stop-gain mutation results in loss of the REDL sequence. When synthesized in a transcription/translation cell free system, all three sequences produce a stable protein. In cells from one proband, the mRNA transcript is stable, but the protein cannot be detected by Western blot and is very poorly detected by immunofluorescence studies in cultured cells. It is possible that loss of the REDL signal results in MESD being secreted by the cell rather than being salvaged and returned to the ER to continue to perform its folding and chaperoning functions. Alternatively, loss of the REDL sequence may destabilize the protein, a possibility suggested by study of other OI-causing genes involved in the collagen synthetic pathway. In the Prolyl-3 Hydroxylase (P3H1)–Cartilage-Associated Protein (CRTAP)–Cyclophilin B (CypB) molecular complex, responsible for the

post-translational modification of type I collagen alpha chains, if either the KDEL-containing P3H1 or the KDEL non-containing CRTAP is null, both proteins are unstable and absent from the cell.[23] It was later reported that loss of the P3H1 KDEL retention sequence alone was sufficient for loss of both P3H1 and CRTAP and the cause of OI in one family, though only intracellular P3H1 and CRTAP were analyzed, leaving open the question of whether stable secreted protein from these cells would be detectable.[24] While we were able to detect LRP5 and LRP6 protein in cell lysates from patient cells, we were not able to determine their localization using immunocytochemistry. We could not determine whether this was due to poor patient cell quality or lack of the chaperone protein MESD. It is unclear whether the expression and activity of MESD, LRP5, LRP6, and the appropriately-interacting WNTs in fibroblasts would be representative of osteogenic cells.

In the three families presented, biallelic frameshifts in the last exon in *MESDC2* led to severe OI phenotypes. These variants are not noted in the NHLBI EVS, the ExAC database, gnomAD, or in dbSNP. In the gnomAD database, there are 7 frameshift variants in the last exon that might have similar effects to those seen here. This represents a carrier frequency of about 1/10,000 individuals meaning homozygosity or compound heterozygosity would lead to a very low frequency of the disorder. *MESDC2* variants accounted for 4.8% of the 63 unsolved OI families we tested but represent 3 of more than 3000 individuals in whom we have identified the causative variants. In the absence of MESD, LRP5 and LRP6 are retained in the ER as high molecular weight aggregates[7]. We expect that loss of functional MESD in these individuals prevents proper formation and localization of the WNT co-receptors LRP5 and LRP6 to the cell surface without which WNTs cannot bind and WNT signaling is blocked. The WNT signaling

pathways that are important to bone development and bone metabolism are not yet fully defined but, given that variants in several genes in this pathway have been linked to bone dysplasia (*WNT1*, *LRP5*, and now *MESDC2*), it is clear they play an integral role. A more complete understanding may require studies in osteogenic cells.

FIGURES & TABLES

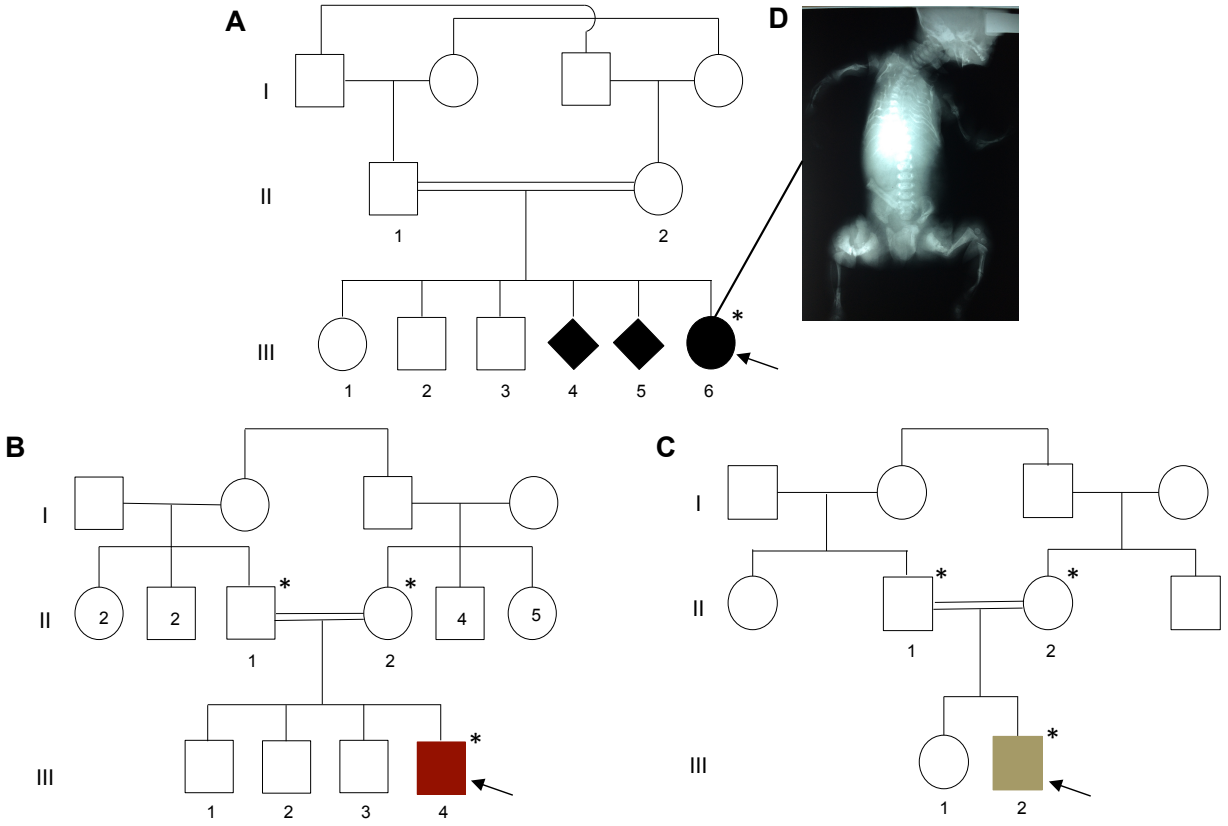

Figure 4-1. Pedigrees Of Families With *MESDC2* Variants. Families (A) 1, (B) 2, and (C) 3. Individual 1:III-6 was exomed leading to the identification of *MESDC2*. The proband in each family is indicated by an arrow. Filled circles represent individuals with OI. Individuals who were studied in each family are noted with asterisks. D) Imaging of individual 1:III-6 shows limited cavarial mineralization, small chest with thin ribs, fractures in upper and lower extremities, and platyspondyly. These findings are compatible with an OI Type III-like presentation.

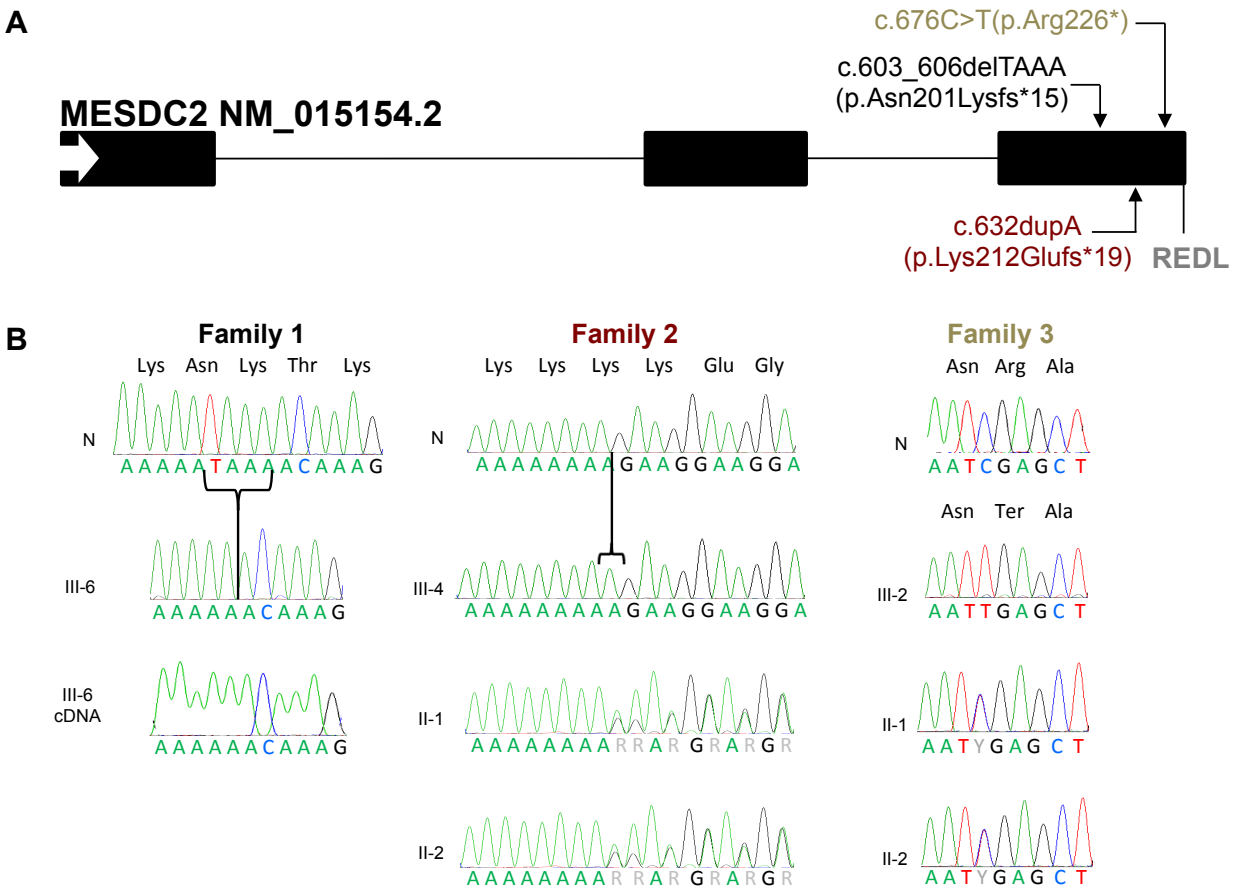

Figure 4-2. *MESDC2* Variants. A) Exon-intron structure of the *MESDC2* coding sequence and location of variants in Family 1, Family 2, and Family 3. B) Variant sequences from available family members confirming the homozygous small deletion (c.603-606delTAAA) in Family 1 (both in proband genomic DNA and cDNA), the duplication (c.632dupA) in Family 2, (in the homozygous proband and in both heterozygous parents), and the substitution mutation (c.676C>T) in Family 3 (in the homozygous proband and in both heterozygous parents). The normal reference sequences are labeled 'N'.

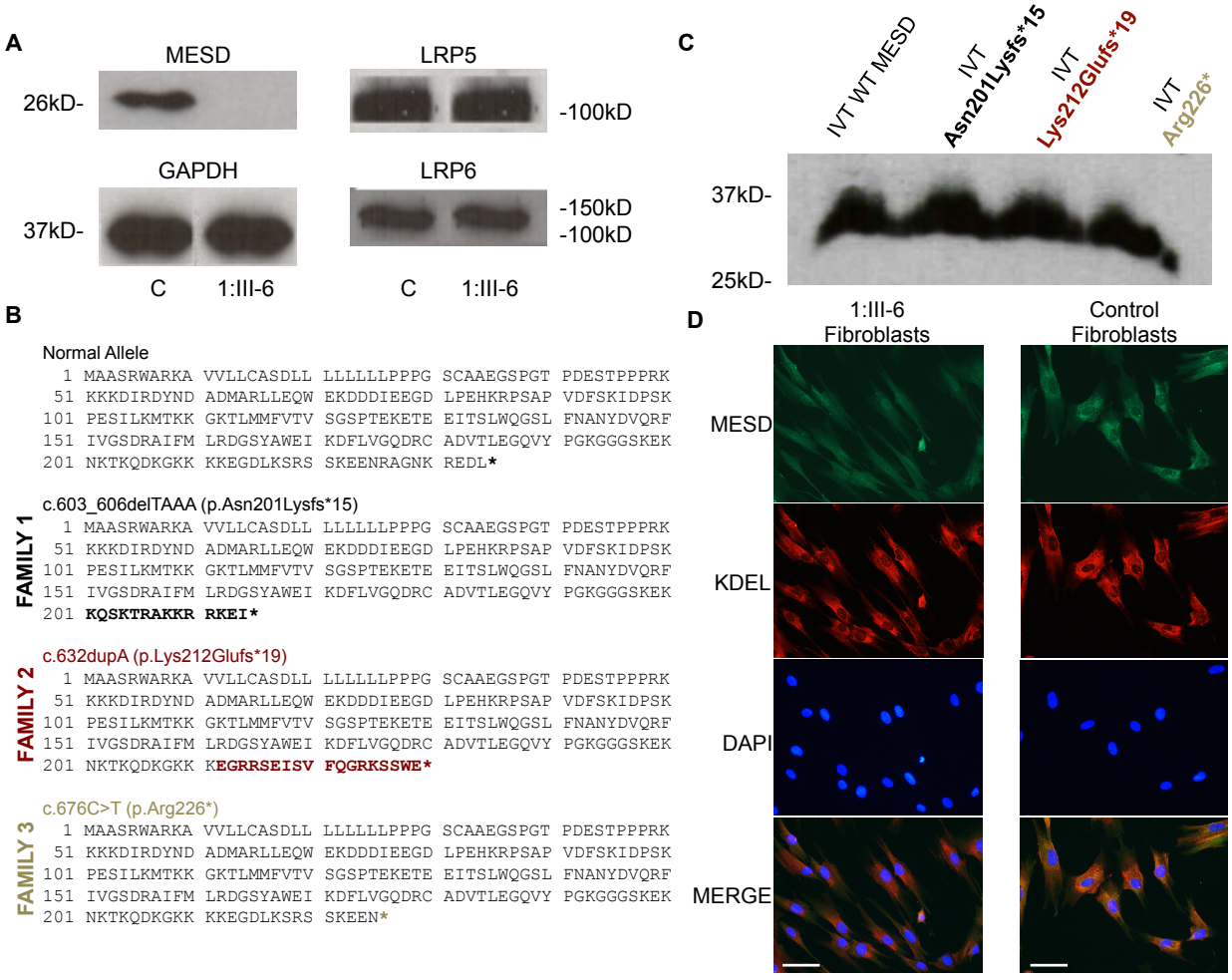

Figure 4-3. Loss Of The REDL Sequence In MESD Is Likely Pathogenic. A) Protein studies on cultured fibroblasts from the proband in Family 1 (1:III-6) demonstrate the absence of MESD protein in the cell lysate. Levels of LRP5 and LRP6 appear normal. Western Blot. B) The variants in Families 1 and 2 cause frameshifts and introduce premature termination codons 15 and 19 codons downstream of the frameshifts, respectively. The variant in Family 3 changes an asparagine residue to a stop codon, resulting in premature termination. All three variants cause the loss of the REDL ER-retention sequence needed for retrieval from the Golgi. C) IVTT of the variant *MESDC2* sequences results in production of stable MESD protein in all cases. D) Variant MESD lacking the REDL sequence is weakly-staining and diffuse throughout the cytoplasm in 1:III-6 primary fibroblasts, while it is properly ER-localized in healthy control cells. Scale Bars = 50µm. ICC.

Table 4-1. Candidate Genes From Exome Analysis

Chromosomal Location	Gene	Protein	Coding Change	Protein Change	Alteration	Clinical Associations
Chromosome 1: 66,533,383-66,748,299	*SGIP1* MIM 611540	SH3-Domain GRB2-Like (Endophilin)-Interacting Protein 1 (SGIP1)	c.1199C>A	p.Pro400His	missense	N/A
Chromosome 1: 205,042,937-205,078,499	*CNTN2* MIM 190197	Contactin 2 (CNTN2)	c.2377C>T	p.Arg793Cys	missense	epilepsy [25]
Chromosome 3: 126,006,355-126,101,561	*SLC41A3* MIM 610803	Solute Carrier Family 41, Member 3 (SLC41A3)	c.533G>A c.776G>A c.806G>A c.884G>A	p.Ile178Thr p.Ile259Thr p.Ile269Thr p.Ile295Thr	missense	N/A
Chromosome 12: 6,693,792-6,700,800	*PIANP* MIM 616065	PILR-Alpha-Associated Neural Protein (PANP)	c.214G>A	p.Arg72Trp	missense	immune regulation (*m. musculus)* [26]
Chromosome 13: 96,090,839-96,839,562	*HS6ST3* MIM 609401	Heparin Sulfate 6-O-Sulfotransferase 3 (HS6ST3)	c.688C>T	p.Arg230Cys	missense	N/A
Chromosome 14: 57,200,507-57,269,008	*EXOC5* MIM 604469	SEC10-Like 1 (SEC10L1)	c.2074C>T	p.Val692Ile	missense	N/A
Chromosome 15: 80,946,289-80,989,878	*MESDC2* MIM 607783	Mesoderm Development Gene (MESD)	c.603-606delTAA	p.Asn201Lysfs*15	frameshift	failure to form mesoderm, patterning defects, embryonic lethality (*m. musculus*) [6; 11]
Chromosome 17: 7,839,904-7,854,796	*KDM6B* MIM 611577	Jumonji Domain-Containing Protein 3 (JMJD3)	c.1825G>A	p.Ala609Thr	missense	Mental Retardation, Autosomal Recessive 33 [MIM 614341] (not confirmed) [27; 28]
Chromosome 19: 11,834,341-11,419,342	*RGL3* MIM 616473	Ral Guanine Nucleotide Dissociation Stimulator-Like 3 (RGL3)	c.1046G>T	p.Ala349Asp	missense	N/A
Chromosome 19: 49,766,968-49,807,113	*AP2A1* MIM 601026	Clathrin Adaptor Complex AP2, Alpha Subunit (AP2-Alpha)	c.2063G>T	p.Gly688Val	missense	N/A
X Chromosome: 73,212,299-73,214,848	*NAP1L2* MIM 300026	Brain Specific Gene BPX (BPX)	c.1285A>G	p.Tyr429His	missense	neural tube defects (*m. musculus*) [29]

REFERENCES

1. Marini, J.C., Forlino, A., Bachinger, H.P., Bishop, N.J., Byers, P.H., Paepe, A., Fassier, F., Fratzl-Zelman, N., Kozloff, K.M., Krakow, D., et al. (2017). Osteogenesis imperfecta. Nat Rev Dis Primers 3, 17052.
2. Tamai, K., Semenov, M., Kato, Y., Spokony, R., Liu, C., Katsuyama, Y., Hess, F., Saint-Jeannet, J., and He, X. (2000). LDL-receptor-related proteins in Wnt signal transduction. Nature 407.
3. Pinson, K., Brennan, J., Monkley, S., Avery, B., and Skarnes, W. (2000). An LDL-receptor-related protein mediates WNT signalling in mice. Nature 407, 535-538.
4. Pyott, S., Tran, T., Leistritz, D., Pepin, M., Mendelsohn, N., Temme, R., Fernandez, B., Elsayed, S., Elsobky, E., Verma, I., et al. (2013). WNT1 mutations in families affected by moderately severe and progressive recessive osteogenesis imperfecta. Am J Hum Genet 92, 590-597.
5. Shaheen, R., Alazami, A.M., Alshammari, M.J., Faqeih, E., Alhashmi, N., Mousa, N., Alsinani, A., Ansari, S., Alzahrani, F., Al-Owain, M., et al. (2012). Study of autosomal recessive osteogenesis imperfecta in Arabia reveals a novel locus defined by TMEM38B mutation. J Med Genet 49, 630-635.
6. Sillence, D., Senn, A., and Danks, D. (1979). Genetic heterogeneity in osteogenesis imperfecta. J Med Genet, 101-116.
7. Hsieh, J., Lee, L., Zhang, L., Wefer, S., Brown, K., DeRossi, C., Wines, M., Rosenquist, T., and Holdener, B. (2003). Mesd encodes an LRP5/6 chaperone essential for specification of mouse embryonic polarity. Cell 112, 355-367.
8. Gong, Y., Slee, R.B., Fukai, N., Rawadi, G., Roman-Roman, S., Reginato, A.M., Wang, H., Cundy, T., Glorieux, F.H., Lev, D., et al. (2001). LDL receptor-related protein 5 (LRP5) affects bone accrual and eye development. Cell 107, 513-523.
9. Boyden, L.M., Mao, J., Belsky, J., Mitzner, L., Farhi, A., Mitnick, M.A., Wu, D., Insogna, K., and Lifton, R.P. (2002). High bone density due to a mutation in LDL-receptor-related protein 5. NEJM 346, 1513-1521.
10. Little, R.D., Carulli, J.P., Del Mastro, R.G., Dupuis, J., Osborne, M., Folz, C., Manning, S.P., Swain, P.M., Zhao, S.C., Eustace, B., et al. (2002). A mutation in the LDL receptor-related protein 5 gene results in the autosomal dominant high-bone-mass trait. Am J Hum Genet 70, 11-19.
11. Van Wesenbeeck, L., Cleiren, E., Gram, J., Beals, R.K., Benichou, O., Scopelliti, D., Key, L., Renton, T., Bartels, C., Gong, Y., et al. (2003). Six novel missense mutations in the LDL receptor-related protein 5 (LRP5) gene in different conditions with an increased bone density. Am J Hum Genet 72, 763-771.
12. Holdener, B.C., Faust, C., Rosenthal, N.S., and Magnuson, T. (1994). msd is required for mesoderm induction in mice. Development 120, 1335-1346.
13. Liu, P., Wakamiya, M., Shea, M.J., Albrecht, U., Behringer, R.R., and Bradley, A. (1999). Requirement for wnt3 in vertebrate axis formation. Nat Genet 22, 361-365.
14. Keupp, K., Beleggia, F., Kayserili, H., Barnes, A.M., Steiner, M., Semler, O., Fischer, B., Yigit, G., Janda, C.Y., Becker, J., et al. (2013). Mutations in WNT1 cause different forms of bone fragility. Am J Hum Genet 92, 565-574.
15. Laine, C.M., Joeng, K.S., Campeau, P.M., Kiviranta, R., Tarkkonen, K., Grover, M., and Makitie, O. (2013). WNT1 mutations in early-onset osteoporosis and osteogenesis imperfecta. NEJM 368, 1809-1816.

16. Fahiminiya, S., Majewski, J., Mort, J., Moffatt, P., Glorieux, F.H., and Rauch, F. (2013). Mutations in WNT1 are a cause of osteogenesis imperfecta. J Med Genet 50, 345-348.
17. Kubota, T., Michigami, T., and Ozono, K. (2009). Wnt signaling in bone metabolism. J Bone Miner Metab 27, 265-271.
18. Fujita, K., and Janz, S. (2007). Attenuation of WNT signaling by DKK-1 and -2 regulates BMP2-induced osteoblast differentiation and expression of OPG, RANKL and M-CSF. Mol Cancer 6, 71.
19. Heo, J.S., Lee, S.Y., and Lee, J.C. (2009). Wnt/B-catenin signaling enhances osteoblastogenic differentation from human periodontal ligament fibroblasts. Mol Cells 30, 449-454.
20. Weiss, M.J., Cole, D.E.C., Ray, K., Whyte, M.P., Lafferty, M.A., Mulivor, R.A., and Harris, H. (1988). A missense mutation in the human liver:bone:kidney alkaliine phosphatase gene causing a lethal form of hypophosphatasia. P Natl Acad Sci USA 85, 7666-7669.
21. Lapunzina, P., Aglan, M., Temtamy, S., Caparros-Martin, J.A., Valencia, M., Leton, R., Martinez-Glez, V., Elhossini, R., Amr, K., Vilaboa, N., et al. (2010). Identification of a frameshift mutation in osterix in a patient with recessive osteogenesis imperfecta. Am J Hum Genet 87, 110-114.
22. Chen, J., Liu, C.C., Li, Q., Nowak, C., Bu, G., and Wang, J. (2011). Two structural and functional domains of MESD required for proper folding and trafficking of LRP5/6. Structure 19, 313-323.
23. Chang, W., Barnes, A.M., Cabral, W.A., Bodurtha, J.N., and Marini, J.C. (2010). Prolyl 3-hydroxylase 1 and CRTAP are mutually stabilizing in the endoplasmic reticulum collagen prolyl 3-hydroxylation complex. Hum Mol Genet 19, 223-234.
24. Takagi, M., Ishii, T., Barnes, A.M., Weis, M., Amano, N., Tanaka, M., Fukuzawa, R., Nishimura, G., Eyre, D.R., Marini, J.C., et al. (2012). A novel mutation in LEPRE1 that eliminates only the KDEL ER- retrieval sequence causes non-lethal osteogenesis imperfecta. PLoS One 7, e36809.
25. Stogmann, E., Reinthaler, E., Eltawil, S., El Etribi, M.A., Hemeda, M., El Nahhas, N., Gaber, A.M., Fouad, A., Edris, S., Benet-Pages, A., et al. (2013). Autosomal recessive cortical myoclonic tremor and epilepsy: association with a mutation in the potassium channel associated gene CNTN2. Brain 136, 1155-1160.
26. Kogure, A., Shiratori, I., Wang, J., Lanier, L.L., and Arase, H. (2011). PANP is a novel O-glycosylated PILRalpha ligand expressed in neural tissues. Biochem Biophys Res Commun 405, 428-433.
27. Najmabadi, H., Hu, H., Garshasbi, M., Zemojtel, T., Abedini, S.S., Chen, W., Hosseini, M., Behjati, F., Haas, S., Jamali, P., et al. (2011). Deep sequencing reveals 50 novel genes for recessive cognitive disorders. Nature 478, 57-63.
28. Kuss, A.W., Garshasbi, M., Kahrizi, K., Tzschach, A., Behjati, F., Darvish, H., Abbasai-Moheb, L., Puettmann, L., Zecha, A., Weibmann, R., et al. (2011). Autosomal recessive mental retardation: homozygosity mapping identifies 27 single linkage intervals, at least 14 novel loci and several mutation hotspots. Hum Genet 129, 141-148.
29. Rogner, U.C., Danoy, P., Matsuda, F., Moore, G.E., Stanier, P., and Avner, P. (2002). SNPs in the CpG island of NAP1L2: a possible link between DNA methylation and neural tube defects? Am J Med Genet 110, 208-214.

Chapter 5: The 'Brittleness' Of OI Bone

INTRODUCTION & BACKGROUND

As a material, bone extracellular matrix is a biological composite of singular quality. While able to match the tensile strength and load-bearing capacity of cast iron, it is also remarkably flexible. The marriage of these two properties is necessary for mechanical support of the body, particularly for locomotion. Strength and flexibility are correspondingly conferred by a mineral reinforcement phase consisting of carbonated apatite and a soft collagenous matrix.[1] However, the material properties of bone, of all composites, are not simply bulk (i.e., the average of their constituent phases), but are also reliant on the relative volumetric contributions of each phase and on the interactions between phases on multiple scales, e.g., fibril-fibril, mineral-collagen, intra-lamellar (the layers of bone secreted by an osteoblast), intra-osteon (the basic unit of structure in compact bone consisting of concentric lamellae surrounding vasculature), etc.[1; 2] Consequently, pathologic changes to bone material properties, e.g., the gracile bones of patients with osteogenesis imperfecta (OI), may originate from disruptions on any of these scales. Our work in human induced pluripotent stem cell (hiPSC)-derived osteoblast-like cells revealed how OI-causing variants in different genes can yield similar cellular phenotypes that account for similar clinical phenotypes (Chapter 3). This chapter will attempt to explain how discrete molecular mechanisms can lead to the same tissue-scale phenotype, the OI-defining feature of "brittle bones", illuminated by research in the fields of biochemistry, biophysics, biomaterials, and biomineralization, among others.

NORMAL BONE

A Hierarchical Structure (Molecular < Fibrillar < Mineralized Matrix < Tissue)

Before a discussion of fragility can be had, the multiscale structure of bone material in its healthy state must be appreciated. The lowest scale of bone structure is the mature collagen type I molecule (known as a "tropocollagen") which has a 1.23nm width and a 300nm length.[3] In lamellar (i.e., mature) bone, tropocollagens self-assemble[4] into a highly-ordered characteristic fibril structure. First, groups of five tropocollagens organize into "microfibrils"[5]; individual molecules are arranged parallel to each other in a quarter-stagger pattern in which adjacent molecules overlap by 27nm with a 40nm gap between tropocollagens axially[6] (Figure 5-1A). The 27nm overlap and 40nm gap regions together (~67nm) define the periodicity of the collagen fiber, referred to as the "D" period[6]; this arrangement gives the fibrillar collagens their characteristic banded appearance in electron microscopy (EM) images. Microfibrils assemble and interdigitate to form fibril structures with diameters of 100-200nm in bone (fibril size ranges widely in other collagenous tissues). Arrangement of microfibrils into a 3D structure occurs such that channels through the fibril are created from the alignment of the gap regions that separate axial molecules.[1]

At first, the fibril structure is stabilized by hydrogen bonding between water molecules that fill the spaces amid adjacent tropocollagens[7] and by immature enzymatic crosslinks directly between tropocollagen molecules which are heavily dependent on the posttranslational modification of collagen type I chains (i.e., aldehyde formation from hydroxylated lysines, the telopeptide lysines especially). As the fibrils mature, so too do the crosslinks, spontaneously converting from divalent to trivalent.[8] These interactions serve to bolster the collagen fibrils when mechanically

loaded. With ageing, non-specific intermolecular cross-links involving glucose begin to form (a process called "glycation"), causing collagen fiber stiffening and contributing to ageing phenotypes, e.g., stiffness of joints, skin, tendon, and bone with implications for ambulation, vascularization, the filtration capability of basement membranes, etc.[8]

The rigidity of bone is attributable to the mineralization of osteoid (the organic collagenous matrix). The inorganic mineral phase of bone is made up of calcium phosphate in a structure ($Ca_{10}[PO_4]_6[OH]_2$) called hydroxyapatite (HA). In collagen fibrils, nucleating HA crystals sit in the 40nm gaps between axially-arranged tropocollagens and grow to fill those spaces and also onto the exterior fibril surface[1] forming nanoplatelets 3-4nm in length.[9] Non-collagenous proteins (NCPs) present in bone extracellular matrix (ECM) (i.e., osteocalcin, osteonectin, osteopontin, bone sialoprotein) have binding affinity for collagen and for calcium and seem to control mineral-collagen interactions including crystal nucleation and growth, effectively regulating matrix mineralization.[10] In the field of biomineralization, there is debate as to whether bone mineral is first deposited as amorphous calcium phosphate which then becomes reordered in mature mineralized matrix.[11] Characterization of a transient octacalcium phosphate (OCP) intermediate in closing cranial sutures in *Mus musculus* was the first reported evidence of such a process occurring in mammalian bone.[12] Another stimulating question is how mineralization is restricted to bony tissues within the body and normally avoided in other collagen-containing tissues. Ectopic ECM mineralization is pathological, e.g., in joints causing osteoarthritis.[13] The first pass at an explanation for the spatial restriction of ECM mineralization was that expression of osteoblast-specific genes was required to initiate the process, but the fact that ectopic mineralization occurs at all (in the absence of osteoblasts in tissues that are not bone) countered

this initial notion.[14] Instead, there seems to be a dual requirement. High levels of pyrophosphate (PP_i), an inhibitor of mineralization, are ubiquitously expressed in tissues and cells, including in osteoblasts. In bone, removal of this inhibition is achieved through the cleavage of PP_i by Tissue Non-Specific Alkaline Phosphatase (TNAP). Joint expression of *TNAP* with expression of high levels of *COL1A1* and *COL1A2* to produce a rich fibrillar matrix are co-requirements for ECM mineralization. Though these genes are widely expressed, they are normally only co-expressed in osteoblasts.[13]

In 1693, Antonie van Leeuwenhoek published his observations of an ox thigh bone as viewed through his state-of-the-art compound microscope and described the presence of several sorts of "tubuli".[15] What he had seen through his glass were osteons, the basic unit of structure in the compact form of bone. In long bones, most commonly affected in OI, there are two subtypes of lamellar bone: "compact" or "cortical" bone which is dense and forms the outer wall of the long bone and "cancellous" or "medullary" bone which consists of networks of trabeculae amongst empty hollow spaces.[16] Histologically, transverse sections of cortical bone reveal circular osteons – concentric layers of lamellae (mineralized bone matrix) encircling a Haversian canal (named for Clopton Havers who had identified them microscopically in 1691)[17] which houses blood vessels, lymphatics, and nerves (Figure 5-1B). The need for this structure is owing to the mineral content of bone which impedes the diffusion of nutrients to resident osteocytes. Unlike cartilage, bone must be vascularized. Formation of an osteon begins with bone-resorptive osteoclasts boring a hole through the matrix. Then, osteoblasts lay down lamellar rings from the outside of this hole inward until the cells are completely surrounded by matrix, becoming inactive osteocytes that reside in empty spaces called lacunae. Osteocytes project their

cytoplasmic processes through fine passages called canaliculi, connecting to other osteocytes in nearby lacunae[16] to form a cell network, the "syncytium".[18] As bone is continuously remodeled, osteons are resorbed and reformed. Leftover lamellae from old resorbed osteons are found between intact Haversian systems (i.e., osteons) and are referred to as interstitial systems.[16]

Mechanical Properties Of Bone

In material science, mechanical properties that dictate material behavior include stiffness, strength, and toughness. Loosely defined, stiffness regards resistance to deformation when acted upon by a force, strength is the maximum force a material can sustain without failing (i.e., breaking), and toughness is a measure of how much energy a material can absorb before failing. Stiffness and toughness are in opposition to each other within a material, one suffering if the other predominates. The properties of mineralized bone matrix lie acceptably between the extremes of either as both properties are necessary in order for bone to serve as the mainframe of the body. The stiffness of bone prevents the skeleton from deforming under the load of body weight and allows for ambulation. Toughness, on the other hand, is the more vital property for fracture resistance.[2]

An exact measure of bone toughness is difficult to obtain as it relies not merely on the average toughness of the inorganic and organic phases (an approach to calculations for inhomogeneous materials that works for other properties, like stiffness), but also on the response of bone to damage, e.g., the progression of cracking, which is governed at any given moment more by the interactions between the phases (e.g., mineral-collagen) and between elements within each phase (e.g., fibril-fibril) than by single phases or single elements themselves. A more correct measure

of toughness is the amount of energy that is dissipated when a crack in the material forms. If the energy dissipated exceeds the energy of impact, e.g., from a boulderer's fall, a crack may nucleate or propagate, but the bone will not break. In bone, following trauma, any resulting damage is repaired through the continuous bone remodeling process.[18] Thus, healthy bone is able to weather the stresses and strains of daily life on the move.

Toughening Mechanisms

While total bone mass and geometry do have a role in determining toughness, they are not sufficient to explain the astonishing properties of a material which, reductively, can be viewed as a recipe of brittle mineral, polymer, and water.[2] It is the multiscale structure of bone, with toughening mechanisms acting on every scale, that explains this marvel. At the smaller scales, stress from an external tensile load is transferred by shearing on multiple scales – between fibers in the tissue, between individual fibrils in a fiber, and between mineral nanoplatelets – causing coupled and cooperative deformation with each structural scale taking up less and less of the overall strain in a ratio of 12:5:2.[19] Energy is dissipated through the "sacrificial" breaking of non-covalent bonds.[2]

Several toughening mechanisms that operate at the tissue scale relate to crack formation. Ahead of a crack tip, there are often thinner microcracks that diverge away from the crack front, which conceivably divert energy, slowing the progression of the greater crack.[2] The presence of this diffuse microdamage may also encourage the remodeling process.[18] Another toughening mechanism is crack deviation, visually evidenced as the zig-zag pattern of cracks, by which crack growth is slowed when encountering different architectures within the bone material, e.g.,

when cracks hit a lamella-lamella interface or when cracks hit an osteon. Indeed, the spherical architecture of the osteon is protective of the vessels within; in other porous brittle materials, pores and cavities are the sites of concentrated stress and are susceptible to the initiation of cracks.[20] Finally, fibers behind the crack front will sometimes reorient, causing the crack to shift, without zig-zagging, jumping or skipping such that a new crack is initiated and fibrous or ligamentous "bridges" are left between bone segments. These crack ligament bridges can then carry some of the applied load and reduce the crack-driving force.[2; 18]

The inhomogeneity of bone material is toughening in and of itself. The crack-driving force is progressively deadened as it travels through different regions of bone material, each of which has its own unique set of mechanical properties, even from lamella to lamella. (Materials like this are called "anisotropic".) While some regions will dissipate less energy, others will dissipate more, and the crack energy is eventually drowned in the troughs of this periodical variation.[2]

FRAGILE BONE

The formula for bone material and the structure of bone tissue are exact. Alteration to either yields bone that is less well suited to the tasks of stabilizing and protecting the body. The changes in OI bone stem from a variety of molecular mechanisms, but all these alterations issue upward through the fibril, matrix, tissue, and skeletal scales, weakening toughening mechanisms and increasing fragility. The disruption of osteoblast differentiation, maturation, and functioning by variants in *SP7*, *TMEM38B*, *WNT1*, and *MESDC2* might be described as the most fundamental OI-causing defects, as they involve the arrest of bone formation initiation.

Alterations At The Molecular Scale, Effects On The Fibrillar Scale

The functional 3D structuring of collagen fibers is dependent on the functional 3D structuring of collagen fibrils, which relies on the production of tropocollagens with typical 3D structure. *COL1A1* and *COL1A2* variants that disrupt collagen folding leading to excessive posttranslational modification (e.g., glycine substitution variants and COOH-propeptide and COOH-telopeptide variants) and variants in genes involved in placing those modifications (*CRTAP*, *P3H1*, *PPIB, FKBP10*) lead to the production of abnormally structured tropocollagens. *BMP1* variants may be expected to fall into this category as well, as failure to remove the COOH-propeptide leads to incorporation of pC-collagen (mature collagen type I with the attached C-propeptide) into forming matrix.[21] Fibrillogenesis still follows, but fibrils do not have the typical dimensions or interactions and the mechanical properties of bone suffer as a result.

Study of the *oim* mouse speaks to what specific effects abnormal tropocollagen may have on matrix ultrastructure. In these mice, a mutation in *Col1a2* prevents collagen α2(I) chains from associating with α1(I) chains. To compromise, α1(I) homotrimers are formed and incorporated into forming bone matrix.[22] The overall collagen content of the bone matrix in these mice was reduced (less 20%), the D periods of the collagen fibers were shortened on average, and the water content of the matrix was higher. The disorganization of the matrix had a net negative effect on both bone stiffness and toughness.[23] Meanwhile, null *COL1A1* variants and recessive variants affecting the chaperoning and secretion of collagen (*SERPINH1*, *CREB3L1*, *MBTPS2*) cut the collagen content of the matrix, throw off the bone material formula, and thus jeopardize bone material properties.

Alterations That Disrupt Matrix Mineralization

A common feature of many OI forms is the hypermineralization of matrix. This increase in mineral density correlates with disease severity (higher in OI Types III, IV, and V than in Type I) and is thought to be a consequence of poor matrix assembly, perhaps by exposing more sites for mineral nucleation.[24] Though there is more mineral, the mineral nanoplatelets themselves are smaller, thinner, and irregularly ordered, again, reflecting the poor collagen matrix organization underneath.[25] This disorganization coupled with the incorporation of a higher proportion of mineral (increasing stiffness and concomitantly moderating toughness) produces fragility.

In other forms of OI, defects in mineralization ruin the good foundation laid by otherwise normal fibrillogenesis. In OI Type VI (caused by variants in *SERPINF1*), histology reveals abundant osteoid with both osteoid thickness and surface area doubled in comparison to normal bone. When viewed under polarized light, OI Type VI lamellar bone has a unique "fish-scale" pattern.[26] A distinctive feature of OI resulting from a recurrent gain-of-function *IFITM5* (encoding BRIL) variant in the 5'UTR (OI Type V) is the formation of dense, but poorly-arranged matrix at fracture sites ("hyperplastic callus").[27] However, variants in the coding region of *IFITM5* cause a clinical phenotype not dissimilar from OI Type VI with characteristic histology and reduced expression of Pigment Epithelium Derived Factor (PEDF, encoded by *SERPINF1*), suggesting there is an interaction between BRIL and PEDF in mineralization.[28] *SPARC* variants are likely to interfere with mineralization as osteonectin is one of the NPCs with a role in policing that process. Along the same lines, variants in *COL1A1* and *COL1A2* that affect binding sites for NCPs may inhibit their association with an equivalent impact on mineralization.

Radiating Effects

Long bone fractures in OI are generally transverse. This fracture pattern indicates an inability to dissipate energy, i.e., insufficient toughness.[23] Poor organization of bone extracellular matrix and defective mineralization along with the prevalence of non-enzymatic crosslinks in collagen fibrils[29] are responsible for reduced energy dissipation on the smaller scales. On larger scales, these failures, in addition to scale-specific failures, e.g., increased intracortical porosity[30], cancel out critical bone toughening mechanisms: crack initiation toughness is a percentage of what it is in normal bone, as is crack extension toughness, and crack paths are linear instead of being successfully deflected.[29] On the scale of the long bone itself, cortical width and cancellous bone volume are both decreased in many cases of classical OI (Types I-IV) and in Types VII and VIII[21], though neither these measurements nor bone mineral density (BMD) measurements can be used to exclude the diagnosis of OI, as many individuals fall within the normal range.[31]

SUMMARY

The hierarchical structure of bone is the origin of its incredible biomaterial properties. This complex inter-reliant architecture is also the primary obstacle to helping patients with OI. Currently employed therapeutics work to increase BMD by tempering bone resorption. As we have seen, however, the failure of OI bone results not from macro-architectural deficiencies, but from defects at smaller scales that alter bone material properties. The OI community awaits the development of effective interventions on these smaller scales.

FIGURE

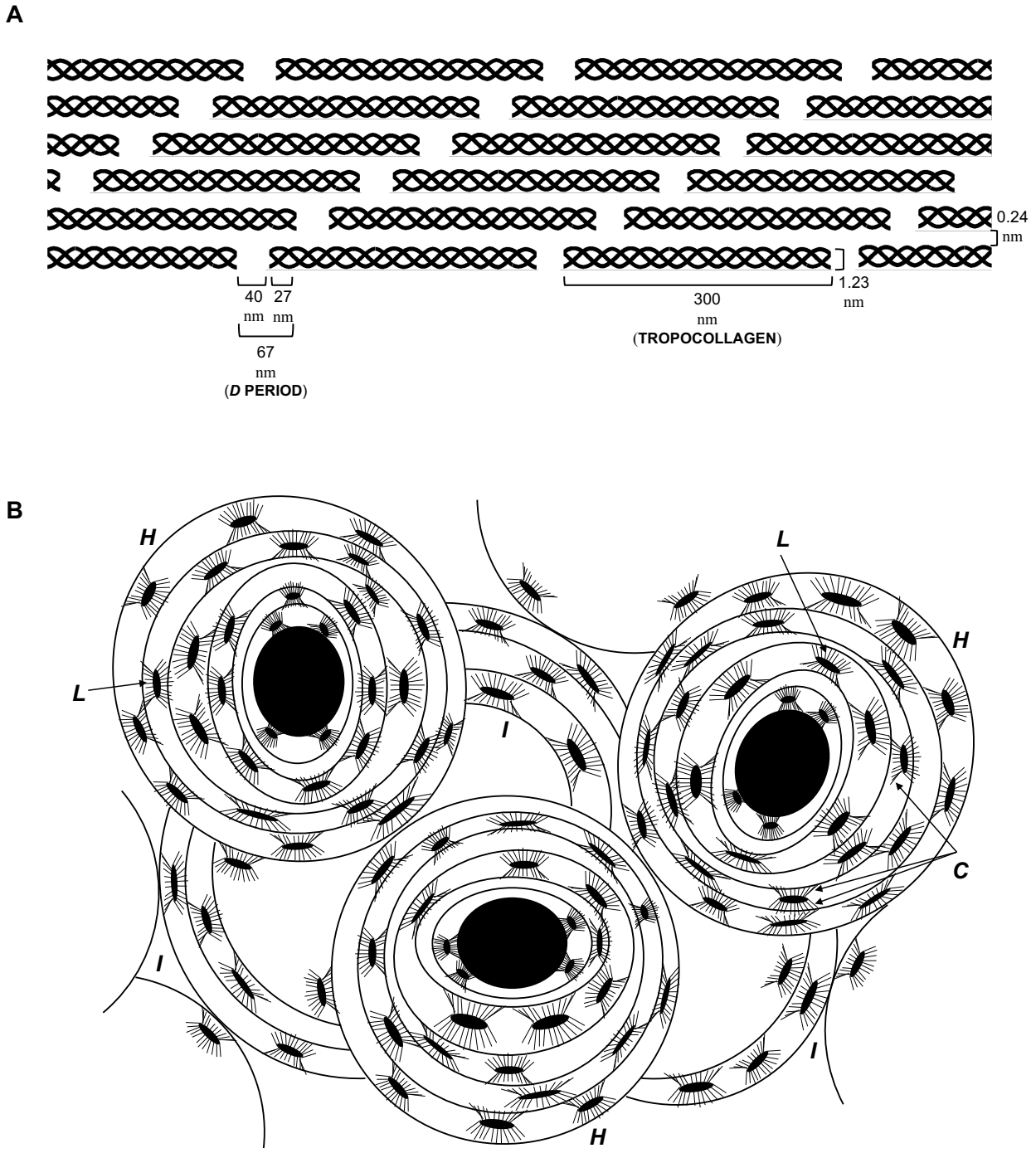

Figure 5-1. The Hierarchical Structure Of Bone. A) 2D representation of the supramolecular arrangement of tropocollagens in a fibril with characteristic quarter-stagger arrangement producing a 67nm periodicity (not shown to scale). B) Illustrated representative morphology of cortical (compact) bone revealed by transverse histological sectioning. **H**, Haversian systems (i.e., osteons) consisting of concentric lamellae (mineralized collagenous matrix) encircling Haversian canals which house blood vessels, nerves, and lymphatics; **I**, interstitial systems (older, partially resorbed osteons); **L**, lacunae; **C**, canaliculi.

REFERENCES

1. Stock, S.R. (2015). The mineral-collagen interface in bone. Calcif Tissue Int 97, 262-280.
2. Wagermaier, W., Klaushofer, K., and Fratzl, P. (2015). Fragility of bone material controlled by internal interfaces. Calcif Tissue Int 97, 201-212.
3. Parry, D., and Craig, A. (1979). Electron microscope evidence for an 80A unit in collagen fibrils. Nature 282, 213-215.
4. Yuan, L., and Veis, A. (1973). The self-assembly of collagen molecules. Biopolymers 12, 1437-1444.
5. Orgel, J., Irving, T., Miller, A., and Wess, T. (2006). Microfibrillar structure of type I collagen in situ. PNAS 103, 9001-9005.
6. Landis, W., Song, M., Leith, A., McEwen, L., and McEwen, B. (1992). Mineral and organic matrix interaction in normally calcifying tendon visualized in three dimensions by high-voltage electron microscopic tomography and graphic image reconstruction. J Struct Biol 110, 39-54.
7. Streeter, I., and de Leeuw, N.H. (2011). A molecular dynamics study of the interprotein interactions in collagen fibrils. Soft Matter 7, 3373-3382.
8. Bailey, A., Paul, R., and Knott, L. (1998). Mechanisms of maturation and ageing of collagen. Mech Ageing Dev 106, 1-56.
9. Fratzl, P., Groschner, M., Vogl, G., Plenk, H.J., Eschberger, J., Fratzl-Zelman, N., Koller, K., and Klaushofer, K. (1992). Mineral crystals in calcified tissues: a comparative study by SAXS. J Bone Miner Res 7, 329-334.
10. George, A., and Veis, A. (2008). Phosphorylated proteins and control over apatite nucleation, crystal growth, and inhibition. Chem Rev 108, 4670-4693.
11. Weiner, S. (2008). Biomineralization: a structural perspective. J Struct Biol 163, 229-234.
12. Crane, N.J., Popescu, V., Morris, M.D., Steenhuis, P., and Ignelzi, M.A., Jr. (2006). Raman spectroscopic evidence for octacalcium phosphate and other transient mineral species deposited during intramembranous mineralization. Bone 39, 434-442.
13. Murshed, M., Harmey, D., Millan, J.L., McKee, M.D., and Karsenty, G. (2005). Unique coexpression in osteoblasts of broadly expressed genes accounts for the spatial restriction of ECM mineralization to bone. Genes Dev 19, 1093-1104.
14. Luo, G., Ducy, P., McKee, M., Pinero, G., Loyer, E., Behringer, R., and Karsenty, G. (1997). Spontaneous calcification of arteries and cartilage in mice lacking matrix GLA protein. Nature 386, 78-81.
15. Van Leeuwenhoek, A. (1693). An extract of a letter from Mr. Anth. Van. Leeuwenhoek, containing several observations on the texture of the bones of animals compared with that of wood: on the bark of trees: on the little scales found on the cuticula, etc. J R Soc, 838-843.
16. Young, B., O'Dowd, G., and Woodford, P. (2014). Wheater's Functional Histology: A Text And Colour Atlas.(Philadelphia: Elsevier).
17. Havers, C. (1691). Osteologia Nova.(London: Samuel Smith).
18. Taylor, D., Hazenberg, J., and Lee, T. (2007). Living with cracks: damage and repair in human bone. Nat Mater 6, 263-268.
19. Gupta, H., Seto, J., Wagermaier, W., Zaslansky, P., Boesecke, P., and Fratzl, P. (2006). Cooperative deformation of mineral and collagen in bone at the nanoscale. PNAS 103, 17741-17746.

20. Currey, J.D., and Shahar, R. (2013). Cavities in the compact bone in tetrapods and fish and their effect on mechanical properties. J Struct Biol 183, 107-122.
21. Marini, J.C., Forlino, A., Bachinger, H.P., Bishop, N.J., Byers, P.H., Paepe, A., Fassier, F., Fratzl-Zelman, N., Kozloff, K.M., Krakow, D., et al. (2017). Osteogenesis imperfecta. Nat Rev Dis Primers 3, 17052.
22. Chipman, S., Sweet, H., McBride, D., Davisson, M., Marks, S., Shuldiner, A., Wenstrup, R., Rowe, D., and Shapiro, J. (1993). Defective proa2(I) collagen synthesis in a recessive mutation in mice: a model of human osteogenesis imperfecta. Proc Natl Acad Sci USA 90, 1701-1705.
23. Bishop, N. (2016). Bone material properties in osteogenesis imperfecta. J Bone Miner Res 31, 699-708.
24. Boyde, A., Travers, R., Glorieux, F., and Jones, S. (1999). The mineralization density of iliac crest bone from children with osteogenesis imperfecta. Calcif Tissue Int 64, 185-190.
25. Fratzl, P., Paris, O., Klaushofer, K., and Landis, W.J. (1996). Bone mineralization in an osteogenesis imperfecta mouse model studied by small-angle x-ray scattering. J Clin Invest 97, 396-402.
26. Glorieux, F., Ward, L., Rauch, F., Lalic, L., Roughley, P., and Travers, R. (2002). Osteogenesis imperfecta type VI: a form of brittle bone disease with a mineralization defect. J Bone Miner Res 17, 30-38.
27. Glorieux, F., Rauch, F., Plotkin, H., Ward, L., Travers, P., Roughley, P., Lalic, L., Glorieux, D., Fassier, F., and Bishop, N. (2000). Type V osteogenesis imperfecta: a new form of brittle bone disease. J Bone Miner Res 15, 1650-1658.
28. Farber, C.R., Reich, A., Barnes, A.M., Becerra, P., Rauch, F., Cabral, W.A., Bae, A., Quinlan, A., Glorieux, F.H., Clemens, T.L., et al. (2014). A novel IFITM5 mutation in severe atypical osteogenesis imperfecta type VI impairs osteoblast production of pigment epithelium-derived factor. J Bone Miner Res 29, 1402-1411.
29. Carriero, A., Zimmermann, E.A., Paluszny, A., Tang, S.Y., Bale, H., Busse, B., Alliston, T., Kazakia, G., Ritchie, R.O., and Shefelbine, S.J. (2014). How tough is brittle bone? Investigating osteogenesis imperfecta in mouse bone. J Bone Miner Res 29, 1392-1401.
30. Albert, C., Jameson, J., Smith, P., and Harris, G. (2014). Reduced diaphyseal strength associated with high intracortical vascular porosity within long bones of children with osteogenesis imperfecta. Bone 66, 121-130.
31. Paterson, C., and Mole, P. (1994). Bone density in osteogenesis imperfecta may well be normal. Postgrad Med J 70, 104-107.

APPENDIX

SUPPLEMENTARY INFORMATION
(CHAPTER 2)

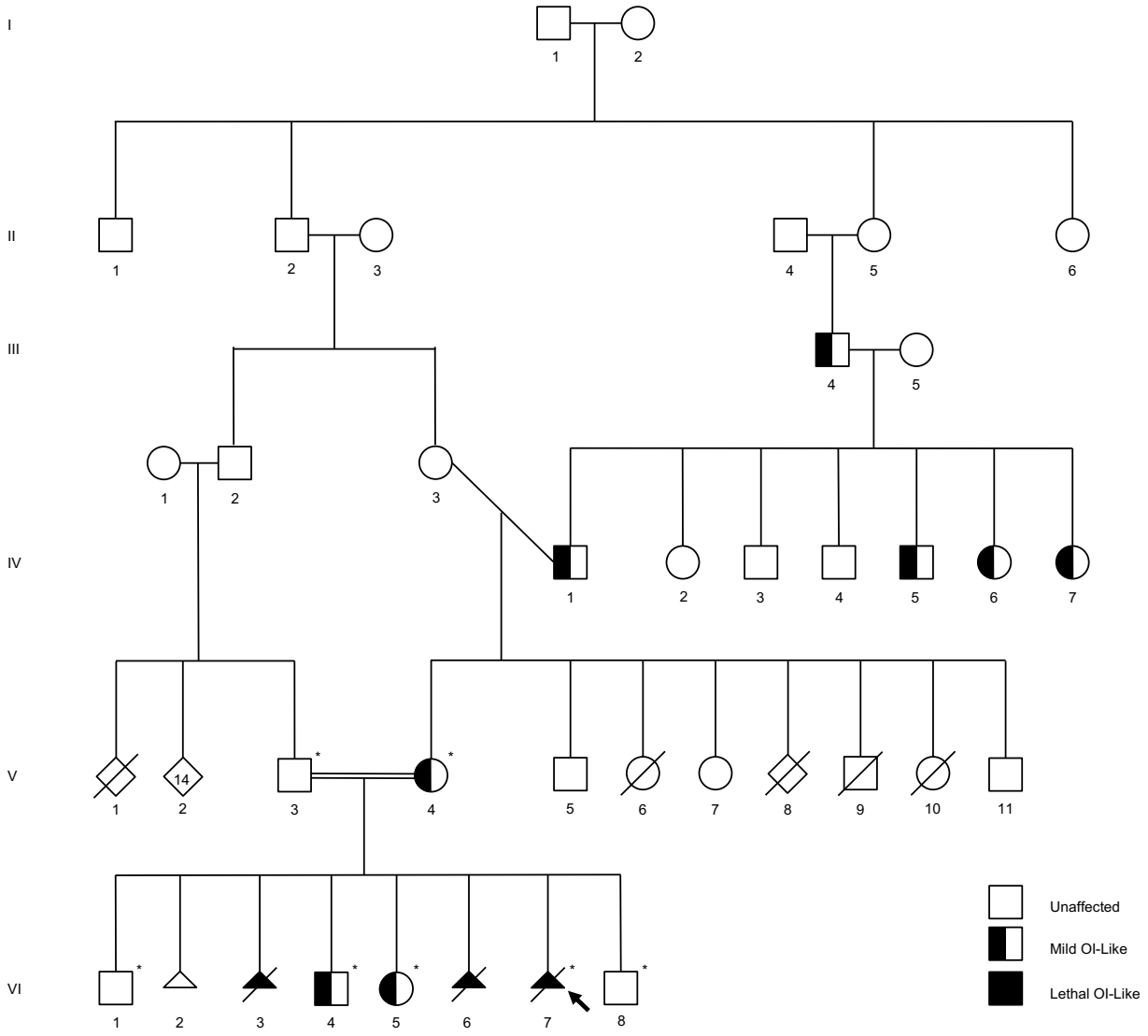

Supplementary Figure 2-1. Expanded Pedigree Of The Family. The arrow indicates the proband. Asterisks denote family members who were exomed.

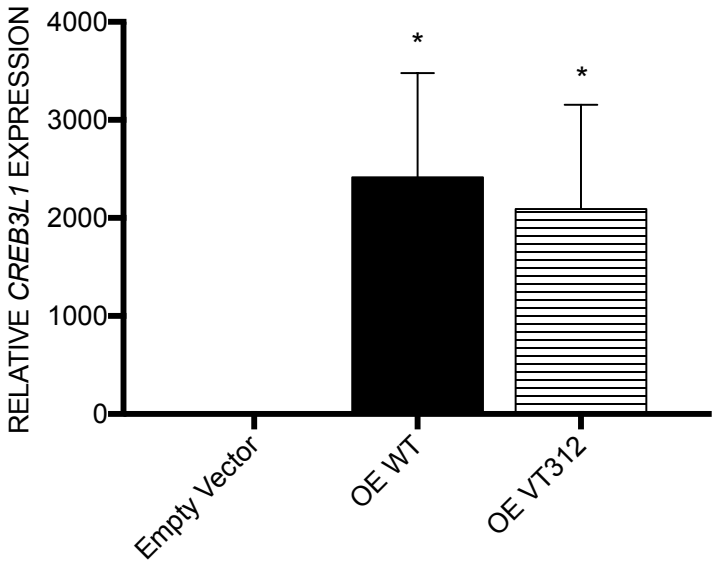

Supplementary Figure 2-2. Efficient Transfection Of HEK293. *CREB3L1*, either wild type (WT) or variant (VT312), is overexpressed in transfected HEK293. *P < 0.05 versus empty vector-transfected control (Dunnett Test). Y-axes represent relative mRNA expression normalized by the level of GAPDH. Values shown are the means of three independent experiments (n = 3). Error bars, S.D. RT-qPCR.

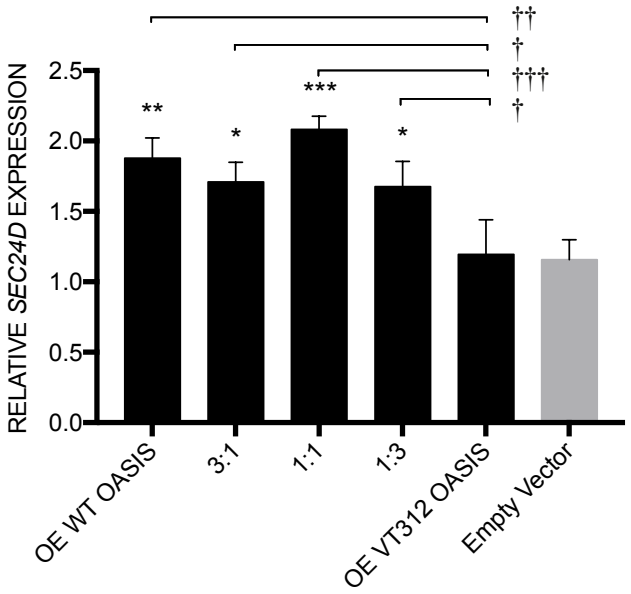

Supplementary Figure 2-3. OASIS Does Not Form Homodimers. While the presence of any WT OASIS yields higher expression of the target *SEC24D*, there is no correlation between increasing amounts of functional WT OASIS and expression. *P < 0.05; **P < 0.01; ***P < 0.001 versus empty vector-transfected control. †P < 0.05; ††P < 0.01; †††P < 0.001 versus the indicated group (Tukey Test). Y-axes represent relative mRNA expression normalized by the level of GAPDH. Values shown are the means of three independent experiments (n = 3). Error bars, S.D. RT-qPCR.

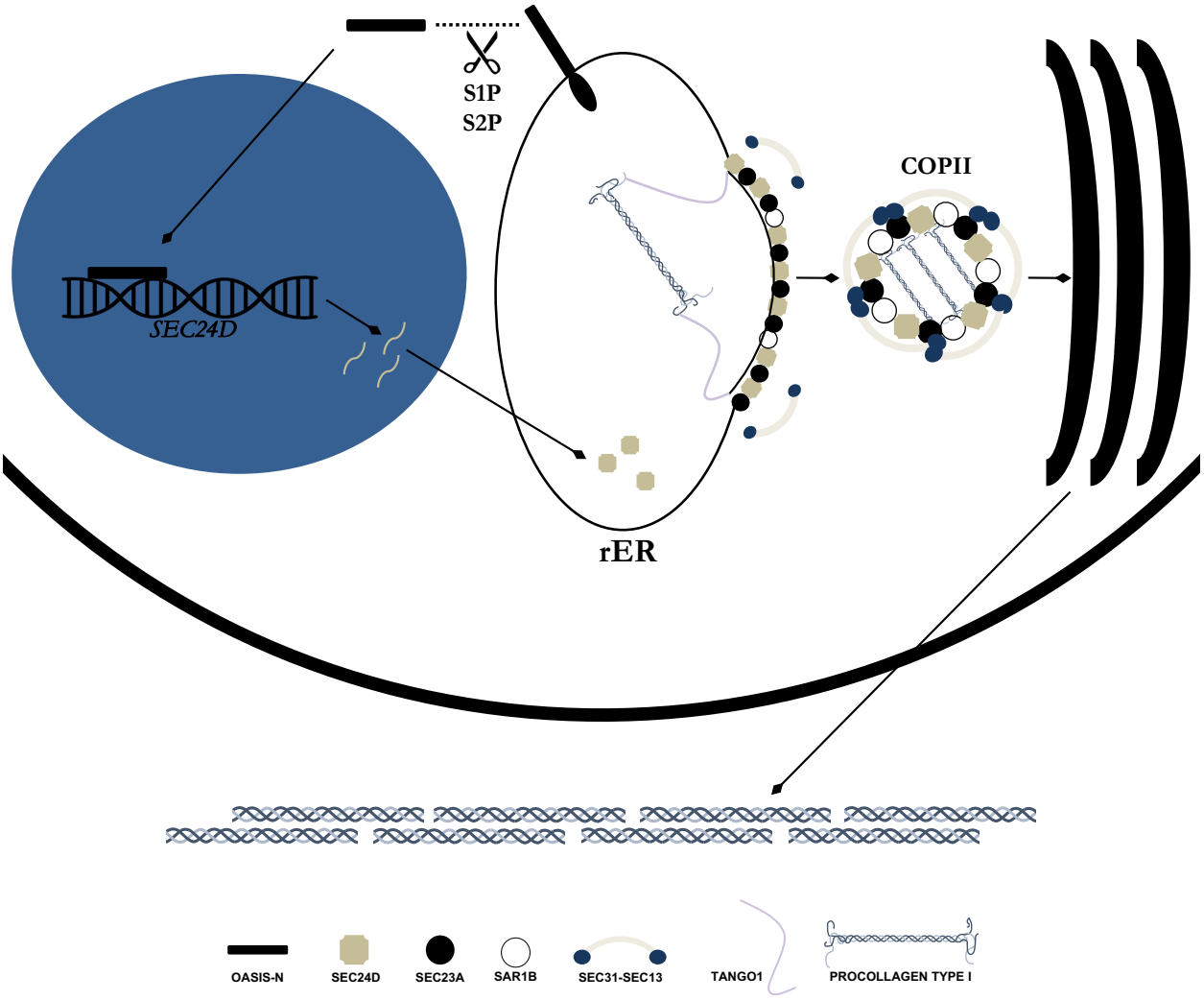

Supplementary Figure 2-4. Role Of OASIS In Osteoblasts. Physiological ER stress imposed by high levels of protein production associated with osteoblast maturation and bone formation causes release of full-length OASIS from the rough endoplasmic reticulum (rER) membrane and cleavage by S1P and S2P yielding an activated form. The NH_2-terminal OASIS fragment (OASIS-N) moves into the nucleus, where it promotes expression of *SEC24D* which encodes a structural protein needed to build COPII carriers for the shuttling of type I procollagen to the Golgi for eventual secretion. OASIS has additional transcriptional targets including the cargo-encoding gene *COL1A1*.[16] Additional COPII structural proteins include SEC13, SEC23, SEC31, SAR1B, and others, while TANGO1 is a helper protein for loading large cargos like type I procollagen. The overall effect of OASIS activation is efficient trafficking of large amounts of type I procollagen, and possibly additional bone matrix proteins, into forming bone matrix.

Supplementary Table 2-1. Primer Sequences

PRIMER	SEQUENCE	REFERENCE \NOTES
CREB3L1-i5S (Exon 7 Mutation Sequencing)	GCCTTGCCCAGGTCATATAG	Collagen Diagnostic Lab (University Of Washington)
CREB3L1-i8A (Exon 7 Mutation Sequencing)	CTCTCCCCTGTCTCCCAGAG	Collagen Diagnostic Lab (University Of Washington)
QuikCREB3L1_ del2159-2161	CCAGGAGAGCCGTCGTAAGAAGGAGTATGTGG	*for* mutagenesis of WT312 expression vector
QuikCREB3L1_ del2159-2161_anti	CCACATACTCCTTCTTACGACGGCTCTCCTGG	*for* mutagenesis of WT312 expression vector
T7UP F	AACGACGGCCAGTGAATTGTAATA	*for* PCR assembly of IVT templates
IRES R	ATGGGTGGTGGCCATATTATCATC	*for* PCR assembly of IVT templates
IVT Sense OASIS	GATGATAATATGGCCACCACCCATATGGACGCCGTCTTGGAA	*for* PCR assembly of IVT templates
IVT Antisense OASIS	TTTTTTTTTTTTTTTTTTTTTCTATGATGGTGGTGTTGGGGC	*for* PCR assembly of IVT templates
COL1A1 UPRE-Like WT Human (Duplex Oligo)	(T O P) CGGCCAGCCGGCCAGCCGACGTGGCTCCCTCCCCTTCTGT GCCGGTCGGCCGGTCGGCTGCACCGAGGGAGGGGAAGACA (B O T T O M)	*for* EMSA
QPCR[SEC23A] F	TCAAGATCTGACCCAGTCTC	*for* RT-qPCR
QPCR[SEC23A] R	GCATATCCTGGTATCCTGAC	*for* RT-qPCR
QPCR[SEC24D] F	GATCCTGACTCTATCCCTAGC	*for* RT-qPCR
QPCR[SEC24D] R	GGTGGCATAAACTTGTCCTC	*for* RT-qPCR
QPCR[GAPDH] F	AACGTGTCAGTGGTGGACC	*for* RT-qPCR
QPCR[GAPDH] R	GACAAAGTGGTCGTTGAGG	*for* RT-qPCR
QPCR[CREB3L1] F	TTGATGACCCTGTGCTGGAT	*for* RT-qPCR
QPCR[CREB3L1] R	CATCTTGATGGGCACAAGGG	*for* RT-qPCR

SUPPLEMENTARY INFORMATION
(CHAPTER 3)

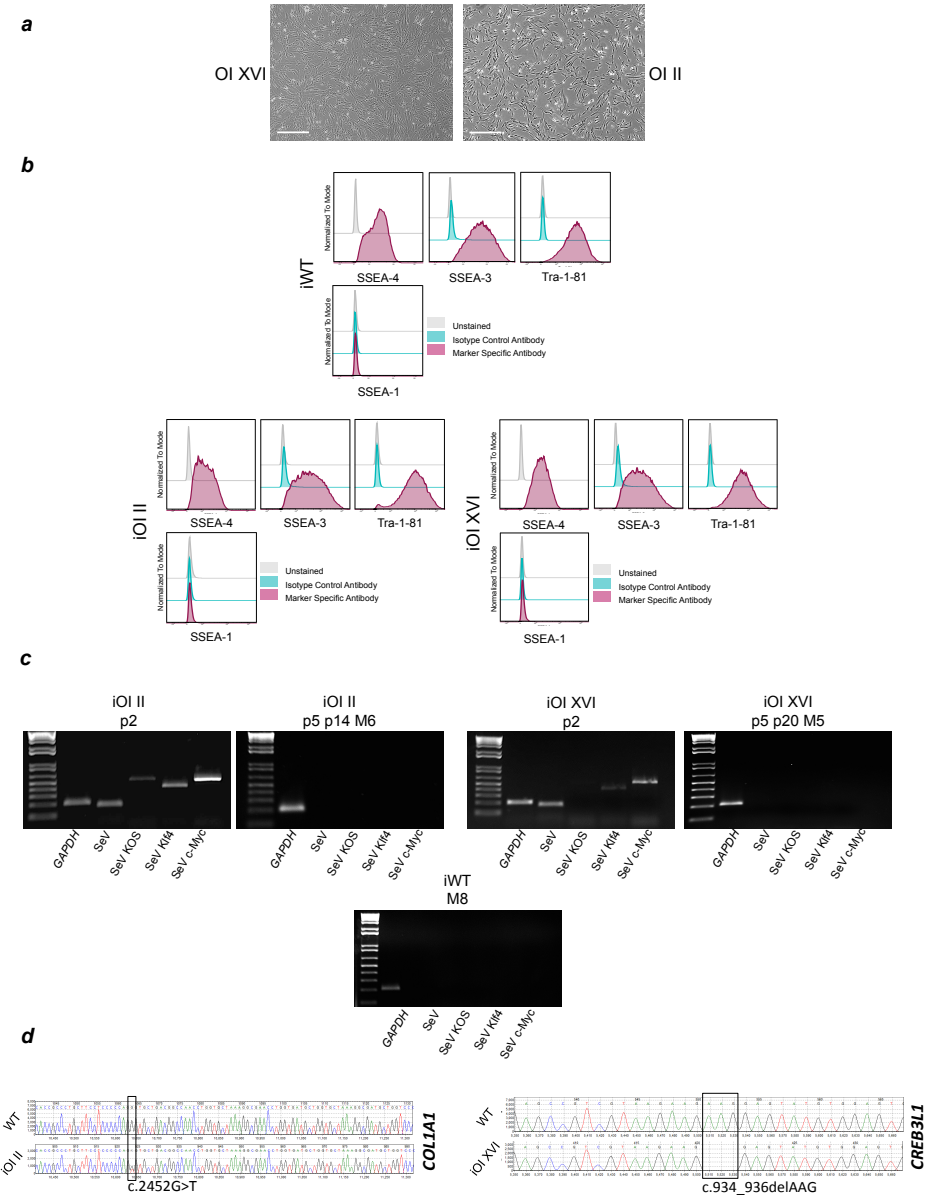

Supplementary Figure 3-1. Additional Characterization Of Established hiPSC Lines. *a*) Primary patient fibroblast lines before reprogramming – OI XVI (p4) with the homozygous *CREB3L1* variant and OI II (p6) with the *COL1A1* variant. Scale Bars = 500µm. *b*) Flow cytometry of reprogrammed cells demonstrates the presence of the pluripotent cell surface markers SSEA-3, SSEA-4, and Tra-1-81, while the cells do not present SSEA-1, an early marker of differentiation. Y-axes represent cell counts normalized to the mode. *c*) Following reprogramming, early passage cells retain viral vector sequences (SeV, SeV OSK, SeV Klf4, SeV c-Myc), but after many passages and clonal expansion, viral sequence is no longer detectable. An early iWT sample was not available for testing because the line was gifted. The nomenclature for passaging (e.g., p5 p20 M5) refers to p5 = passages after reprogramming before picking individual clones, p20 = clonal expansion on feeders, and M5 = feeder-free passages. RT-PCR. *d*) Confirmation of patient mutations in the patient hiPSC clones – *CREB3L1* c.934_936delAAG (p.Lys312del) in iOI XVI and *COL1A1* c.2452G>T (p.Gly818Cys) in iOI II. Sanger Sequencing.

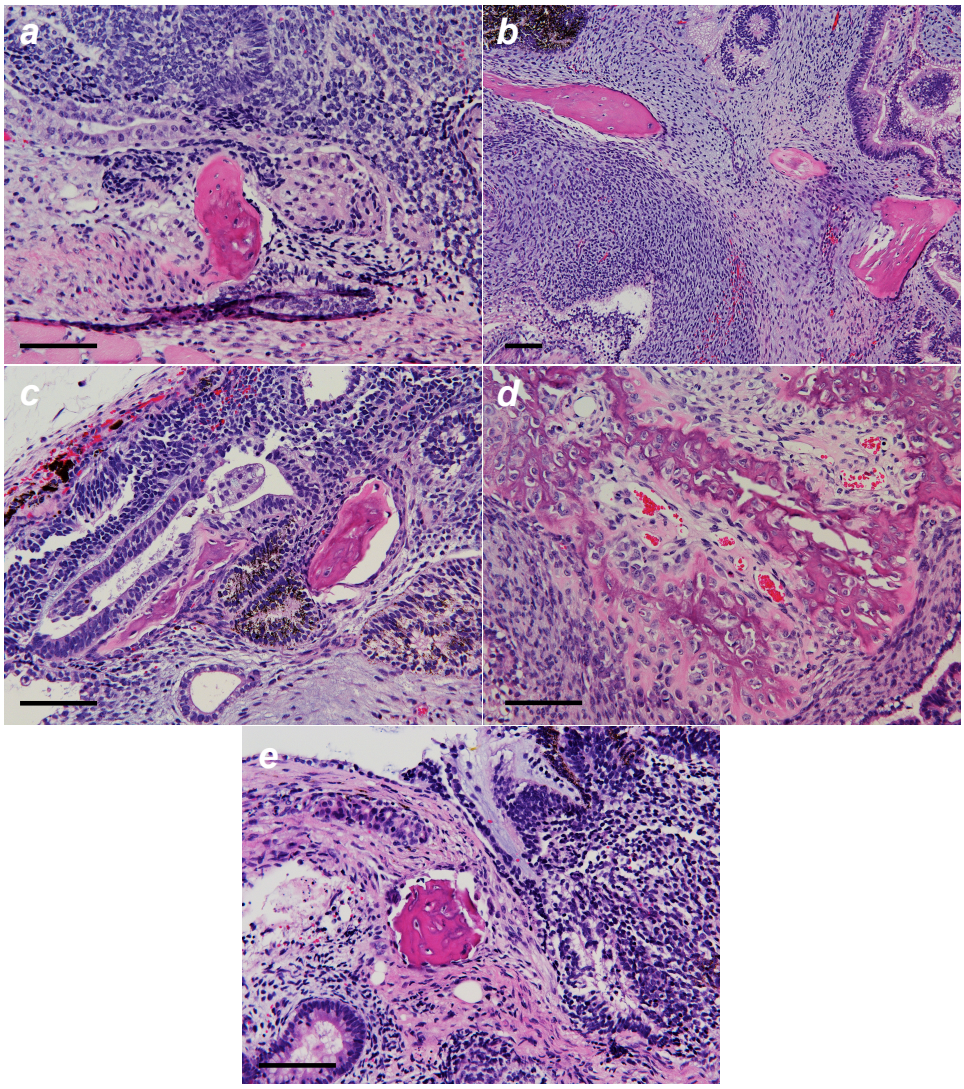

Supplementary Figure 3-2. Foci Of Bone From Teratomas. *a*) iWT-T2. *b*) iWT-T2. *c*) iOI II-T1. *d*) Possible endochondral bone formation in iOI II-T2. e) iOI XVI-T2, the only focus of bone observed in iOI XVI-generated tumors (n = 4). Scale Bars = 100mm. H&E.

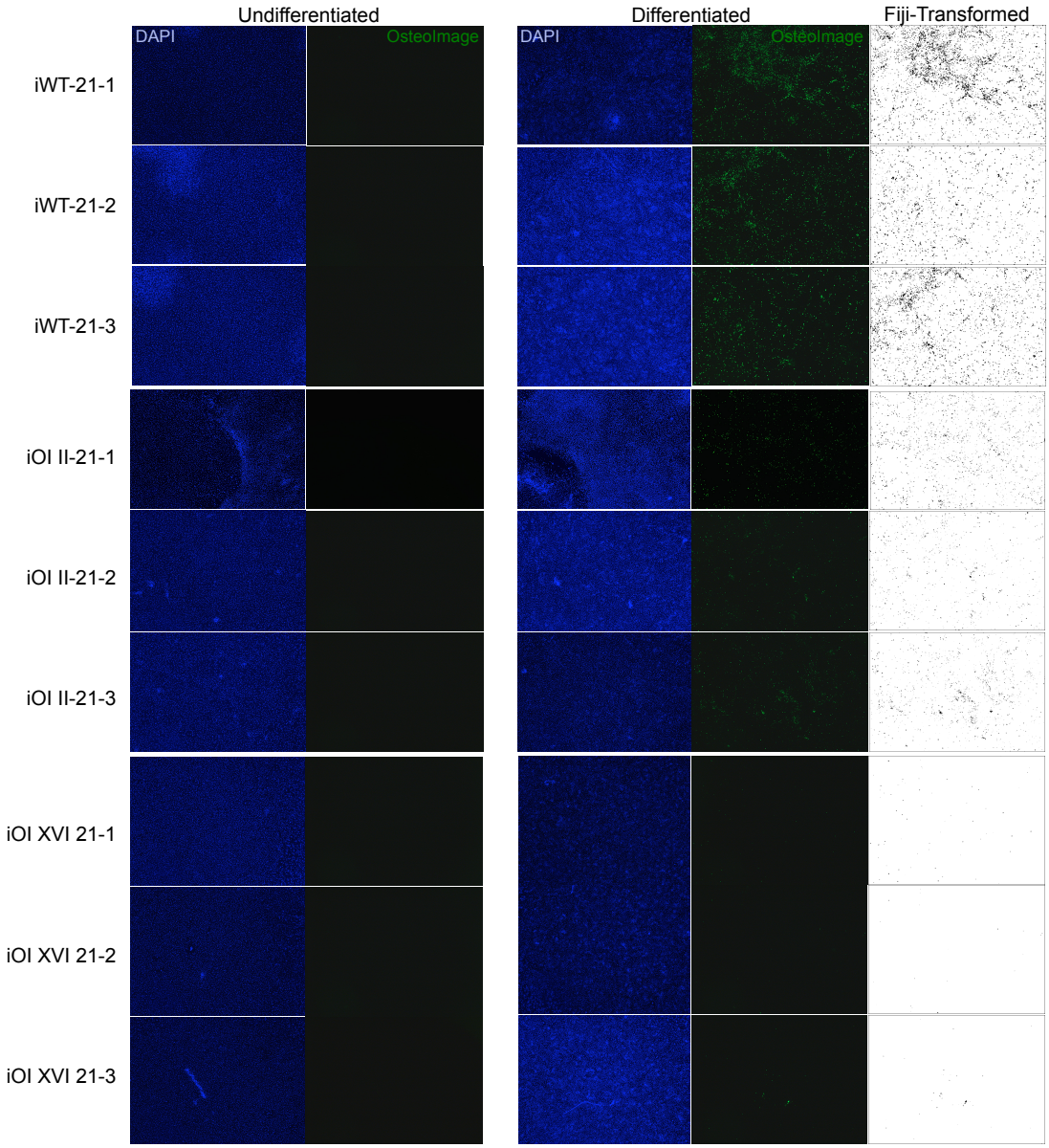

Supplementary Figure 3-3. Quantification Of OsteoImage Mineralization Assay. The mineralization assay was performed on cells cultured for 21 days either in basal media without factors (αMEM 10% FBS) or in osteoblast differentiation media (αMEM 10% FBS w\ dexamethasone, ascorbic acid, and β-glycerophosphate). Cells were counterstained with DAPI to demonstrate the presence of cells in the absence of mineralization. Fiji (Image J) was used to transform the images and measure fluorescence as follows: Image<Color<Split Channels<Select Green. Image<Adjust<Threshold<Auto Select Threshold. Tick "Dark Background". If signal was very low, auto threshold selected background instead, in which case opened the original image and adjusted sliders until signals approximately matched. Analyze<Analyze Particles<Tick "Summarize".

Supplementary Table 3-1. Primer Sequences

PRIMER	SEQUENCE	REFERENCE \NOTES
QPCR [OCT4] F	AGT TTG TGC CAG GGT TTT TG	Ruhola-Baker Lab (University Of Washington)
QPCR [OCT4] R	ACT TCA CCT TCC CTC CAA CC	Ruhola-Baker Lab (University Of Washington)
QPCR [SOX2] F	ATG GAC AGT TAC GCG CAC ATG	
QPCR [SOX2] R	AGC TGG TCA TGG AGT TGT ACT GCA G	
QPCR [NANOG] F	TCC TGG AAC ACT CAG ACC TGG TG	
QPCR [NANOG] R	TCC AAG TCA CTG GCA GGA G	
QPCR [GAPDH] F	AAC GTG TCA GTG GTG GAC C	
QPCR [GAPDH] R	GAC AAA GTG GTC GTT GAG G	
QPCR DIFF [COL1A1] F	GTG CTA AAG GTG CCA ATG GT	Kanke *et al.* 2014 *Stem Cell Reports*
QPCR DIFF [COL1A1] R	CTC CTC GCT TTC CTT CCT CT	Kanke *et al.* 2014 *Stem Cell Reports*
QPCR DIFF [RUNX2] F	TTA CTT ACA CCC CGC CAG TC	Arpornmaeklong *et al.* 2009 *Stem Cells Dev*
QPCR DIFF [RUNX2] R	TAT GGA GTG CTG CTG GTC TG	Arpornmaeklong *et al.* 2009 *Stem Cells Dev*
QPCR DIFF [BGLAP] F	GGC AGC GAG GTA GTG AAG AG	Kanke *et al.* 2014 *Stem Cell Reports*
QPCR DIFF [BGLAP] R	AGC AGA GCG ACA CCC TAG AC	Kanke *et al.* 2014 *Stem Cell Reports*
QPCR DIFF [ALPL] F	GGA CAT GCA GTA CGA GCT GA	Arpornmaeklong *et al.* 2009 *Stem Cells Dev*
QPCR DIFF [ALPL] R	CCA CCA AAT GTG AAG ACG TG	Arpornmaeklong *et al.* 2009 *Stem Cells Dev*
QPCR DIFF [SP7] F	AAG CTG ATC TGG TGG TGC AT	
QPCR DIFF [SP7] R	GAC TCC ACA AAG GGC ATG AT	
QPCR DIFF [IBSP] F	TTC ATT GAA TGG TTT GAG GTT G	Kanke *et al.* 2014 *Stem Cell Reports*
QPCR DIFF [IBSP] R	AGT GTT GCA TAG GTA GTG CGA TT	Kanke *et al.* 2014 *Stem Cell Reports*
QPCR DIFF [SPARC] F	TGA GGT ATC TGT GGG AGC TAA TC	PrimerBank ID 365777426c1
QPCR DIFF [SPARC] R	CCT TGC CGT GTT TGC AGT G	PrimerBank ID 365777426c1
QPCR [CREB3L1] F	TTG ATG ACC CTG TGC TGG AT	
QPCR [CREB3L1] R	CAT CTT GAT GGG CAC AAG GG	
QPCR [SEC24D] F	GAT CCT GAC TCT ATC CCT AGC	
QPCR [SEC24D] R	GGT GGC ATA AAC TTG TCC TC	
SeV RT-PCR F	GGA TCA CTA GGT GAT ATC GAG C	Life Technologies (Invitrogen) CytoTune-iPS 2.0 Sendai Reprogramming Kit
SeV RT-PCR R	ACC AGA CAA GAG TTT AAG AGA TAT GTA TC	Life Technologies (Invitrogen) CytoTune-iPS 2.0 Sendai Reprogramming Kit

SeV RT-PCR KOS F	ATG CAC CGC TAC GAC GTG AGC GC	Life Technologies (Invitrogen) CytoTune-iPS 2.0 Sendai Reprogramming Kit
SeV RT-PCR KOS R	ACC TTG ACA ATC CTG ATG TGG	Life Technologies (Invitrogen) CytoTune-iPS 2.0 Sendai Reprogramming Kit
SeV RT-PCR Klf4 F	TTC CTG CAT GCC AGA GGA GCC C	Life Technologies (Invitrogen) CytoTune-iPS 2.0 Sendai Reprogramming Kit
SeV RT-PCR Klf4 R	AAT GTA TCG AAG GTG CTC AA	Life Technologies (Invitrogen) CytoTune-iPS 2.0 Sendai Reprogramming Kit
SeV RT-PCR c-Myc F	TAA CTG ACT AGC AGG CTT GTC G	Life Technologies (Invitrogen) CytoTune-iPS 2.0 Sendai Reprogramming Kit
SeV RT-PCR c-Myc R	TCC ACA TAC AGT CCT GGA TGA TGA TG	Life Technologies (Invitrogen) CytoTune-iPS 2.0 Sendai Reprogramming Kit
CREB3L1-i5S (OI XVI Mutation Sequencing)	GCC TTG CCC AGG TCA TAT AG	Collagen Diagnostic Lab (University Of Washington)
CREB3L1-i8A (OI XVI Mutation Sequencing)	CTC TCC CCT GTC TCC CAG AG	Collagen Diagnostic Lab (University Of Washington)
COL1A1-IN32S (OI II Mutation Sequencing)	CCT CTC AGG AAA CCC AGA CAC AAG CA	Collagen Diagnostic Lab (University Of Washington)
COL1A1-x38A (OI II Mutation Sequencing)	CTC CAG GAG CAC CAA CAT TA	Collagen Diagnostic Lab (University Of Washington)

Supplementary Methods

Flow Cytometry: For flow cytometry of hiPSC lines, cells were harvested with Accutase (Corning). Approximately 3 x 10^5 cells were resuspended in 0.1% FBS in PBS and incubated at 4 °C with conjugated antibody in the dark for 30 minutes. The following antibodies were used in the analysis: SSEA-1, SSEA-3, and Tra-1-81 from the StemFlow Human Pluripotent Stem Cell Sorting & Analysis Kit (Cat No. 560461; BD Biosciences) at the recommended dilution (20uL/1 x 10^6 cells) and SSEA-4 (FCMA116P; Millipore) at 1:50. Non-specific fluorescence was accounted for by the inclusion of isotype controls (AlexaFluor647 Mouse IgM κ, FITC Mouse IgM κ, PE Rat IgM κ) for each specific antibody except for SSEA-4. A minimum of 10,000 events were acquired for each sample using a FACSCanto II (BD Biosciences) and cell cytometry data were analyzed using FlowJo software (BD Biosciences).

RT-PCR – SeV: RT-PCR to detect the SeV genome and transgenes in hiPSC lines was performed according to a protocol in the CytoTune-iPS 2.0 User Guide. Briefly, total RNA was extracted from late-passage hiPSCs using the RNeasy Mini Kit (Qiagen). RNA from early-passage (p2 after transduction) cells was also collected as a positive control. Reverse transcription of 850ng of RNA was performed with iScript Reverse Transcription Supermix (BIORAD) in 20μl reactions. PCR was carried out using 1μl of cDNA and HotStarTaq (Qiagen) with the following parameters: 95 °C for 15 minutes followed by 95 °C for 30 seconds, 55 °C for 30 seconds, 72 °C for 30 seconds for 32 cycles, then, 72 °C for 10 minutes. Products were analyzed on a 2% agarose gel.

Mutation Confirmation: Confirmation of patient-specific mutations in *CREB3L1* and *COL1A1* was achieved with Sanger sequencing. Primers for mutation confirmation are listed in Supplementary Table 3-1 (Integrated DNA Technologies). Relevant exons were amplified using AmpliTaq Gold Polymerase (Applied Biosystems). The cycling program was: 95°C for 12 minutes, 95 °C for 10 seconds, 61 °C for 40 seconds, 72 °C for 50 seconds for 35 cycles, then, 72 °C for 7 minutes. Amplicons were treated with ExoSAP according to a standard protocol. Sequencing reactions were assembled using Big Dye v3.1 (Applied Biosystems) with the following program: 96°C for 10 seconds, 50 °C for 5 seconds, 60 °C for 4 minutes for 40 cycles. Sequencing was run on an ABI 3730. Sequences were analyzed using Mutation Surveyor v4.0.9 software (Softgenetics).

SUPPLEMENTARY INFORMATION
(CHAPTER 4)

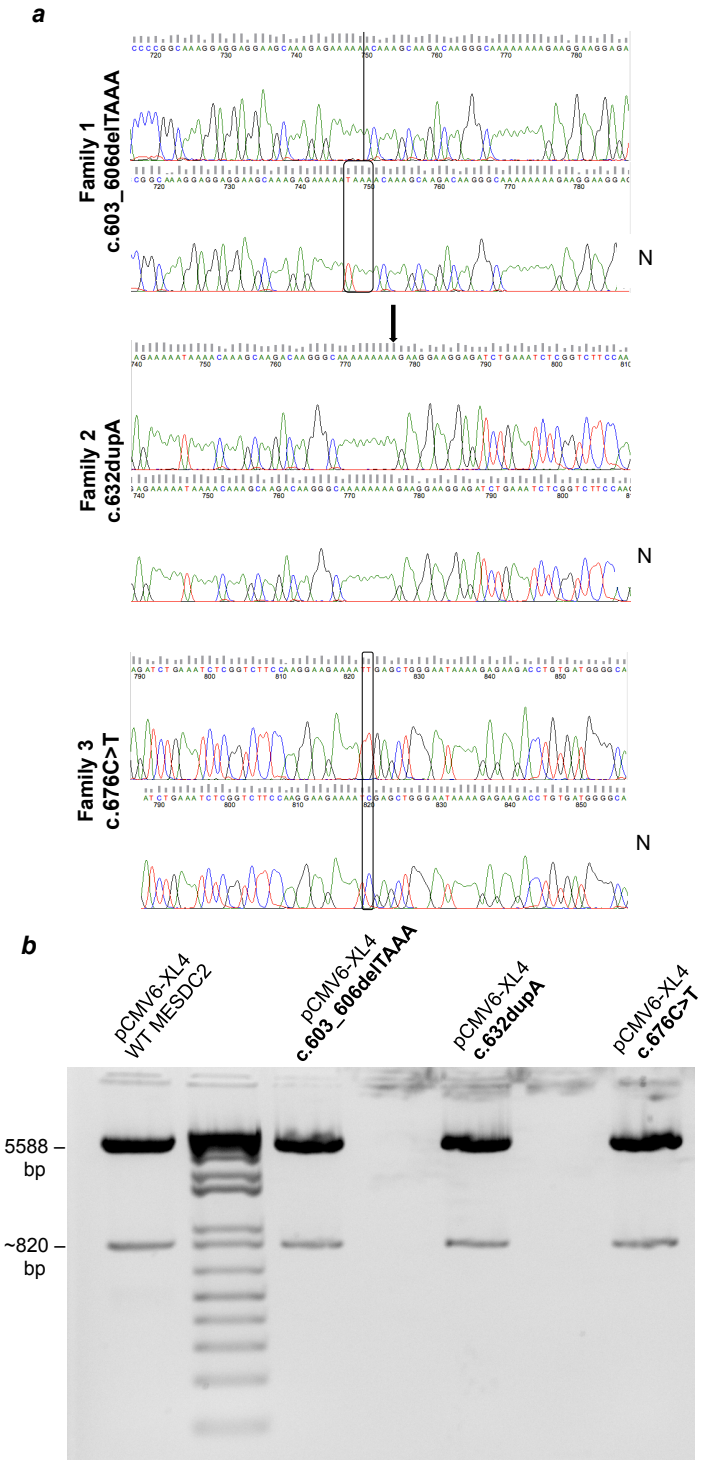

Supplementary Figure 4-1. IVTT DNA Templates. *a*) Mutagenesis introducing family variants in *MESDC2* was confirmed by Sanger sequencing. The normal reference sequences are labeled 'N'. *b*) Sac-I digestion of T7-MESDC2 cDNA fragments away from pCMV6-XL4 expression plasmid backbone.

ABBREVIATIONS

α1(I) – collagen 1 alpha 1 chain
α2(I) – collagen 1 alpha 2 chain
AA – ascorbic acid
βGP – β-glycerophosphate
BMD – bone mineral density
bZIP – basic leucine zipper
CaP – calcium phosphate
consScoreGERP – Genomic Evolutionary Rate Profiling Conservation Score
COPII – coat protein II
CREB/ATF – cyclic AMP response element binding/activating transcription factor
dbSNP – Single Nucleotide Polymorphism Database (https://www.ncbi.nlm.nih.gov/SNP/)
DEX – dexamethasone
DI – Dentinogenesis Imperfecta
EB – embryoid body
ECM – extracellular matrix
EDS – Ehlers-Danlos Syndrome
EMSA – electrophoretic mobility shift assay
ER – endoplasmic reticulum
ESC – embryonic stem cell (h – human i.e., hESC)
ExAC – Exome Aggregation Consortium (http://exac.broadinstitute.org)
FGF – fibroblast growth factor
FZD – frizzled receptor
gnomAD – Genome Aggregation Database (http://gnomad.broadinstitute.org)
HA – hydroxyapatite; $Ca_{10}(PO_4)_6(OH)_2$
HBM – high bone mass
ICC – immunocytochemistry
iPSC – induced pluripotent stem cell (h – human i.e., hiPSC)
IVT/IVTT – in vitro transcription/translation
μCT – micro-computed tomography
MEF – mouse embryonic fibroblast
MIM/OMIM – Mendelian Inheritance In Man/Online MIM (https://www.omim.org)
MLBR – major ligand binding region
MSC – mesenchymal stem cell
NCP – non-collagenous protein
NGS – Next Generation Sequencing
NHLBI EVS – National Heart, Lung, & Blood Institute Exome Variant Server (http://evs.gs.washington.edu/EVS/)
ODM – osteoblast differentiation media
OI – Osteogenesis Imperfecta
OC – osteocalcin (an NCP)
OCP – octacalcium phosphate
OE – over-expression
ON – osteonectin (an NCP)
OPN – osteopontin (an NCP)
OPPG – Osteoporosis-Pseudoglioma Syndrome
ORF – open reading frame
PEDF – Pigment Epithelium Derived Factor
PhastCons – Phylogenetic Analysis With Space/Time Models Conservation Score (http://compgen.cshl.edu/phast/)
PPi – pyrophosphate; $P_2O_7^{4-}$
rER – rough endoplasmic reticulum
RIP – Regulated Intramembrane Proteolysis
ROH – region of homozygosity
RT-qPCR – quantitative reverse transcription polymerase chain reaction
SeV – Sendai virus; murine parainfluenza virus type 1; hemagglutinating virus of Japan (HVJ)

SNP – single nucleotide polymorphism
SREBP – sterol regulatory element binding protein
TEM – transmission electron microscopy
TM – transmembrane
TSH – thyroid-stimulating hormone/thyrotropin
UPR – Unfolded Protein Response
UPRE – unfolded protein response element
VT – variant
WES – Whole Exome Sequencing
WT – wild type